Title
Defining the Molecular and Functional Diversity of Stem Cell-Derived Motor Neurons

Author
Adams, Katrina

Publication Date
2014

Peer reviewed|Thesis/dissertation

UNIVERSITY OF CALIFORNIA

Los Angeles

Defining the Molecular and Functional Diversity of Stem Cell-Derived Motor Neurons

A dissertation submitted in partial satisfaction of the requirements for the degree Doctor of Philosophy in Molecular Biology

by

Katrina Louise Adams

2014

ABSTRACT OF THE DISSERTATION

Defining the Molecular and Functional Diversity

of Stem Cell-Derived Motor Neurons

by

Katrina Louise Adams

Doctor of Philosophy in Molecular Biology

University of California, Los Angeles, 2014

Professor Bennett G. Novitch, Chair

Spinal motor neurons (MNs) are a diverse group of specialized neurons that innervate and control all muscles of the body, thereby allowing locomotion and respiration. Over the past decade, many groups have used directed differentiation of pluripotent stem cells into MNs to model human MN development and disease *in vitro*. Despite these efforts, it remains unknown whether stem cell-derived MNs fully recapitulate endogenous MN populations. To address this question, this thesis presents the characterization of human embryonic and stem cell-derived MNs on molecular and physiological levels. We find that the processes of MN development and organization are largely conserved between mice and humans. However, the majority of stem cell-derived MNs only express characteristics of MNs that normally innervate axial muscles *in vivo*. To expand the diversity of stem cell-derived MNs, we propose an alternative method of differentiation using overexpression of MN fate determinants. Specifically, we find that overexpression of the transcription factor Foxp1 during stem cell differentiation results in a large number of dorsal and ventral limb-innervating MNs. Finally, we demonstrate that stem cell-derived MNs are capable of forming functional synapses with muscle cells *in vitro*. Together,

this work provides a detailed analysis of the strengths and weaknesses of current MN differentiation protocols, and presents new approaches for increasing the functional diversity of stem cell-derived MNs. In addition to valuable insights into human development, this body of work provides important information for ongoing efforts of modeling MN disease with stem cells.

The dissertation of Katrina Louise Adams is approved.

Douglas L. Black

Ellen M. Carpenter

Amander T. Clark

William E. Lowry

Bennett G. Novitch, Committee Chair

University of California, Los Angeles

2014

DEDICATION

For my parents, Stephen and Catharine Adams – my first scientific role models

TABLE OF CONTENTS

LIST OF FIGURES

ACKNOWLEDGMENTS

This work would not have been possible without the help and support of so many people. First, I must thank my mentor Ben Novitch for all of his hard work, guidance, and patience over the past 6 years. Thanks to Ben, I have learned how to be an independently thinking scientist. I greatly admire his constant dedication and passion for his work. I would also like to thank all of my thesis committee members: Amander Clark, Bill Lowry, Doug Black, and Ellen Carpenter for their helpful discussions and advice over the years.

I thank all the current and past Novitch lab members, without whom this work would not have been successful. First, I would like to thank David Rousso, whose guidance during my first years in Ben's lab was vital to my success. His endless enthusiasm for science remains an inspiration to me. I would also like to thank Destaye Moore for all of her hard work and help with the human motor neuron project. She spent hours upon hours culturing motor neurons and stem cells, and I am eternally grateful! I thank Caroline Pearson for all of her helpful discussions and advice on my research and career plans. I thank Jennifer Kong for her endless amount of support and laughter. Navigating all the ups and downs of grad school was a lot easier having you all to go through it with me.

In addition, I would like to thank Samantha Butler and all the members of her laboratory for their advice on my projects over the years, especially in regards to axon guidance assays. I would also like to thank all of our wonderful collaborators at UCLA who have helped me through my graduate career, including Joy Umbach, Cameron Gunderson, Bill Lowry, Michaela Patterson, Ben van Handel, Matteo Pelligrini, Artur Jaroszewicz , Doug Black, Meera Pratap, and Tom Otis.

Finally, I would like to thank my family and friends for their support and never-ending encouragement. My parents, thank you for always reassuring me that experiments are not supposed to work most of the time and for never asking the dreaded "when are you

graduating?" question. And lastly, Andrew Harmon, thank you for your constant love and encouragement over the past 5 years.

Chapter 2 is a version of a manuscript in preparation, authored by Katrina Adams, Destaye Moore, Joy Umbach, Meera Pratap, Tom Otis, and Bennett Novitch.

Chapter 3 is a version of a manuscript submitted for publication, authored by Katrina Adams, David Rousso, Joy Umbach, and Bennett Novitch. We thank Samantha Butler, Willliam Lowry, and Artur Kania for helpful discussion and comments on the manuscript; Kathrin Plath and Marianne Bonner for experimental instruction; Cameron Gunderson, Nick Brecha for reagents; Albert Han for collecting RNA from Foxp1$^{+/-}$ and Foxp1$^{-/-}$ embryonic spinal MNs.

Chapter 4 is a version of a published manuscript: Umbach JA, Adams KL, Gunderson CB, and Novitch BG. Functional neuromuscular junctions formed by embryonic stem cell-derived motor neurons. *PLoS One* 7, e36049. doi: 10.1371/journal.pone.0036049 (2012). We thank Hynek Wichterle for the generous gift of *Hb9::eGFP* mESCs; Amy Hurwitz and Destaye Moore for technical assistance, Lou Ignarro for facilities, and Samantha Butler, Harley Kornblum, and Felix Schweizer for helpful discussions and comments on the manuscript.

Lastly, I would like to thank my funding sources. This thesis work was supported by the UCLA Cellular and Molecular Biology Training program (Ruth L. Kirschstein NIH GM00785), the UCLA-California Institute for Regenerative Medicine Training Grant, and a UCLA Graduate Division Dissertation Year Fellowship.

VITA

EDUCATION

University of California, San Diego (UCSD) 2004-2008

Bachelor of Science in Biochemistry and Cell Biology.

Graduate with cum laude honors.

AWARDS

Dissertation Year Fellowship, UCLA Graduate Division 2013-2014

Pre-doctoral Training Fellowship, Broad Stem Cell Research Center, 2012-2013

California Institute for Regenerative Medicine.

Cellular and Molecular Biology Training Fellowship, 2009-2011

Ruth L. Kirschstein National Research Service Award GM007185

PUBLICATIONS

Adams KL, Rousso DL, Umbach JA, and Novitch BG. (2014) Foxp1-mediated directed differentiation of limb-innervating motor neurons from embryonic stem cells. ***In review.***

Adams KL, Moore DM, Umbach JA, Pratap M, Otis TS, and Novitch BG. Characterization and comparison of human embryo and stem cell-derived spinal motor neurons. ***In preparation.***

Umbach JA, **Adams KL**, Gunderson CB, and Novitch BG. (2012) Functional neuromuscular junctions formed by embryonic stem cell-derived motor neurons. PLoS One 7, e36049.

Takashima S, **Adams KL**, Ortiz PA, Ying CT, Moridzadeh R, Younossi-Hartenstein A, and Hartenstein V. (2011) Development of the Drosophila entero-endocrine lineage and its specification by the Notch signaling pathway. Developmental Biology 353, 161-172.

Hartenstein V, Takashima S, and **Adams KL**. (2010) Conserved genetic pathways controlling the development of the diffuse endocrine system in vertebrates and Drosophila. General and Comparative Endocrinology 166, 462-469.

Takimoto JK, **Adams KL**, Xian Z, and Wang L. (2009) Improving orthogonal tRNA-synthetase recognition for efficient unnatural amino acid incorporation and application in mammalian cells. Molecular Biosystems 5, 931-934.

CHAPTER 1 – INTRODUCTION

1-1: An overview of stem cells and regenerative medicine

One of the most exciting scientific discoveries of the 20th century was the derivation of embryonic stem cells (ESCs) from the inner cell mass of mouse[1] and human blastocysts[2]. ESCs are self-renewing and pluripotent cells, which are able to differentiate into any cell lineage of the three germ layers: endoderm, mesoderm, and ectoderm. Therefore, ESCs theoretically provide an unlimited source of cells that can be used to replace any damaged or diseased cells of the human body. However, the regenerative potential of stem cells is largely dependent upon efficient differentiation protocols that produce specific cell types of interest.

Much progress has been made over the past 10-20 years in creating and refining differentiation protocols for generating a myriad of cell populations from ESCs. The majority of differentiation protocols rely upon addition of signaling molecules, identified from developmental studies, to direct the ESCs towards a germ layer and then a specific cell population. For example, many different types of neurons (motor neurons, dopaminergic neurons, cortical neurons) can now be generated *in vitro* from neural stem cells derived from ESCs, as long as appropriate sequential signaling cues are used[3]. In addition to the nervous system, protocols for ESC differentiation into cardiomyocytes[4], lung cells[5], intestinal cells[6], germ cells[7], and many other cell types have been created. These stem cell-derived populations have brought significant insight into human developmental processes that would otherwise remain largely unknown.

Despite these scientific advances, use of ESCs for regenerative medicine remains controversial for several reasons. First, there are ethical concerns over the destruction of human embryos for the generation of new human ESC (hESC) lines, although the majority of these lines are generated from leftover human embryos from In Vitro Fertilization (IVF) cycles[8]. Second, there remains the issue of immune rejection if non-autologous hESC-derived cells are

transplanted into patients. One solution to this problem is the creation of tissue banks for collecting a large variety of hESC lines to represent a high percentage of the world's population[9]. Another solution, which has shifted some research focus away from ESCs, is the use of induced pluripotent stem cells (iPSCs).

iPSCs were first produced through viral overexpression of several key transcription factors (Oct4, Sox2, c-Myc, Klf4) in mouse fibroblasts, reprogramming the fibroblasts back to a pluripotent state[10]. Since then, iPSCs have been generated from human fibroblasts[11], urine samples[12], blood cells[13], and more. iPSCs have been shown to be similar to ESCs in their differentiation capabilities and epigenetic landscape, although some controversy remains over how identical these populations are[14]. iPSCs have great potential for regenerative medicine in that patient-specific iPSC lines can be generated and subsequently used for transplantation therapies, thereby, avoiding the issue of immune rejection. An even more powerful application has been the generation of iPSC lines from patients with disease-causing genetic mutations. Differentiation of these mutant iPSCs lines into the cell populations normally affected by disease has resulted in great insight into early disease processes, as well as potential new drug treatments. One example of this – the use of iPSCs to investigate motor neuron disease – will be further discussed in chapter 5.

Overall, the discoveries of ESCs and iPSCs have ushered in a new era of regenerative medicine. Diseases that were once thought to be incurable, such as Alzheimer's and Parkinson's, are now viewed as potentially treatable. However, many questions of stem cell research and disease modeling remain to be answered before their full potential can be realized. It remains unknown how faithfully stem cell-derived populations recapitulate the molecular and functional properties of their endogenous counterparts. Furthermore, it is unclear whether certain stem cell-derived populations behave appropriately both *in vitro* and *in vivo.* This body of work will address these questions, using the MN model system.

1-2: Introduction to MN biology

The central nervous system is made up of thousands upon thousands of different neurons, glial support cells, and their synaptic connections. This enormous diversity allows all animals to receive and interpret information from the environment, thereby learning and adapting to changes. One group of neurons – the spinal MNs – have been extensively characterized and used as a model system for neuronal differentiation processes and neural circuit formation[15]. Spinal MNs are a group of neurons located in the ventral horn of the spinal cord and are responsible for all voluntary and involuntary muscle movement. Somatic MNs are classified into three subtypes: alpha MNs that innervate extrafusal muscle fibers of skeletal muscles (involved in muscle contraction), gamma MNs that innervate intrafusal muscle fibers of muscle spindles (involved in muscle stretching), and beta MNs that innervate both the muscle fibers and spindles[16]. Alpha MNs have been the most thoroughly characterized, and will be the focus of this dissertation.

Spinal MNs are responsible for connecting central nervous system processes with peripheral actions. They receive pre-synaptic inputs from proprioceptive sensory afferents and spinal interneurons, as well as descending cortical tracts in the spinal cord[16]. Upon sufficient stimulation, MNs release the neurotransmitter acetylcholine at their post-synaptic nerve terminals to induce contraction of muscle fibers. These specialized synapses are called neuromuscular junctions (NMJs). From studies with rodent and chick embryos, the differentiation of MNs and their functional role in the spinal neural circuitry have been well characterized.

Patterning of the neural tube

In the mouse embryo, stem and progenitors cells in the developing neural tube receive instructional cues from several signaling molecules. Sonic hedgehog (Shh) is secreted from the notochord and floor plate of the neural tube, Bone morphogenetic proteins (BMPS) are secreted

from the roof plate, and retinoic acid (RA) is secreted from the paraxial mesenchyme (**Fig. 1-1a**)[17]. Shh and BMP signaling creates a dorsoventral patterning gradient in which class I and class II homeodomain proteins are activated in different neural progenitors. The cross-repressive activities of these transcription factors result in the formation of different progenitor domains along the dorsovental axis of the neural tube (**Fig. 1-1b**)[17]. These progenitor domains give rise to different populations of spinal neurons, followed by oligodendrocytes and astrocytes at later stages in development. In the ventral region of the neural tube, high levels of Shh induce expression of the basic-helix-loop-helix (bHLH) protein Olig2 in a subset of progenitors[18]. These are the MN progenitors in the pMN domain (**Fig. 1-1 b-c**). Around embryonic day (E) 9-9.5, these $Olig2^{+}$ progenitors begin to differentiate into postmitotic MNs by detaching from the lumen and migrating laterally into the mantle zone of the spinal cord[19]. As MN progenitors exit the cell cycle, Olig2 expression is rapidly down-regulated, while expression of Lin1/Isl1/Mec3 (LIM)-homedomain transcription factors (Lhx3, Lhx4, Islet 1, Islet 2) and the transcription factor Hb9 are up-regulated (Figure 1-1c)[19]. These newly born MNs then diversify into the different subtypes present in the mature spinal cord.

MN diversity and organization

In vertebrate embryos, spinal MNs are organized into columns at specific positions along the rostrocaudal axis, largely controlled by the actions of Hox proteins[20]. These motor columns can be identified by their position in the spinal cord, their transcription factor profile, and their target muscles (**Fig. 1-2**). Medial motor column (MMC) MNs are found along the entire length of the spinal cord, express Hb9, Islet 1 (Isl1) and Lhx3, and innervate axial muscles[21]. Lateral motor column (LMC) MNs are present at forelimb and hindlimb levels and are divided into medial (LMCm) and lateral (LMCl) populations that innervate ventral and dorsal limb muscles, respectively. LMCm MNs express Isl1 and Foxp1, while LMCl MNs express Hb9, Lhx1, and Foxp1[22, 23]. Hypaxial motor column (HMC) MNs innervate muscles at all body segments

involved with respiration, including the diaphragm, intercostal, and abdominal muscles[24] (unpublished data). HMC MNs express Isl1 and Hb9, but lack Lhx3 or Foxp1 expression[22]. Lastly, pregangiolic motor column (PGC) MNs are located only at thoracic levels, innervate the sympathetic ganglia, and express Foxp1 and nNOS[22]. This diversity of MN populations is critical for the correct functioning of motor circuitry, and therefore survival.

Each motor column is further subdivided into motor pools, or small clusters of MNs that innervate the same muscle, which can be identified by their shared expression of certain transcription factors, including ETS proteins[25] (**Fig. 1-3c**). The limb-innervating or LMC motor pools at hindlimb levels have been the most extensively characterized in the mouse embryo. Retrograde labeling experiments have indicated that motor pools are organized into a topographical map in the ventral horn of the spinal cord (**Fig. 1-3a**)[26]. Motor pools that are located at rostral lumbar regions innervate more proximal hindlimb muscles (ie. quadriceps), while motor pools at caudal lumbar regions innervate distal hindlimb muscles (ie. the foot) (**Fig. 1-3b**). The correct formation of these motor columns and pools is dependent upon the combined activity of different MN fate determinants.

MN fate determinants

A large amount of work has been done to characterize the proteins required for MN development *in vivo*. Certain members of the LIM homedomain protein family have been found to be critical for the differentiation of all MNs and/or specific subtypes of MNs from Olig2$^+$ MN progenitors. Isl1 is required for MN generation as *Isl1* mutant embryos lack all MN populations[27]. Islet 2 (Isl2) is expressed by all MN populations initially and later down-regulated by visceral MN populations (ie. the PGC MNs)[28]. Loss of Isl2 in MNs results in a switch from visceral to somatic MN character[28]. Interestingly, Lhx3 has been shown to be important for both overall MN generation and for specification of MMC MN populations. Misexpression of Lhx3 in combination with Isl1 results in formation of ectopic MNs in dorsal regions of the spinal cord[29]. Misexpression

of Lhx3 in spinal MNs converts LMC and PGC MNs into MMC MNs, demonstrated by changes in molecular expression and axonal projections[30]. Lastly, Lhx1 has been found to be critical for the formation of LMCl MNs and therefore, the correct innervation of dorsal limb muscles[31]. Together, the actions of these proteins are known as the "LIM code" of MN development.

Another family of proteins – the Hox proteins – plays an important role in the specification and restriction of motor columns to distinct rostrocaudal domains along the spinal cord. Hox protein expression appears to be largely controlled by rostrocaudal patterning signals, including RA, Fibroblast growth factors (FGFs), and Wnt proteins[32]. Hoxc9, expressed only at thoracic levels of the spinal cord, has been shown to be responsible for restricting the formation of LMC MNs to cervical and lumbar levels[33]. In contrast, a complicated array of Hox5, Hox6, and Hox8 proteins are required in the cervical spinal cord for the correct formation of LMC MNs and motor pools[34]. Furthermore, Hox5 activity was recently found to be required for formation of phrenic (HMC) MNs at cervical levels[24]. Therefore, combinatorial actions of Hox proteins and LIM-homeodomain proteins result in the correct segregation of MN subtypes both between and within different regions of the spinal cord.

Another fate determinant that is of significant interest is the Forkhead domain transcription factor Foxp1. Foxp1 has been previously described to be critical for the development of several organ systems, such as the lungs[35], heart[36], and immune system[37], usually acting as a transcriptional repressor[38]. Our lab previously examined the role of Foxp1 in spinal MN populations and found it to be a critical regulator of MN diversity[22]. All LMC and PGC MNs express Foxp1, and these MNs populations are dramatically reduced in *Foxp1* mutant embryos[22, 23]. Furthermore, when floxed *Foxp1* alleles are selectively removed from spinal MNs using *Olig2*-driven Cre recombination, surviving mice are unable to move their forelimb and hindlimb muscles[26]. Conversely, Foxp1 misexpression in all spinal MNs results in increased numbers of LMC and PGC MNs, and subsequent decreased numbers of MMC and HMC

populations[22, 23]. Therefore, Foxp1 appears to act as a fate determinant for LMC and PGC MNs, thus introducing another level of regulation for MN diversity at limb levels.

MN axon guidance

Although the direct gene targets of the MN fate determinants described above have yet to be identified, one of the ways that these proteins are believed to influence the post-mitotic activity of MNs is through regulating expression of axon guidance receptors. One example of this is seen with the role of Lhx3 in MMC MNs, which was found to promote the expression of FGFR1 selectively in MMC MNs[39]. This allows MMC MN axons to innervate the developing dermomyotome through FGF-mediated attraction[39]. Another example is the relationship between Lhx1 and EphA4 expression in LMCl MNs, resulting in repulsion of LMCl axons away from the EphrinA$^+$ ventral limb[40]. A similar role has been identified for EphB1 in LMCm MNs, which repels LMCm axons away from the EphrinB$^+$ dorsal limb[41]. It is important to note that manipulating expression of MN fate determinants, such as Lhx3 and Foxp1, *in vivo* results in altered MN axon trajectories; therefore, it is very likely that these transcription factors regulate networks of genes involved in axon guidance and synapse formation.

1-3: Current approaches for generating spinal MNs from stem cells

Thanks to the knowledge gained from developmental studies, a variety of different protocols have been created for generating spinal MNs from mouse and human ESCs. The majority of these protocols rely upon the use of signaling molecules that were identified from *in vivo* studies as being critical for MN formation. Recently, an interest in reprogramming has also resulted in the generation of direct conversion methods. Each method presents its own advantages and limitations, and it is especially important to consider the types of MNs that are produced in each case.

RA and Shh dependent protocols

The first study to provide evidence for formation of stem cell-derived MNs was published in 2002 by Wichterle et al., in which MNs were generated from mouse ESCs using a step-wise procedure mimicking normal development[42]. This involves formation of embryoid bodies (EBs), or floating aggregates of cells, from mouse ESCs in a differentiation media that pushes the cells towards a neural fate. RA and Shh (or small molecule agonists of Shh) are added to the EBs at specific concentrations found to induce MN progenitor fate. After ~1 week of culture, mature functional ESC-derived MNs are produced, which express multiple molecular markers of MNs and fire repetitive action potentials – the hallmark of a mature MN. This protocol was then adapted for use with hESCs in a variety of different approaches. The most standard approach is a similar EB-dependent differentiation protocol, in which hESCs are induced to form neural progenitors through removal of pluripotency-promoting factors (FGFs), EB formation, and RA addition[43]. Once neural progenitors are isolated, Shh is added to induce expression of MN progenitor markers OLIG2 and NKX6.1. Postmitotic MNs can be identified starting around 5 weeks after the initiation of differentiation, marked by expression of HB9 and ISL1/2, and further maturation of hESC-derived MNs can take up to 2 months.

Because of the lengthy time required to generate mature hESC-derived MNs in culture, alternative protocols have been created with goals of shortening the differentiation timeline and maximizing the number of MNs generated. For example, one protocol uses inhibition of the transforming growth factor beta (TGF-β) and BMP pathways to repress non-neural lineages early in differentiation, resulting in highly efficient production of neural progenitors from hESCs and hiPSCs[44]. Another protocol uses a similar approach in combination with multiple Shh agonists (Purmorphamine and SAG) and RA, to induce MN formation efficiently within 3 weeks of differentiation[45]. Despite the small alterations in timing and efficiency among these different protocols, all depend upon use of RA and Shh for instructing MN cell fate.

In order to accurately use ESC-derived MN populations to model MN development and disease, it is essential that the full diversity of endogenous MNs is represented *in vitro.* Unfortunately, the majority of published papers describing novel hESC differentiation methods do not include analyses of different MN subtype markers or muscle preference assays. However, it has been shown that the majority of mouse ESC-derived MNs from RA/Shh-dependent protocols express molecular markers and characteristics of cervical MMC MNs[46]. For example, upon transplantation into developing chick embryos, mouse ESC-derived MNs preferentially project axons towards axial muscles[46]. Therefore, efforts have been made in recent years to expand the types of MNs generated from ESCs to other regions of the spinal cord.

Spontaneous differentiation of ESCs

From developmental studies, it is known that RA, FGF, and Wnt proteins are important regulators of posteriorization of the neural tube[47]. Therefore, it is possible that manipulating levels of these proteins during differentiation protocols will result in a more complete representation of MN subtypes from ESCs. However, this has yet to be definitively proven. Instead, interestingly, it has been recently shown that removal of RA and Shh during differentiation of mouse ESCs results in caudal cervical and thoracic MN populations[48]. Removal of high RA levels likely allows mouse ESC-derived MNs to escape from a cervical spinal cord identity. However, this increase in diversity comes at a great cost to efficiency, as only ~7% of spontaneous ESC-derived cells expressed MN markers[48]. Furthermore, this method has yet to be repeated with hESCs or hiPSCs, and may not represent a useful approach for generating large numbers of human MNs to be used for drug screening or transplantation.

Direct conversion of cells into MNs

An alternative approach to using developmental signaling molecules is the use of transcription factors to reprogram cell fates. This was first seen with the transcription factor MyoD, which was found to promote muscle identify when overexpressed in fibroblasts[49]. With the discovery of iPSCs, scientists have since become more interested in understanding the limits and plasticity of cell fate. Overexpression of several transcription factors (Ascl1, Brn2, and Myt1l) in mouse and human embryonic and postnatal fibroblasts was found to result in βIII-Tubulin $(TUJ1)^+$ neurons that express synaptic proteins[50, 51]. Furthermore, overexpression of 7 transcription factors (Ascl1, Brn2, Myt1l, Ngn2, Hb9, Isl1, and Lhx3) resulted in conversion of mouse and human fibroblasts to functional MNs, defined by their molecular and physiological properties[52]. Interestingly, these "induced" MNs clustered separately from embryonic and ESC-derived MNs in microarray analyses, suggesting that induced MNs retain some epigenetic memory of their fibroblast origin. Another study found that overexpression of Isl1, Ngn2, and Lhx3 transcription factors in hESCs generated functional MNs within 11 days after infection[53]. The advantage of these approaches is that they can produce large numbers of functional cells in a small amount of time. However, the types of MNs generated from these methods have not been characterized. Because Lhx3 was used to generate induced MNs, it is likely that these induced MNs expressed characteristics of MMC MNs.

1-4: Strategies to evaluate stem cell-derived MN function

In order to determine that stem cell-derived populations are similar to endogenous populations, an array of different techniques have been used to characterize and compare these two populations. The best evidence is integration of stem cell-derived neurons into developing or mature neural circuitry. For spinal MNs, this integration requires that spinal MNs are able to project axons towards and form synapses with the appropriate type of muscle, fire action potentials (APs), and receive pre-synaptic inputs from other neurons. Currently, there are

several different approaches used in the MN field to assess the functional maturation of ESC-derived MNs.

Electrophysiology

A great deal of work has been done to understand the electrophysiological properties of developing and mature spinal MNs, using mouse, chick, and rat model organisms[54]. This has allowed for analyzes of ESC-derived MNs, which have been found to exhibit physiological characteristics that match their natural counterparts. For example, mouse ESC-derived MNs express voltage-activated ion channels, including Na^{2+}, K^{+}, and Ca^{2+} channels[55]. Mouse ESC-derived MNs also generate repetitive trains of APs under current-clamp conditions[55], the hallmark of a mature MN. These properties have also been found to be true of hESC and hiPSC-derived MN populations. Furthermore, hESC and hiPSC-derived MNs have shown physiological maturation with additional time in culture, including an increase in cell soma size, an increase in dendritic branching, and a transition from firing single APs to multiple APs in response to current injection[56, 57]. However, no studies of human embryonic MN physiology have been performed; therefore, evaluation of hESC and hiPSC-derived MNs is currently based upon rodent models.

Muscle co-cultures

In order to qualify as functional, MNs must form synapses or NMJs with muscle fibers in the developing embryo. Therefore, many studies have used *in vitro* muscle and MN co-cultures to show evidence of ESC-derived MN functionality. Both mouse and human ESC-derived MNs have been found to form NMJs *in vitro*, when cultured with C2C12 myotubes or primary chick myotubes[52, 55]. These NMJs are normally characterized by clustering of acetylcholine receptors around the MN endplate, labeled with a fluorescently conjugated bungarotoxin. Contraction of myotubes has also been observed in these co-cultures, suggesting functional synapses.

However, C2C12 myotubes have been found to contract spontaneously in culture, even without the addition of MNs (unpublished data). Therefore, there is a need for *in vitro* assays that measure the different properties of synapse formation and maturation. In addition to validating stem cell-derived MN function, these assays would provide a platform for investigating synaptic defects in MN diseases.

Transplantations

Overall, transplantation studies provide the best evidence that stem cell-derived MNs recapitulate their endogenous counterparts. The majority of studies have used transplantation into the developing chick embryo, likely because of experimental ease, and found that both mouse and human ESC-derived MNs engraft in the ventral horn of the spinal cord when injected into the lumen[42, 45, 48]. Transplanted mouse ESC-derived MNs project axons robustly to the developing muscles, and have been found to express synaptic proteins and form NMJs with host chick muscles[42, 46]. Interestingly, when the number of transplanted mouse ESC-derived MNs was decreased, transplanted MNs only projected axons towards axial muscles – in agreement with their MMC phenotype[46]. Since then, transplantation of spontaneously differentiated ESCs has been found to result in a higher number of projections towards limb muscles, although synapse formation was not shown[48]. Therefore, transplantation of ESC-derived MNs into the developing chick embryo, at least for mouse ESCs, represents a reliable and detailed method for analyzing MN function and muscle preference *in vivo*.

In addition to chick embryos, transplantation of stem cell-derived neural progenitors and MNs into mouse and rat spinal cords has also been performed. For example, transplanted mouse ESC-derived MNs in the tibial nerves of adult mice formed functional NMJs with mouse host muscles[58]. Human iPSC-derived MNs were also found to integrate into neural circuitry when transplanted into the injured musculocutaneous nerves of rats, protecting the muscles from atrophy[59].

1-5: Summary

The creation of pluripotent stem cells has allowed human development and disease to be studied at levels that were not previously possible. This is especially true for MN diseases Amyotrophic lateral sclerosis (ALS) and Spinal muscular atrophy (SMA), which have been greatly investigated over the past decade using hESC and hiPSC-derived MNs. However, it still remains unknown how similar hESC-derived MNs are to endogenous MNs, largely because molecular studies of human MN development have not been performed. Characterizations of mouse ESC-derived MNs have shown that the majority express characteristics of cervical MMC MNs. Therefore, additional approaches for generating a wider diversity of MN subtypes, especially limb-innervating MNs, are needed. I present my work that addresses these concerns in the following chapters.

In chapter two, I characterize and compare hESC-derived MNs to human embryonic MNs, both on molecular and functional levels. I find that human embryonic MNs are organized into the same motor columns and pools present in mouse embryos, with some differences in pool size. In addition, human embryonic and hESC-derived MNs appear to follow a similar functional maturation timeline, suggesting that differentiation protocols mimic normal developmental progression. However, I find that hESC-derived MNs represent only a limited subset of endogenous populations, largely expressing cervical MMC and HMC MN markers. .

In chapter three, I investigate whether overexpression of MN fate determinants can direct the formation of specific MN subtypes from ESCs. I find that Foxp1 misexpression is sufficient to push mouse ESC-derived MNs from an MMC-like fate to an LMC-like fate. Furthermore, using multiple *in vitro* and *in vivo* assays to characterize the functional behavior of Foxp1-programmed MNs, I find that they display many hallmark characteristics of LMC MNs.

In chapter four, I present a low-density co-culture system that can be used to analyze formation of NMJs between ESC-derived MNs and muscle myotubes *in vitro*. Using dual patch clamp recordings, spontaneous and multi-quantal responses in myotubes can be detected that

are similar to *in vivo* responses. Therefore, ESC-derived MNs are capable of forming functional synapses *in vitro*. This system presents a platform for investigating NMJ formation and synaptic dysfunction in stem cell models of MN diseases.

Finally, in chapter five, I summarize the findings presented in this body of work and present future implications for the use of ESC-derived MNs to model human development and MN disease.

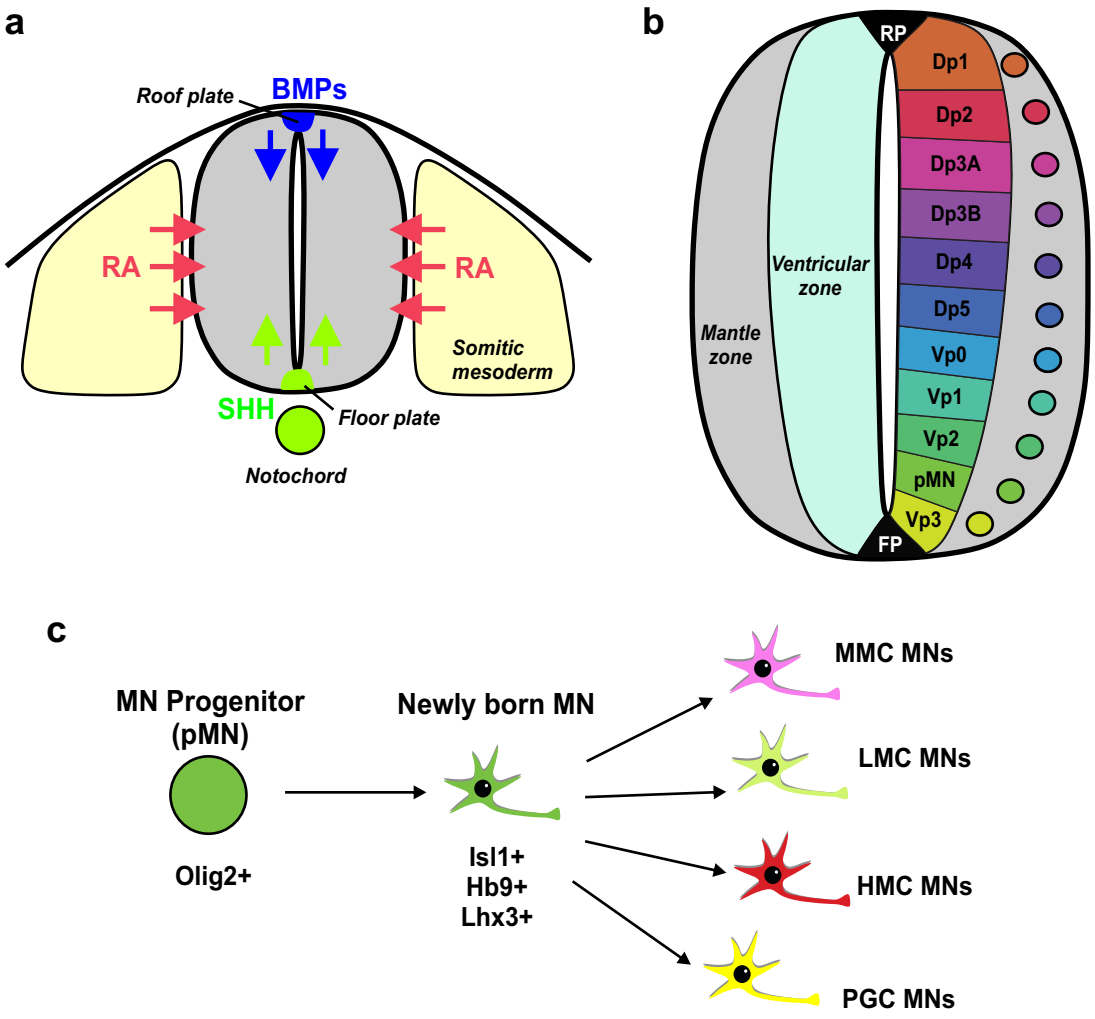

Figure 1-1 Development of the mouse spinal cord.

(**a**) Progenitors in the developing neural tube receive Sonic hedgehog (Shh) from the floor plate and notochord, Bone morphogenetic proteins (BMPs) from the roof plate, and retinoic acid (RA) from the surrounding somitic mesoderm.

(**b**) These signaling molecules initiate expression of patterning genes that set up a dorsoventral organization of different progenitor domains (Vp3 to Dp1) in the ventricular zone. Each domain gives rise to different neurons that migrate into the mantle zone.

(**c**) MN progenitors in the pMN domain express Olig2. When these progenitors differentiate, they turn off Olig2 and turn on Isl1, Hb9, and Lhx3 expression. These newly born MNs then diversify into the different MN subtypes.

a

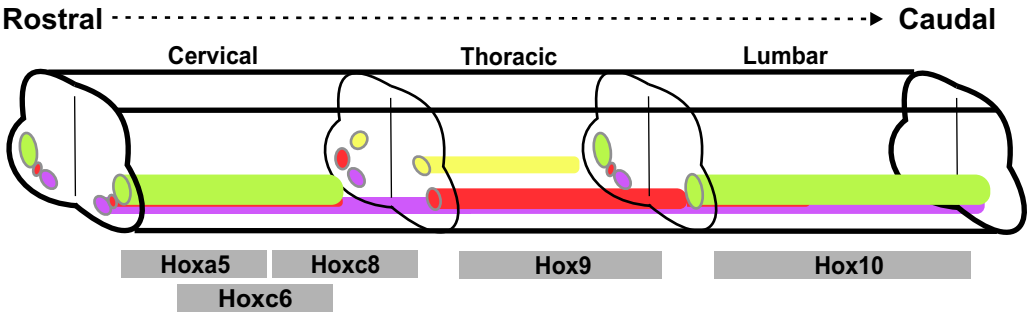

Motor Column	Molecular Markers	Muscle Targets
MMC	Hb9, Isl1/2, Lhx3	Axial (back) muscles
LMCm	Hb9, Isl1/2, Foxp1, Raldh2	Ventral limb muscles
LMCl	Hb9, Foxp1, Lhx1, Raldh2	Dorsal limb muscles
PGC	Hb9, Isl1/2, Foxp1, nNOS	Sympathetic ganglia
HMC	Hb9, Isl1/2	Respiratory muscles

b

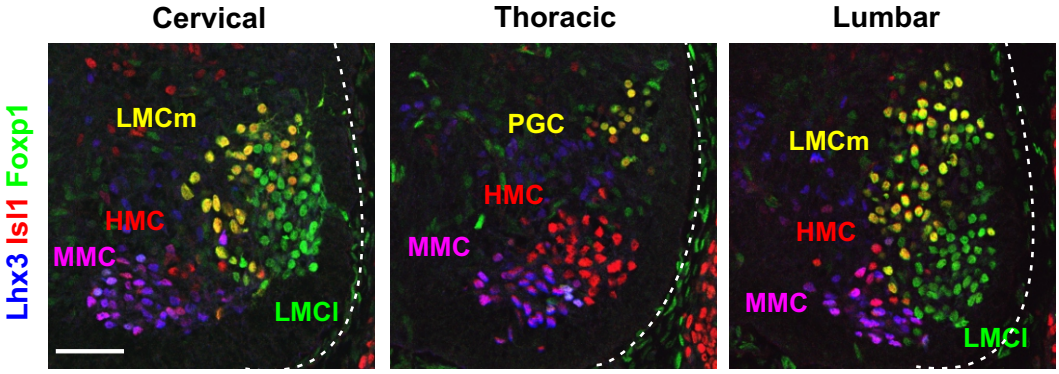

c

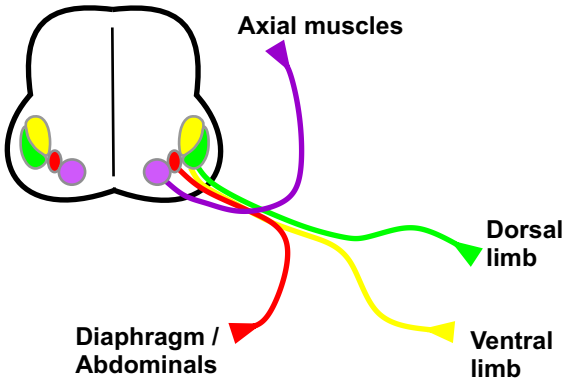

d

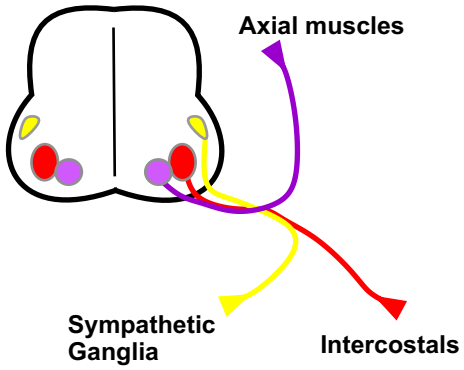

Figure 1-2 MN diversity in the developing mouse spinal cord.

(a) MNs are organized into columns that extend along the rostrocaudal axis of the spinal cord. These columns are restricted to certain levels of the spinal cord by the actions of different Hox proteins. The motor columns can be distinguished by their expression of different transcription factors and their muscle targets.

(b) Transverse sections of E12.5 mouse spinal cord, showing the MN cell bodies in the ventral horn of the spinal cord. The different MN populations can be distinguished by their differential expression patterns and their cell body position. Scale bar = 50 μm.

(c) MN axon trajectories at limb levels (cervical and lumbar regions). Purple = MMC MNs. Red = HMC MNs. Yellow = LMCm MNs. Green = LMCl MNs.

(d) MN axon trajectories at thoracic spinal cord levels. Purple = MMC MNs. Red = HMC MNs. Yellow = PGC MNs.

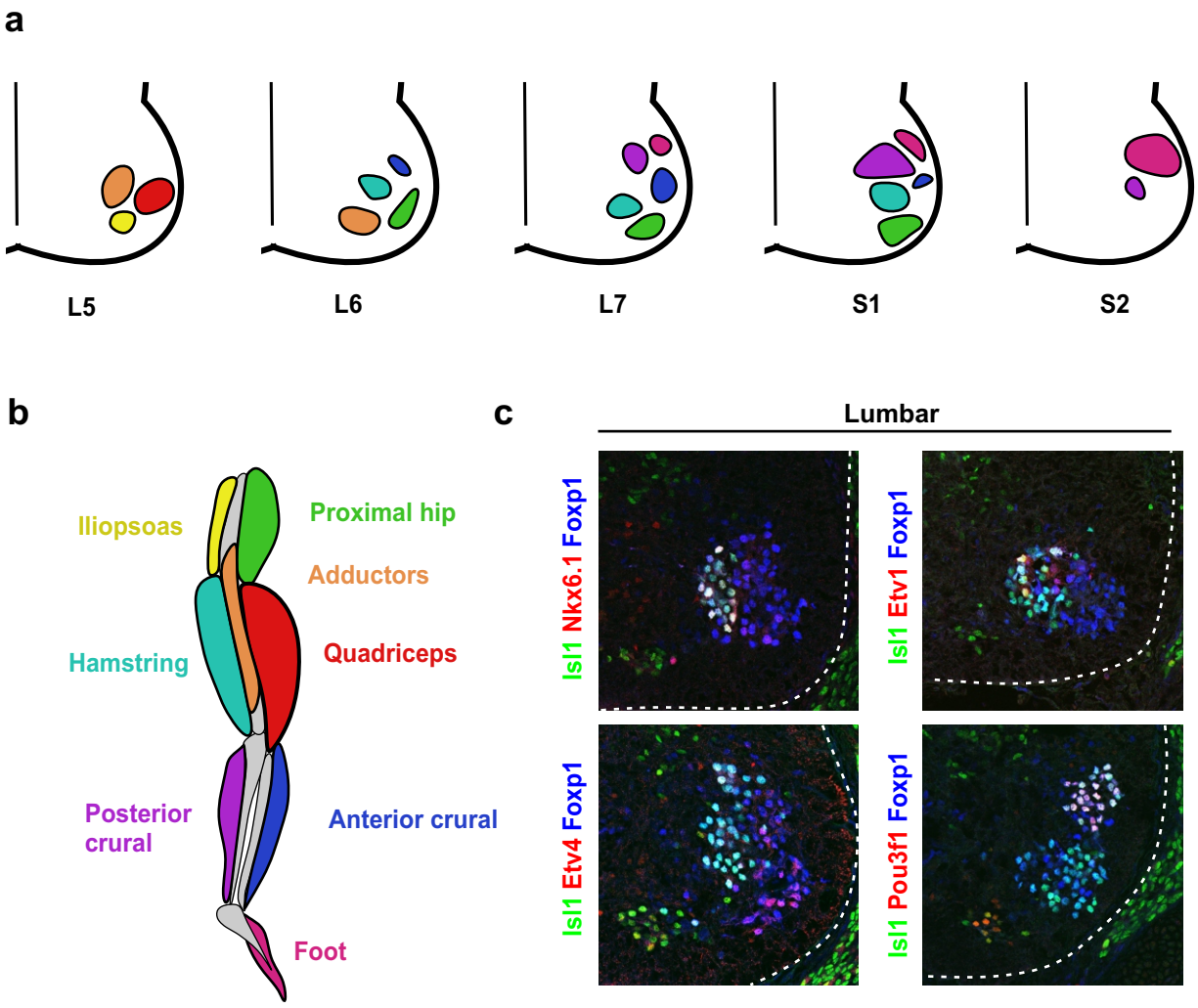

Figure 1-3. Organization of hindlimb LMC motor pools in mice.

(**a**) LMC MNs are segregated into small motor pools that are located at specific rostrocaudal positions in the lumbar spinal cord. The position of the motor pool in the ventral spinal cord is related to it's target muscle.

(**b**) The muscles of the hindlimb that are innervated by each motor pool in the spinal cord, as shown in (a). The most distal muscles (ie. foot) are innervated by MNs at caudal S1-2 spinal levels.

(**c**) Motor pools can be identified in the spinal cord ventral horn of mouse embryos by their unique expression of certain transcription factors (Nkx6.1, Etv1, Etv4, Pou3f1).

BIBLIOGRAPHY

1. Evans, M.J. & Kaufman, M.H. Establishment in culture of pluripotential cells from mouse embryos. *Nature* **292**, 154-156 (1981).

2. Thomson, J.A.*, et al.* Embryonic stem cell lines derived from human blastocysts. *Science* **282**, 1145-1147 (1998).

3. Chambers, S.M., Mica, Y., Studer, L. & Tomishima, M.J. Converting human pluripotent stem cells to neural tissue and neurons to model neurodegeneration. *Methods Mol. Biol.* **793**, 87-97 (2011).

4. Xu, C., Police, S., Rao, N. & Carpenter, M.K. Characterization and enrichment of cardiomyocytes derived from human embryonic stem cells. *Circ. Res.* **91**, 501-508 (2002).

5. Huang, S.X.*, et al.* Efficient generation of lung and airway epithelial cells from human pluripotent stem cells. *Nat. Biotechnol.* **32**, 84-91 (2014).

6. McCracken, K.W., Howell, J.C., Wells, J.M. & Spence, J.R. Generating human intestinal tissue from pluripotent stem cells in vitro. *Nat Protoc* **6**, 1920-1928 (2011).

7. Hayashi, K. & Saitou, M. Generation of eggs from mouse embryonic stem cells and induced pluripotent stem cells. *Nat Protoc* **8**, 1513-1524 (2013).

8. Lo, B. & Parham, L. Ethical issues in stem cell research. *Endocr. Rev.* **30**, 204-213 (2009).

9. Lott, J.P. & Savulescu, J. Towards a global human embryonic stem cell bank. *The American journal of bioethics : AJOB* **7**, 37-44 (2007).

10. Takahashi, K. & Yamanaka, S. Induction of pluripotent stem cells from mouse embryonic and adult fibroblast cultures by defined factors. *Cell* **126**, 663-676 (2006).

11. Takahashi, K.*, et al.* Induction of pluripotent stem cells from adult human fibroblasts by defined factors. *Cell* **131**, 861-872 (2007).

12. Zhou, T.*, et al.* Generation of human induced pluripotent stem cells from urine samples. *Nat Protoc* **7**, 2080-2089 (2012).

13. Haase, A.*, et al.* Generation of induced pluripotent stem cells from human cord blood. *Cell Stem Cell* **5**, 434-441 (2009).

14. Bilic, J. & Izpisua Belmonte, J.C. Concise review: Induced pluripotent stem cells versus embryonic stem cells: close enough or yet too far apart? *Stem Cells* **30**, 33-41 (2012).

15. Davis-Dusenbery, B.N., Williams, L.A., Klim, J.R. & Eggan, K. How to make spinal motor neurons. *Development* **141**, 491-501 (2014).

16. Kanning, K.C., Kaplan, A. & Henderson, C.E. Motor neuron diversity in development and disease. *Annu. Rev. Neurosci.* **33**, 409-440 (2010).

17. Briscoe, J. & Novitch, B.G. Regulatory pathways linking progenitor patterning, cell fates and neurogenesis in the ventral neural tube. *Philos. Trans. R. Soc. Lond. B. Biol. Sci.* **363**, 57-70 (2008).

18. Novitch, B.G., Chen, A.I. & Jessell, T.M. Coordinate regulation of motor neuron subtype identity and pan-neuronal properties by the bHLH repressor Olig2. *Neuron* **31**, 773-789 (2001).

19. Arber, S.*, et al.* Requirement for the homeobox gene Hb9 in the consolidation of motor neuron identity. *Neuron* **23**, 659-674 (1999).

20. Dasen, J.S. & Jessell, T.M. Hox networks and the origins of motor neuron diversity. *Curr. Top. Dev. Biol.* **88**, 169-200 (2009).

21. Sharma, K.*, et al.* LIM homeodomain factors Lhx3 and Lhx4 assign subtype identities for motor neurons. *Cell* **95**, 817-828 (1998).

22. Rousso, D.L., Gaber, Z.B., Wellik, D., Morrisey, E.E. & Novitch, B.G. Coordinated actions of the forkhead protein Foxp1 and Hox proteins in the columnar organization of spinal motor neurons. *Neuron* **59**, 226-240 (2008).

23. Dasen, J.S., De Camilli, A., Wang, B., Tucker, P.W. & Jessell, T.M. Hox repertoires for motor neuron diversity and connectivity gated by a single accessory factor, FoxP1. *Cell* **134**, 304-316 (2008).

24. Philippidou, P., Walsh, C.M., Aubin, J., Jeannotte, L. & Dasen, J.S. Sustained Hox5 gene activity is required for respiratory motor neuron development. *Nat. Neurosci.* **15**, 1636-1644 (2012).

25. Lin, J.H.*, et al.* Functionally related motor neuron pool and muscle sensory afferent subtypes defined by coordinate ETS gene expression. *Cell* **95**, 393-407 (1998).

26. Surmeli, G., Akay, T., Ippolito, G.C., Tucker, P.W. & Jessell, T.M. Patterns of spinal sensory-motor connectivity prescribed by a dorsoventral positional template. *Cell* **147**, 653-665 (2011).

27. Pfaff, S.L., Mendelsohn, M., Stewart, C.L., Edlund, T. & Jessell, T.M. Requirement for LIM homeobox gene Isl1 in motor neuron generation reveals a motor neuron-dependent step in interneuron differentiation. *Cell* **84**, 309-320 (1996).

28. Thaler, J.P.*, et al.* A postmitotic role for Isl-class LIM homeodomain proteins in the assignment of visceral spinal motor neuron identity. *Neuron* **41**, 337-350 (2004).

29. Thaler, J.P., Lee, S.K., Jurata, L.W., Gill, G.N. & Pfaff, S.L. LIM factor Lhx3 contributes to the specification of motor neuron and interneuron identity through cell-type-specific protein-protein interactions. *Cell* **110**, 237-249 (2002).

30. Sharma, K., Leonard, A.E., Lettieri, K. & Pfaff, S.L. Genetic and epigenetic mechanisms contribute to motor neuron pathfinding. *Nature* **406**, 515-519 (2000).

31. Kania, A., Johnson, R.L. & Jessell, T.M. Coordinate roles for LIM homeobox genes in directing the dorsoventral trajectory of motor axons in the vertebrate limb. *Cell* **102**, 161-173 (2000).

32. Mazzoni, E.O.*, et al.* Saltatory remodeling of Hox chromatin in response to rostrocaudal patterning signals. *Nat. Neurosci.* **16**, 1191-1198 (2013).

33. Jung, H.*, et al.* Global control of motor neuron topography mediated by the repressive actions of a single hox gene. *Neuron* **67**, 781-796 (2010).

34. Lacombe, J.*, et al.* Genetic and functional modularity of Hox activities in the specification of limb-innervating motor neurons. *PLoS Genet* **9**, e1003184 (2013).

35. Shu, W.*, et al.* Foxp2 and Foxp1 cooperatively regulate lung and esophagus development. *Development* **134**, 1991-2000 (2007).

36. Zhang, Y.*, et al.* Foxp1 coordinates cardiomyocyte proliferation through both cell-autonomous and nonautonomous mechanisms. *Genes Dev.* **24**, 1746-1757 (2010).

37. Hu, H.*, et al.* Foxp1 is an essential transcriptional regulator of B cell development. *Nature immunology* **7**, 819-826 (2006).

38. Li, S.*, et al.* Foxp1/4 control epithelial cell fate during lung development and regeneration through regulation of anterior gradient 2. *Development* **139**, 2500-2509 (2012).

39. Shirasaki, R., Lewcock, J.W., Lettieri, K. & Pfaff, S.L. FGF as a target-derived chemoattractant for developing motor axons genetically programmed by the LIM code. *Neuron* **50**, 841-853 (2006).

40. Kania, A. & Jessell, T.M. Topographic motor projections in the limb imposed by LIM homeodomain protein regulation of ephrin-A:EphA interactions. *Neuron* **38**, 581-596 (2003).

41. Luria, V., Krawchuk, D., Jessell, T.M., Laufer, E. & Kania, A. Specification of motor axon trajectory by ephrin-B:EphB signaling: symmetrical control of axonal patterning in the developing limb. *Neuron* **60**, 1039-1053 (2008).

42. Wichterle, H., Lieberam, I., Porter, J.A. & Jessell, T.M. Directed differentiation of embryonic stem cells into motor neurons. *Cell* **110**, 385-397 (2002).

43. Hu, B.Y. & Zhang, S.C. Differentiation of spinal motor neurons from pluripotent human stem cells. *Nat Protoc* **4**, 1295-1304 (2009).

44. Chambers, S.M.*, et al.* Highly efficient neural conversion of human ES and iPS cells by dual inhibition of SMAD signaling. *Nat. Biotechnol.* **27**, 275-280 (2009).

45. Amoroso, M.W.*, et al.* Accelerated high-yield generation of limb-innervating motor neurons from human stem cells. *J. Neurosci.* **33**, 574-586 (2013).

46. Soundararajan, P., Miles, G.B., Rubin, L.L., Brownstone, R.M. & Rafuse, V.F. Motoneurons derived from embryonic stem cells express transcription factors and develop phenotypes characteristic of medial motor column neurons. *J. Neurosci.* **26**, 3256-3268 (2006).

47. Maden, M. Retinoids and spinal cord development. *J. Neurobiol.* **66**, 726-738 (2006).

48. Peljto, M., Dasen, J.S., Mazzoni, E.O., Jessell, T.M. & Wichterle, H. Functional diversity of ESC-derived motor neuron subtypes revealed through intraspinal transplantation. *Cell Stem Cell* **7**, 355-366 (2010).

49. Davis, R.L., Weintraub, H. & Lassar, A.B. Expression of a single transfected cDNA converts fibroblasts to myoblasts. *Cell* **51**, 987-1000 (1987).

50. Vierbuchen, T.*, et al.* Direct conversion of fibroblasts to functional neurons by defined factors. *Nature* **463**, 1035-1041 (2010).

51. Pang, Z.P.*, et al.* Induction of human neuronal cells by defined transcription factors. *Nature* **476**, 220-223 (2011).

52. Son, E.Y.*, et al.* Conversion of mouse and human fibroblasts into functional spinal motor neurons. *Cell Stem Cell* **9**, 205-218 (2011).

53. Hester, M.E.*, et al.* Rapid and efficient generation of functional motor neurons from human pluripotent stem cells using gene delivered transcription factor codes. *Mol Ther* **19**, 1905-1912 (2011).

54. Gao, B.X. & Ziskind-Conhaim, L. Development of ionic currents underlying changes in action potential waveforms in rat spinal motoneurons. *J. Neurophysiol.* **80**, 3047-3061 (1998).

55. Miles, G.B.*, et al.* Functional properties of motoneurons derived from mouse embryonic stem cells. *J. Neurosci.* **24**, 7848-7858 (2004).

56. Karumbayaram, S.*, et al.* Directed differentiation of human-induced pluripotent stem cells generates active motor neurons. *Stem Cells* **27**, 806-811 (2009).

57. Takazawa, T.*, et al.* Maturation of spinal motor neurons derived from human embryonic stem cells. *PLoS One* **7**, e40154 (2012).

58. Yohn, D.C., Miles, G.B., Rafuse, V.F. & Brownstone, R.M. Transplanted mouse embryonic stem-cell-derived motoneurons form functional motor units and reduce muscle atrophy. *J. Neurosci.* **28**, 12409-12418 (2008).

59. Su, H.*, et al.* Transplanted motoneurons derived from human induced pluripotent stem cells form functional connections with target muscle. *Stem Cell Res* **11**, 529-539 (2013).

CHAPTER 2 – Characterization and Comparison of Human Embryo and Stem Cell-Derived Motor Neurons

ABSTRACT

Directed differentiation of human pluripotent stem cells into specific cell types has allowed for modeling of human development and disease at unprecedented levels. Despite these advances, it remains unknown whether stem cell-derived populations truly mimic endogenous populations, both in molecular and functional properties. We present the first characterization of human embryonic motor neurons (MNs), and find that they are organized into the same rostrocaudal columns and motor pools that are present in mouse embryos. However, we find that the majority of human embryonic stem cell (hESC)-derived MNs express markers of cervical MMC and HMC populations, and generate very few LMC MNs. Despite these differences, hESC-derived MNs functionally mature along a similar time course as endogenous MNs, suggesting that differentiation protocols mimic development. Overall, these results provide a valuable analysis of human MN development and present significant differences between embryonic and stem cell-derived MNs with important implications for future MN disease studies.

This chapter is modified from:

Adams KL, Moore DM, Umbach JA, Pratap M, Otis TS, and Novitch BG. (2014) Characterization and comparison of human embryo and stem cell-derived motor neurons. *In preparation for publication.*

KLA performed a majority of the experiments and wrote the manuscript. DMM generated and helped characterize the hESC-derived MNs. JAU performed the electrophysiology of the human embryonic MNs. MP performed the electrophysiology of the hESC-derived MNs.

INTRODUCTION

Human pluripotent stem cells are an invaluable tool for modeling human development and disease *in vitro*, as well as for generating unlimited numbers of cells for transplantation therapies. Patient tissue biopsies are not feasible for many neurodegenerative diseases; therefore, directed differentiation of human stem cells provides information about early disease processes that would otherwise remain unknown. One such example is the use of human embryonic stem cells (hESCs) and human induced pluripotent stem cells (hiPSCs) to model spinal motor neuron (MN) development and diseases such as Amyotrophic lateral sclerosis (ALS) and Spinal muscular atrophy (SMA). Differentiation of ALS and SMA patient-derived iPSCs into MNs has allowed for insights into MN dysfunction, cell autonomous and non-autonomous roles, and potential treatments[1-6]. However, many of these studies rely on the assumption that stem cell-derived MNs faithfully recapitulate endogenous populations.

Current knowledge of vertebrate spinal MN development and function is largely based on studies performed using mouse and chick models. In the developing mouse embryo, around embryonic day (E) 9-9.5, neural progenitors in the ventral spinal cord expressing the basic helix loop helix (bHLH) protein Olig2 begin to differentiate into MNs[7-9]. These progenitors exit the cell cycle, turn off Olig2 expression, and turn on expression of Hb9, Isl1/2, and Lhx3 transcription factors[7, 8]. By E12.5, all MNs have differentiated and separated into their different motor columns. These motor columns can be identified by their cell body position in the spinal cord, their transcription factor profile, and their target muscles[10, 11]. Medial motor column (MMC) MNs are present along the length of the spinal cord, express Hb9, Isl1, and Lhx3, and innervate axial muscles. Lateral motor column (LMC) MNs are present at limb levels and are divided into medial (LMCm) and lateral (LMCl) populations that innervate ventral and dorsal limb muscles, respectively. LMCm MNs express Isl1 and Foxp1, while LMCl MNs express Hb9, Lhx1, and Foxp1[11, 12]. Hypaxial motor column (HMC) MNs innervate muscles involved with respiration, including the diaphragm, intercostal, and abdominal muscles[11] (unpublished data). HMC MNs

express Isl1 and Hb9, but lack Lhx3 or Foxp1 expression. Lastly, preganglionic motor column (PGC) MNs are located only at thoracic levels, innervate the sympathetic ganglia, and express Foxp1 and nNOS. This diversity of MN populations *in vivo* is critical for the correct functioning of motor circuitry, and therefore survival.

In recent years, many studies have reported different approaches for generating spinal MNs from hESCs and hiPSCs. The majority of these protocols rely upon the addition of signaling molecules retinoic acid (RA) and Sonic hedgehog (Shh) or Shh agonists, identified from mouse and chick studies as being critical for MN formation[10, 13, 14]. However, very little molecular and functional characterization of endogenous human MNs has been performed, largely because of the difficulty in obtaining human embryonic tissue. Therefore, a majority of studies rely upon the assumptions that human MN development mirrors mouse development and that cell markers identified from mouse studies will label the same populations in human MN cultures. Surprisingly, it remains unknown how similar mouse and human MN populations are, and to what extent hESC-derived MNs recapitulate endogenous populations.

Here we characterize human spinal cord development during the first trimester and find that human MN development is remarkably similar to mouse MN development during this time period. Human embryonic MNs are organized into the same motor columns and motor pools found in mouse spinal cords, with the exception of some differences in motor pool size. We also characterize hESC-derived MNs and find that they represent only a limited subset of the endogenous populations found *in vivo,* with the majority representing cervical MN subtypes. Despite this, we find that hESC-derived MNs follow a similar maturation timeline as human embryonic MNs, suggesting that differentiation protocols mimic natural developmental. Overall, these findings present the first detailed molecular description of human MN development and a direct comparison of human embryonic and hESC-derived MNs.

MATERIALS AND METHODS

Mouse husbandry and tissue collection. All mice were maintained and tissue collected in accordance with guidelines set forth by the UCLA Institutional Animal Care and Use Committee. Timed matings were performed using male and female wild-type mice (strain C57BL6). The morning the plug was observed was designated E0.5. Embryos were collected in ice-cold Phosphate Buffered Saline (PBS) and visceral organs were removed. Embryos were fixed in 4% Paraformaldehyde (Fisher) for 2 – 4 hours, depending on tissue size, and incubated in 30% sucrose (in 0.1M PB) overnight. Embryos were frozen in OCT (Tissue TEK) on dry ice.

Human embryo tissue collection. Human embryonic spinal cord samples were obtained from Novogenix Laboratories following informed consent and elective termination. Developmental age was determined by ultrasound and confirmed by analysis of developmental characteristics of samples. All ages are reported as developmental week (time after fertilization). For cryosection analysis: samples were fixed in 4% Paraformaldehyde for 1 – 4 hours, depending on tissue size. Samples were then incubated in 30% sucrose overnight and frozen in OCT on dry ice. 12µm cryosections were then processed for immunostaining.

hESC Culture. All hESC experiments were conducted with prior approval from the UCLA Embryonic Stem Cell Research Oversight (ESCRO) Committee. H9 hESCs (Madison, Wisconsin) were maintained on irradiated mouse embryonic fibroblasts (MEFs) in hESC media [DMEM/F12, 20% Knockout serum replacement, 1% Nonessential amino acids, 1% Glutamax, 0.1 mM 2-Mercaptoethanol, and 10 ng/ml of basic fibroblast growth factor (bFGF)]. All reagents were from Invitrogen, unless otherwise noted. hESCs were passaged weekly using manual dissection. For all experiments, hESCs were used between passages 35 and 50.

hESC differentiation to MNs. hESCs were differentiated to MNs as previously described[13]. Briefly, hESC colonies were dissociated with dispase (Stem Cell Tech) and plated in low-adhesion 6-well plates in hESC media without bFGF. Embryoid bodies (EBs) formed within 1-2 days. After 4 days, EBs were moved into Neural differentiation media [DMEM/F12, 1x N2 supplement, 1% Nonessential amino acids, 1% Glutamax, and 2 µg/ml Heparin]. After 3 days, EBs were attached to poly-ornithine/laminin coated dishes, in media supplemented overnight with 10% fetal bovine serum (FBS) to facilitate adhesion. Retinoic Acid (RA; 0.1 µM; Sigma) was added to the attached EBs 3 days later, and neural rosette structures appeared within 5-7 days. Neural rosettes were manually isolated and transferred into neural differentiation media with 0.1 µM RA and 1 µM Sonic hedgehog agonist (SAG; Calbiochem). After ~15 days, EBs were re-attached to poly-ornithine/laminin coated dishes in MN maturation media [neural differentiation media with 0.1 µM RA, 50 nM SAG, cyclic AMP (0.1 µM; Sigma), Ascorbic Acid (200 ng/ml; Sigma), Insulin growth factor 1 (IGF1; 10 ng/ml; Peprotech) and neurotrophic factors (GDNF, BDNF, CNTF; all 10 ng/ml; Peprotech)]. For immunostaining, hESC-derived MNs were lightly dissociated using 20% TrypLE (Invitrogen) and plated on poly-ornithine/laminin coated glass coverslips in MN maturation media. hESC-derived MNs were fixed in 4% PFA for 10 mins at room temperature before being processed for immunostaining.

Immunostaining. Antibody staining of cryosections was performed as previously described[11]. Fixed adherent cell cultures were washed in block solution (PB, 1% heat-inactivated horse serum, 0.1% Triton X100) for 10 minutes, followed by incubation with primary antibodies overnight at 4°C. The following primary antibodies were used: rabbit anti-Caspase3 (1:400; Cell Signaling), goat anti-ChAT (1:200; Millipore), rabbit anti-Etv1 (1:32,000), rabbit anti-Etv4 (1:1000), guinea pig anti-Foxp1 (1:16,000), rabbit anti-Hb9 (1:8000); guinea pig anti-Hoxa5 (1:8000), goat anti-Hoxa9 (1:1000; Santa Cruz SC-17155), rabbit anti-Hoxa10 (1:32,000), mouse anti-Hoxb4 (I12; 1:100; Developmental Studies Hybridoma Bank), rabbit anti-Hoxc6

(1:1000; Santa Cruz SC-66925), mouse anti-Hoxc8 (1:2,000; Covance MMS-266R), goat anti-Isl1 (1:8,000, R&D Systems AF1837), mouse anti-Isl1/2 (39.4D5; 1:100; Developmental Studies Hybridoma Bank), mouse anti-Lhx1 (4F2; 1:100; Developmental Studies Hybridoma Bank), mouse anti-Lhx3 (67.4E12; 1:100; Developmental Studies Hybridoma Bank), rabbit anti-mCherry (1:1000; BioVision), mouse anti-MNR2 (81.5C10; 1:100; Developmental Studies Hybridoma Bank), mouse anti-Neun (1:2000; Millipore), rabbit anti-Nkx6.1 (1:2,500); rabbit anti-nNOS (1:10,000; ImmunoStar 24287), rabbit anti-Olig2 (1:8000), rabbit anti-p75 (1:400; Promega), rabbit anti-Pou3f1 (1:2,000); goat anti-Sox2 (1:2,000, Santa Cruz SC-17320), rabbit anti-βIII Tubulin (1:3,000; Covance MRB-435P), and mouse anti-βIII Tubulin (1:3,000; Covance MMS-435P). Monoclonal antibodies obtained from the DSHB were developed under the auspices of the NICHD and maintained by the University of Iowa, Department of Biology, Iowa City, IA 52242. Cells were incubated with Alexa488-, FITC-, Cy3-, Cy5-, and DyLight649-conjugated secondary antibodies (Jackson Immunoresearch) for 1 hour at room temperature the following day, and coverslips were mounted with Prolong Gold (Invitrogen).

Image analysis. Fluorescent images were collected using either a Zeiss LSM5 Exciter, Zeiss LSM700, or Zeiss LSM780 confocal imaging system. Images were processed using Adobe Photoshop and CorelDraw Software. Cell number quantification was performed using the NIH ImageJ software suite with an ITCN add-in for automated cell counting.

Electrophysiology of human embryonic MNs. Week 6-9 human spinal cord samples were dissociated using Papain (0.5 U/ml; Worthington) for about 15-20 mins and plated at low density on matrigel-coated dishes [~2 x 10^4 cells/dish]. Electrophysiology was performed using standard whole-cell, current-clamp techniques, described previously[15]. Patch pipettes were filled with the following: 140mM potassium gluconate, 10mM Na HEPES, 1mM EGTA, 4mM ATP-Mg, 0.3 mM GTP, pH 7.2 (adjusted with KOH). Cells were bathed in 120 mM NaCl, 1.2 mM KH_2PO_4, 1.9 mM

KCl, 26 mM $NaHCO_3$, 2.2 mM $CaCl_2$, 1.4 mM $MgSO_4$, 10 mM D-Glucose, 7.5 mM Na HEPES (pH with NaOH to 7.2). Resting potentials were maintained at about -70 mV. For single action potential (AP) recordings, 0.5 msec current pulses of +2.5 nA were administered. For multiple AP recordings, a depolarizing 100 pA, 250 msec current pulse was administered to cells. For ion current measurements, cells were held under voltage clamp conditions at a holding potential of -60 mV. Responses to 10 msec duration voltages steps of 10 mV increments between -50 to +60 mV were recorded. Data were collected using Axopatch 2B patch clamp amplifiers with 4-pole Bessel filtering at 5 kHz. Signals were digitized, stored and analyzed using pClamp software (Axon Instruments).

Electrophysiology of hESC-derived MNs. hESC-derived MNs were dissociated with Papain (0.5 U/ml; Worthington) and plated on matrigel-coated glass coverslips. Electrophysiological recordings were performed as previously described[5]. Cells were placed in extracellular solution [119 mM NaCl, 26 mM $NaHCO_3$, 11 mM glucose, 2.5 mM KCl, 2.5 mM $CaCl_2$, 1.3 mM $MgCl_2$, and 1 mM NaH_2PO_4 (pH 7.4), when gassed with 5% CO_2 and 95% O_2]. hESC-derived MNs were identified by their characteristic trapezoidal shape, with more than two dendritic processes visualized with an upright microscope (Leica) with a 40x water immersion objective. Cells were constantly perfused with carbogen-bubbled extracellular solution at a rate of 2.8 to 3 ml/min. Recordings were made with borosilicate glass pipettes with resistances between 4 and 5 megohms when filled with internal pipette solution [135 mM $KMSO_4$, 10 mM NaCl, 10 mM Hepes, 3 mM MgATP, 0.3 mM Na_2GTP, 0.1 mM EGTA, and 100 μM Alexa Fluor 594 hydrazide (Molecular Probes), adjusted to pH 7.4]. Whole-cell recordings were made with a MultiClamp 700B amplifier (Molecular Devices) in current-clamp mode. Each cell was subjected to a series of increasing current injections from –10 to +70 pA in steps of 5 or 10 pA. Currents were filtered at 4 kHz and sampled at 20 kHz with Digidata 1440 (Axon Instruments). Spike detection and

analysis was performed with pClamp 10, and further analysis was carried out in Excel or Igor software. Figures were made in Igor.

Quantification. For analysis of human embryonic MN columns: 2 sections of cervical, thoracic, and lumbar regions of week 6 and 9 spinal cords were averaged. Three week 6 spinal cords were obtained (exact ages: weeks 6, 6.2, and 6.6), and MN percentages from these samples were averaged to generate mean ± SEM values. Two week 9 spinal cords were obtained (exact ages: weeks 9.1 and 9.3), and MN percentages from these samples were averaged to generate mean ± SEM values. Not all human spinal cord samples contained intact cervical to lumbar regions; therefore, some regions were quantified from only 1 sample. For analysis of human embryonic LMC motor pools: three week 7 human spinal cord samples were obtained (exact ages: week 7, 7.1, 7.1) and motor pools were quantified from rostral to caudal cervical levels, aligned using HOX protein expression, and averaged to generate mean ± SEM values. For analysis of hESC-derived MNs: 3 images (~300 cells) were quantified per antibody stain for each differentiation experiment.

RESULTS

Characterization of human spinal cord development during the first trimester.

Histological studies have previously reported that human spinal MN populations are born between weeks 3-5.5 of development, based on the presence of neuronal populations in the ventral spinal cord[16, 17]. However, very few molecular analyses of human embryonic spinal cord have been performed. To address this, we characterized donated human embryonic spinal cords from weeks 6 to 9 of development. At week 6, the majority of neurons in the spinal cord had differentiated, identified by large numbers of lateral $NEUN^+$ cells (**Fig. 2-1 a**). Consistent with previous reports, all MNs had been born by week 6 and had segregated into their distinct motor columns in the ventral spinal cord, marked by expression of HB9 and ISL1 (**Fig. 2-1 i**). A

small population of OLIG2$^+$ progenitors remained in the ventricular zone at week 6 (**Fig. 2-1 e**). This population, which likely represents the oligodendrocyte progenitor pool in the pMN domain, expanded at week 7 of development to include migrating OLIG2$^+$ cells outside of the ventricular zone (**Fig. 2-1 f**). By weeks 8 and 9, there were large numbers of OLIG2$^+$ cells present in the lateral ventral horns (**Fig. 2-1 g,h**). During this time period, we also observed a decrease in the number of SOX2$^+$ progenitors in the ventricular zone – especially in the dorsal spinal cord (**Fig. 2-1 c-d**). Together these results suggest that the spinal cord transitions from neurogenesis to gliogenesis during weeks 6 to 9 of human development.

We then examined spinal MN maturation during this developmental period. MN populations maintained expression of HB9 and ISL1 up to week 9 (**Fig. 2-1 i-l**). The acetylcholine-synthesis enzyme CHAT was expressed at low levels in week 6 and 7 human embryonic MNs (**Fig. 2-1 m,n**), but increased dramatically around week 8 (**Fig. 2-1 o**). This suggests that human embryonic MNs become physiologically functional around this point in development. Lastly, we observed that p75^{NTR} levels greatly increased in week 7 MN populations (**Fig. 2-1 r-t**). p75^{NTR} has been found to be involved in neurotrophin-mediated MN survival and axon guidance, as well as mechanisms for programmed cell death[18]. Therefore, human embryonic MNs are likely undergoing these processes around week 7 of development and later. Interestingly, we also observed p75^{NTR+} sensory axons entering the dorsal spinal cord around week 7. These axons appeared to reach the MNs at week 9 (**Fig. 2-1 t**), indicating that proprioceptive sensory-motor circuits form during this developmental period.

Spinal cord developmental processes are conserved between mice and humans

To understand how the progression of human spinal cord development during the first trimester aligns with mouse embryonic development, we performed the same characterization for mouse spinal cords from E12.5 to E15.5 (**Supplementary Fig. 2-S1**). At E12.5 and E13.5, a small pool of Olig2$^+$/Sox2$^+$ progenitors remained in the pMN domain of cervical mouse spinal

cords (**Supplementary Fig 2-S1 e-f**). Migrating Olig2^{+} progenitors were first identified at E13.5 and were observed in the mantle zone of the ventral spinal cord at E14.5 and E15.5 (**Supplementary Fig. 2-S1 g-h**). This progression is very similar to what we observed with OLIG2 expression in human spinal cords from week 6 to 9. At E12.5, all mouse MNs had differentiated and segregated into columns (**Supplementary Fig. 2-S1 i**). At E14.5, ChAT expression increased in MNs (**Supplementary Fig. 2-S1 o**), reminiscent of the increase seen in week 8 human spinal cord samples. In addition, p75^{NTR} expression was up-regulated in E14.5 MNs, and p75^{NTR+} sensory axons were present in the dorsal spinal cord around E13.5-E14.5 (**Supplementary Fig. 2-S1 r,s**). Overall, the developmental processes occurring in the mouse spinal cord from E12.5 to E15.5 appear to match those of week 6 to 9 human embryos. Interestingly, this suggests that one day of mouse development is roughly equivalent to one week of human development.

During this analysis of human and mouse spinal cord development, we noticed that Hb9 expression differed slightly between the two species. Hb9 was strongly expressed by postmitotic MNs in the mouse spinal cord and was not expressed by Sox2^{+} progenitor populations (**Supplementary Fig. 2-S2 a-c**). However, in the human spinal cord we saw high HB9 expression in the MNs *and* low HB9 expression in the ventral ventricular zone (**Supplementary Fig. 2-S2 d-f**). Therefore, it is possible that HB9 has multiple roles in different cell populations during human spinal cord development.

Characterization of human embryonic MN subtype organization

To further characterize human MN development, we examined week 6 and 9 spinal cords for the presence of different MN subtype markers along the length of the spinal cord. We identified cervical, thoracic, and lumbar regions of the spinal cord based on the HOX protein expression profile. At cervical regions, identified by HOXA5^{+} cells, we found that week 6 human embryonic MNs were organized into two MMC populations, identified by their expression of

LHX3 (**Fig. 2-2 a-d**). The smaller and more lateral MMC population expressed lower levels of LHX3, and is likely the population that innervates the rhomboideous (Rb) muscle (**Fig. 2-2 b,d**). In addition, there was a large lateral FOXP1$^+$ MN population that was divided into ISL1$^+$ and LHX1$^+$ populations, which represent the LMCm and LMCl MN populations, respectively (**Fig. 2-2 b-d**). When we examined cervical MN populations at week 9, we found that LMCl MNs had down-regulated LHX1 expression (**Fig. 2-2 g**). At thoracic levels of week 6 spinal cords, identified by HOXA9$^+$ cells, MNs were organized into MMC (LHX3$^+$), HMC (ISL1$^+$ only), and PGC (FOXP1$^+$) populations (**Fig. 2-2 i-l**). At week 6, PGC MNs also expressed low levels of nNOS (**Fig. 2-2 k**), and this expression greatly increased by week 9 (**Fig. 2-2 o**). Lastly, at HOXA10$^+$ lumbar levels of week 6 spinal cords, MNs were organized into a medial LHX3$^+$ MMC population and a lateral FOXP1$^+$ LMC population (**Fig. 2-2 q-t**). The dorsal LMCm MNs expressed ISL1 and the ventral LMCl MNs expressed LHX1 (**Fig. 2-2 r,s**). At week 9, only a portion of the LMCl MNs expressed LHX1, suggesting that LHX1 was undergoing down-regulation (**Fig. 2-2 w**). The fact that LHX1 had completely turned off in cervical MNs, but not lumbar MNs, is in agreement with the observations in mouse embryos that development proceeds from rostral to caudal regions of the spinal cord.

The most striking difference between week 6 and 9 human MN populations was the reduction in MN numbers by week 9. Quantification of the total MN numbers at cervical, thoracic, and lumbar levels revealed that ~50% of total MNs were lost between weeks 6 and 9 of development. (**Fig. 2-2 z**). This suggests that MNs undergo programmed cell death – a process that has been described in mouse and chick development, with the purpose of removing MNs that make incorrect connections with muscle cells[19]. In confirmation, we found Caspase3$^+$ MNs in weeks 6 and 7 thoracic spinal cords (**Supplementary Fig. 2-S3 a,b**). To determine whether programmed cell death affected one MN population more than others, we quantified the percentage of each MN column at cervical, thoracic, and lumbar levels of week 6 and 9 spinal cords (**Fig. 2-2 y**). At cervical and lumbar levels, the percentage of MMC MNs

decreased by ~20% between weeks 6 and 9, while thoracic MMC MN populations remained the same. The percentages of cervical LMCm ($FOXP1^+/ISL^+$) populations remained similar, but cervical LMCl ($FOXP1^+/LHX1^+$) populations decreased drastically by week 9 in parallel with an increase in "other LMC" MNs ($FOXP1^+/ISL1^-/LHX1^-$). This population is most likely LMCl MNs that have down-regulated LHX1 expression. Interestingly, the percentage of "other LMC" MNs increased at lumbar levels between weeks 6 and 9, despite LMCl MN percentages remaining constant (**Fig. 2-2 y**). This indicates that lumbar LMCl MN populations are further subdivided into two groups of MNs, based on their LHX1 expression at week 9. Overall, these results illustrate that human embryonic MNs are organized into the same rostrocaudal columns present in mouse embryos.

LMC motor pool organization is largely conserved between mice and humans, but with small differences in motor pool size.

To further investigate any differences between human and mouse MN populations, we analyzed human embryonic MNs for expression of motor pool markers. Motor pools are small groups of MNs that innervate the same muscle, and therefore the size of a motor pool is directly related to the degree of control needed for certain muscle movements. LMC motor pools have been well characterized in mouse and chick embryos, resulting in identification of transcription factors that are expressed by distinct motor pools and required for the correct innervation of target muscles[20-23]. To determine whether these transcription factors are also expressed by human LMC MNs, we analyzed week 7 spinal cords at cervical and lumbar levels. At cervical levels, LMCm ($ISL1^+/FOXP1^+$) MNs expressed NKX6.1, *Etv4*, and POU3F1 at specific rostrocaudal levels (**Fig. 2-3 a-d**). ETV1 was not expressed by any cervical LMC MNs. A small population of cervical LMCl ($ISL1^-/FOXP1^+$) MNs also expressed *Etv4*. At lumbar levels, LMCm MNs expressed all 4 motor pool markers at different rostrocaudal levels and a small number of

LMCl MNs also expressed *Etv4* (**Fig. 2-3 e-h**). Therefore, human embryonic LMC MNs express the same motor pool markers found in mouse LMC MNs.

We then asked whether there are any differences in the size and/or position of motor pools between mice and humans, which could be related to muscle function and anatomical differences. From our previous analysis of human and mouse spinal cord development, we knew that E13.5 mouse spinal cord was approximately equivalent to week 7 human. Therefore, we quantified the percentage of each motor pool from rostral ($HOXA5^+$) to caudal ($HOXC8^+$) cervical levels for both E13.5 mouse embryos and week 7 human embryos (**Fig. 2-3 i-k**). Overall, the cervical LMC motor pool organization was very similar between mouse and human spinal cords, but with two differences in motor pool size. First, the $Etv4^+$/$ISL1^+$ population was reduced from ~30% of mouse LMC MNs at $Hoxc6^+$/$Hoxc8^+$ regions to ~15% of human LMC MNs (**Fig. 2-3 i,j**). This motor pool innervates the cutaneous maximus muscle in mouse embryos, which is responsible for contraction of the skin for defensive behaviors[24, 25]. Interestingly, humans lack this muscle, which is consistent with a decrease in this motor pool population. It is likely that the remaining 15% $Etv4^+$/$ISL1^+$ MNs present in the human spinal cord innervate a different muscle involved in limb and shoulder movement. The second difference was a ~2-fold increase in the size of the $NKX6.1^+$ LMCm pool at caudal $HOXC8^+$ levels in human spinal cord, compared to mouse. This motor pool has not been previously described in mouse embryos and therefore does not have a known muscle target. However, because of its position at caudal cervical levels, it likely innervates a distal limb muscle. The $Pou3f1^+$ LMC motor pool is at a similar axial position in the spinal cord and innervates the flexor carpi ulnaris muscle (found in the lower forearm); therefore, it's likely that the Nkx6.1 population innervates a similar, if not the same, muscle.

Human embryonic MNs functionally mature from week 7 to 9 of development

To analyze the electrophysiological properties of human embryonic MNs during the first trimester, we performed single cell patch clamp recordings of dissociated human spinal cord samples. At week 7 of development, ~70% of human embryonic MNs fired a single action potential (AP) in response to a +2.5 nA, 0.5 msec current injection (**Fig. 2-4 b**). These APs generally had smaller amplitudes and slower kinetics, indicating immature electrical properties (**Fig. 2-4 a**). In addition, 0% of week 7 MNs fired multiple APs in response to a longer (250 msec, 100 pA) current injection. At week 8 of development, ~50% of human embryonic MNs fired single APs and ~30% fired multiple APs (**Fig. 2-4 b**). Finally, by week 9, ~60% of human embryonic MNs fired multiple APs, while only ~5% showed no response (**Fig. 2-4 b**). Furthermore, single APs had increased amplitudes at week 9 of development (**Fig. 2-4 a**).

Lastly, we analyzed the ion currents of human embryonic MNs using whole cell patch clamp recordings in the voltage clamp mode. We found that prominent inward and outward currents began to appear around week 8, coinciding with the appearance of multiple APs (**Fig. 2-4 a**). The onset and kinetics of the ion currents changed with developmental age. Together, these results suggest that human embryonic MNs become functionally mature around weeks 8-9 of development.

hESC-derived MNs acquire markers of maturation from weeks 5 to 9 of differentiation

In order to determine how well hESC-derived MNs represent endogenous populations, we generated spinal MNs from H9 hESCs, using a standard embryoid body (EB) differentiation approach with RA and SAG addition (**Fig. 2-5 a**). Differentiating hESC cultures were analyzed 25-28 days after removal of basic fibroblast growth factor (bFGF) for the presence of MN progenitor markers OLIG2 and NKX6.1 (**Fig. 2-5 b**). Cultures that contained high numbers of MN progenitors were then analyzed several weeks after transition into maturation media. We confirmed generation of spinal MNs by expression of MN-specific and general neuronal markers HB9, ISL1, CHAT, and βIII-Tubulin (TUJ1) (**Fig. 2-5 c-e**).

We found that HB9 expression peaked around week 7 of differentiation, with very few $HB9^+$ cells at weeks 5 and 9 (**Supplementary Fig. 2-S4 a-c**). In addition, CHAT levels gradually increased from week 5 to 9, suggesting that hESC-derived MNs became functionally mature during this time period (**Supplementary Fig. 2-S4 d-f**). Finally, we examined hESC-derived MNs for $p75^{NTR}$ expression and found it significantly up-regulated at week 7 of differentiation. However, we also observed $p75^{NTR+}$ cells that did not co-express ISL1/2, indicating that non-MN populations in the cultures expressed $p75^{NTR}$ as well (**Supplementary Fig. 2-S4 g-i**).

The majority of hESC-derived MNs express cervical HOX proteins

To determine the rostrocaudal identity of hESC-derived MNs, we analyzed week 5 MNs for expression of different HOX proteins (**Fig. 2-5 f**). The majority of hESC-derived MNs (identified by $ISL1^+$ cells) expressed HOXA5 (**Fig. 2-5 h**), a marker of cervical human neurons. A smaller number of hESC-derived MNs also expressed HOXC6 (**Fig. 2-5 i**). We did not observe expression of more caudal HOX proteins, such as HOXC8, HOXA9, and HOXA10 (**Fig. 2-5 j-l**). In addition, we did not observe any $HOXB4^+$ cells, which would indicate a hindbrain identity (**Fig. 2-5 g**). Together, these results indicate that differentiation of hESCs into MNs results in largely cervical spinal populations.

hESCs generate a limited diversity of MN populations

From our analysis of human spinal cord, we know that $HOXA5^+$ human embryonic MNs are segregated into MMC, LMCm, and LMCl populations. We next wanted to determine whether hESC-derived MNs are segregated into these same columns *in vitro*. To address this, we analyzed hESC-derived MNs at 5, 7, and 9 weeks of differentiation for expression of MN subtypes markers LHX3, FOXP1, and LHX1. At week 5 of differentiation, the majority of hESC-derived MNs (identified by $ISL1^+$ cells) expressed LHX3, and very few expressed LMC markers FOXP1 and LHX1 (**Fig. 2-6 a-c**). Two weeks later, we saw a dramatic decrease in the number

of LHX3$^+$ MNs from ~65% to ~10% of total MNs (**Fig. 2-6 d,m**). In parallel, the number of FOXP1$^+$/ISL1$^+$ hESC-derived MNs increased from ~7% to ~20% from weeks 5 to 7. These MNs likely represent LMCm-like MNs. Only ~10% of hESC-derived MNs expressed LHX1 and FOXP1, indicative of an LMCl identity. Additionally, the percentage of ISL1$^+$ only cells increased from ~20% to ~60% from week 5 to 7 (**Fig. 2-6 m**), which potentially include a mixture of HMC-like MNs and MMC-like MNs that have down-regulated Lhx3 expression. By week 9, LHX3 expression had turned off in the majority of hESC-derived MNs, while FOXP1$^+$ and LHX1$^+$ populations remained constant (**Fig. 2-6 g-i**). Therefore, it appears that the molecular profile of hESC-derived MNs alters dramatically between weeks 5 and 7 of differentiation. While the majority of hESC-derived MNs initially expressed MMC markers, only ~20-30% of hESC-derived MNs expressed LMC MN markers at any point during differentiation.

We next analyzed hESC-derived MNs for expression of LMC motor pool markers. At 9 weeks of differentiation, we found that a percentage (~20%) of ISL1$^+$/FOXP1$^+$ hESC-derived MNs co-expressed NKX6.1 (**Fig. 2-6 j**), suggesting formation of an LMCm motor pool. We did not see any expression of ETV1 or POU3F1 in FOXP1$^+$ MNs (**Fig. 2-6 k-l**). Due to the identification of only NKX6.1$^+$ LMCm MNs at HOXA5$^+$ regions in human embryonic spinal cords, these results agree with the rostrocaudal identify of the hESC-derived MNs.

Functional maturation of hESC-derived MNs mirrors the endogenous human developmental timeline

Previous studies of stem cell-derived MNs have shown that hESC-derived MNs fire multiple APs in response to depolarizing current injections, indicating functional maturation[15, 26, 27]. Recently, a study reported that hESC-derived MNs transition from an immature physiological profile to a more mature profile within the span of two weeks, by examining cell soma size, dendritic branching, and AP firing[28]. To determine the functional maturity of our hESC-derived MNs, we used whole cell patch clamp recordings to measure MN activity at 6, 8, and 10 weeks

of differentiation. For all ages examined, we found a mixed population of responses ranging from zero APs to multiple continuous APs in response to increasing 10pA current injections (**Fig. 2-7 a**). This suggests that there is high degree of variability within hESC-derived MN cultures at any time of differentiation. We quantified the percentage of cells that displayed each type of response and found that ~60% of week 6 hESC-derived MNs fired only a single AP, while ~20% fired multiple APs (**Fig. 2-7 b**). At 8 weeks of differentiation, ~40% of cells fired a single AP and ~40% fired multiple APs. This trend was also seen at week 10 of differentiation (**Fig. 2-7 b**). Furthermore, these APs were abolished when 1 μM Tetrodotoxin (TTX) was added to the cultures, which selectively blocks voltage-dependent sodium channels (**Fig. 2-7 e**). Therefore, it appears that the majority of hESC-derived MNs become functionally mature around week 8.

To directly compare hESC-derived MNs with endogenous MN populations, we then repeated the analysis of human embryonic MNs at week 8 of development, using the same physiological conditions and experimental parameters used to analyze the hESC-derived MNs. We found that ~40% of human embryonic MNs fired a single AP and ~20% fired repetitive APs at week 8 (**Fig. 2-7 c**). There was no significant difference between the distribution of responses shown by human embryonic and hESC-derived MNs (**Fig. 2-7 c**). In addition, all recorded cells were filled with Alexa^{594} dye and analyzed for the presence of MN markers ISL1/2 and CHAT to confirm MN identity (**Fig. 2-7 d**). Overall, these results suggest that hESC-derived MNs become functionally mature around week 8 of differentiation, and resemble endogenous MN populations in their physiological properties.

DISCUSSION

Current approaches for modeling human diseases *in vitro* with directed differentiation of hESCs and hiPSCs rely upon the assumption that stem cell-derived populations recapitulate most, if not all, qualities of endogenous cells. In this study we illustrate significant differences

between stem cells and their natural counterparts in the context of spinal MNs. We present the first molecular and functional characterization of human embryonic MNs, and find that they are organized into the same columns and motor pools that are present in mouse embryos, with several notable differences in motor pool size. We find that the majority of hESC-derived MNs express markers of cervical MMC and HMC populations, and that very few LMC MN populations are generated. Despite these differences, hESC-derived MNs appear to mature functionally around the same time as endogenous MNs, suggesting that differentiation protocols mimic development.

Our discovery that MN development and organization are largely conserved between humans and mice is not completely surprising, seeing as both species are four-limbed terrestrial mammals. However, we did observe two differences in cervical LMC motor pool size between human and mouse spinal cords, both of which can be attributed to anatomical differences. The reduction of the ISL1^{+}/*Etv4*$^{+}$ motor pool in human spinal cord is consistent with the absence of the cutanenous maximus muscle in humans. A fascinating potential explanation for the expanded NKX6.1^{+}/HOXC8^{+} motor pool in humans is that it is involved in hand movement, and it's size is required for increased hand dexterity. Further characterization of mouse embryos, as well as other primate species, will be needed to make a compelling argument for the developmental mechanisms underlying the evolution of hand motor control. Despite these two differences, the overall similarities between human and mouse embryonic MNs validate the use of mouse models for investigating developmental mechanisms of neuronal differentiation and circuit formation in the spinal cord. However, future studies using an unbiased profiling approach will also be needed to potentially identify unique regulatory genes restricted to human MN populations.

Because of the difficulty in obtaining human embryonic tissue early in gestation, few studies of early human neuronal development have been performed. The majority of human studies over the past several years have focused on the development of the human cortex from

weeks 9.5 to 15 of development, focusing on an expanded progenitor population in the outer subventricular zone of human brains[29]. Interestingly, this population is thought to be one of the mechanisms behind humans' increased brain size compared to other species[29, 30]. More recently, a study of early human development was published that characterized progenitor populations in the spinal cord, hindbrain, and midbrain of human samples from weeks 4-10 of gestation (or weeks 2-8 of development)[17]. The expression profiles of many regulatory genes were found to be very similar between human, mouse, and chick embryos, again suggesting conserved developmental programs. However, spinal MNs were observed to be derived from two distinct progenitor domains (an $OLIG2^{+}/NKX2.2^{-}$ domain and an $OLIG2^{+}/NKX2.2^{+}$ domain) in the developing human neural tube, unlike mouse embryonic MNs[17]. We were not able to replicate these findings in our study due to the fact that our analysis was limited to a time period after MN differentiation. Perhaps this second MN progenitor population is required for the increased number of MNs in developing human embryos compared to mouse embryos (data not shown), reminiscent of the outer subventricular zone progenitors in the developing human cortex.

A variety of differentiation protocols have been created for generating spinal MNs from hESCs and hiPSCs[13-15]. Unfortunately, the majority of these studies did not characterize the types of MNs generated in culture; therefore, it is difficult to compare these studies with our results. Using a standard EB approach with RA and SAG addition, we found several interesting differences between endogenous and stem cell-derived MNs. First, HB9 expression was maintained by MNs in the human spinal cord until at least week 9 of development, but was only expressed by hESC-derived MNs from week 7 to 9 of differentiation. Second, the majority of hESC-derived MNs initially expressed LHX3 at week 5 of differentiation, but this number rapidly decreased with additional time in culture. Endogenous human MMC MNs, however, continued to express LHX3 until at least week 9 of development, although the number of MMC MNs did decrease with time. It is possible that LHX3 expression was not down-regulated by hESC-

derived MNs, but rather that these MNs selectively underwent cell death in a similar mechanism as seen *in vivo*. Another possible explanation is that this initial LHX3$^+$/ISL1$^+$ population of hESC-derived MNs represented newly-born MNs, which have been shown to temporarily express Lhx3 in mouse studies[31]. This explanation agrees with the low HB9 expression and immature electrophysiological properties of week 5 hESC-derived MNs. Lastly, we found that the majority of hESC-derived MNs did not express markers of LMC MNs, most likely because they expressed high levels of HOXA5 and low levels of more caudal HOX proteins. A recent study found that addition of RA, SAG, and Purmorphamine (another Shh agonist) during hESC differentiation resulted in a large number of FOXP1$^+$ MNs[27]. Therefore, it is possible to expand the diversity of hESC-derived MNs by altering the differentiation protocol.

Lastly, this study presents important insight into stem cell-derived MN populations that are used to model human development and MN disease pathogenesis *in vitro*. MN populations are differently affected in MN diseases[32]; therefore, it is likely that extending the diversity of hESC and hiPSC-derived MNs will reveal new disease phenotypes.

Figure 2-1

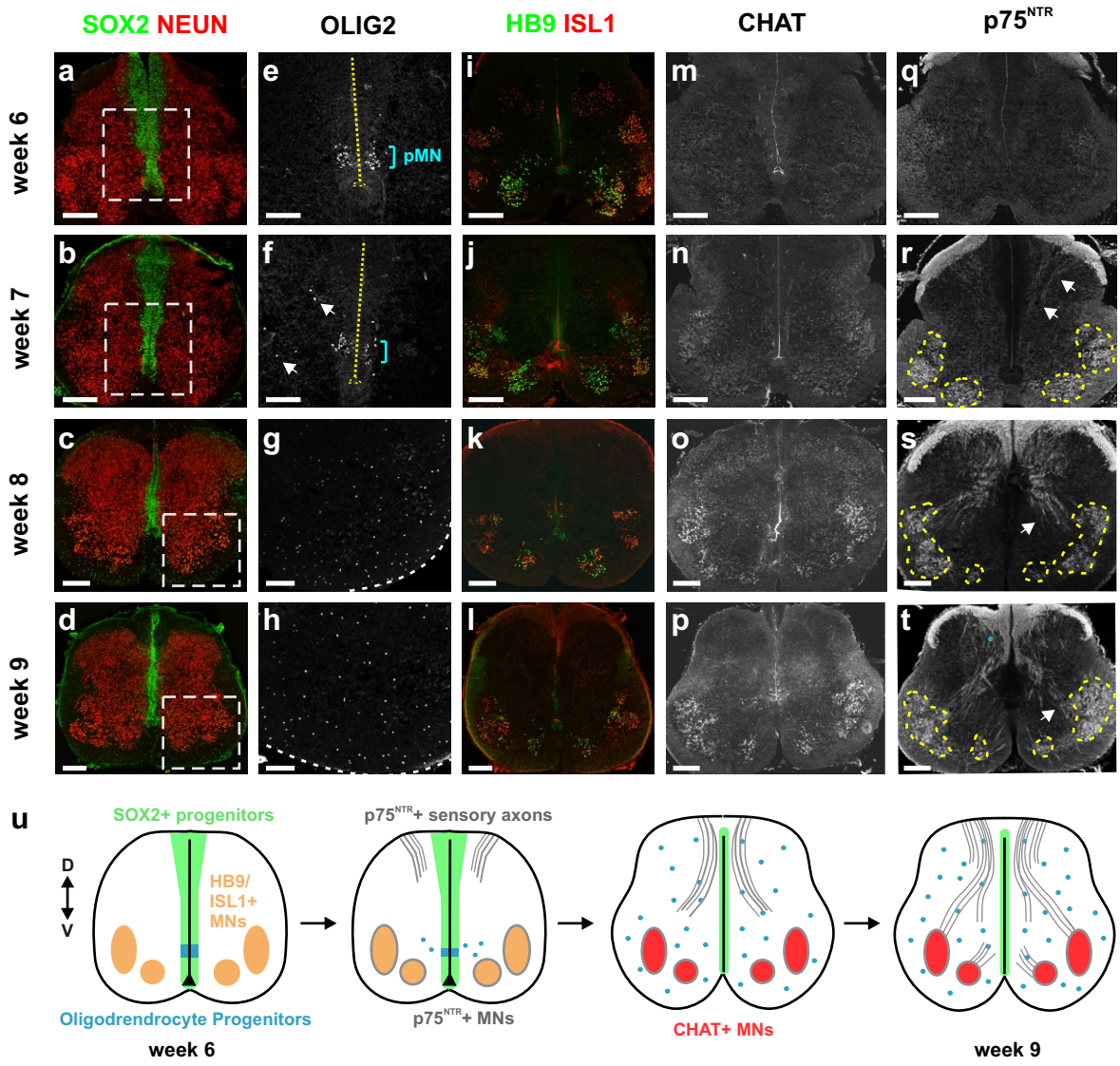
SOX2 NEUN
OLIG2
HB9 ISL1
CHAT
p75NTR
week 6
week 7
week 8
week 9
pMN
u
SOX2+ progenitors
p75NTR+ sensory axons
D
V
HB9/
ISL1+
MNs
Oligodrendrocyte Progenitors
week 6
p75NTR+ MNs
CHAT+ MNs
week 9

Figure 2-1 Postmitotic human embryonic MNs are present by week 6 of development and further mature during the switch from neurogenesis to gliogenesis.

Human embryonic spinal cord samples were analyzed at cervical levels from weeks 6 to 9 of development.

(**a-d**) At week 6, the majority of the ventral spinal cord consisted of postmitotic $NEUN^+$ neurons, while the dorsal spinal cord contained a large $SOX2^+$ progenitor population. Within two weeks, dorsal neuronal populations were born and the number of $SOX2^+$ cells decreased. Scale bars = 200 μm. Boxes depict areas shown in e-h.

(**e-h**) $OLIG2^+$ progenitors in the pMN domain were still present at weeks 6 and 7, but absent at later stages. Migrating $OLIG2^+$ cells were first present at week 7 and migrated out to the mantle zone by weeks 8 and 9. Scales bar = 100 μm.

(**i-l**) $HB9^+$/$ISL1^+$ spinal MNs had segregated into motor columns by week 6. HB9 and ISL1 expression was maintained in MNs to week 9, although the total number of MNs decreased with time. Scale bars = 200 μm.

(**m-p**) CHAT expression levels increased in MNs around week 8. Scale bars = 200 μm.

(**q-t**) $p75^{NTR}$ levels increased in MNs at week 7 (outlined in yellow). At week 7, $p75^{NTR+}$ sensory axons could be identified entering the dorsal spinal cord (arrows in r). These axons reached the MNs by week 9 (arrows in t). Scale bars = 200 μm.

(**u**) Schematic summary of human embryonic spinal cord development from weeks 6 to 9.

Figure 2-2

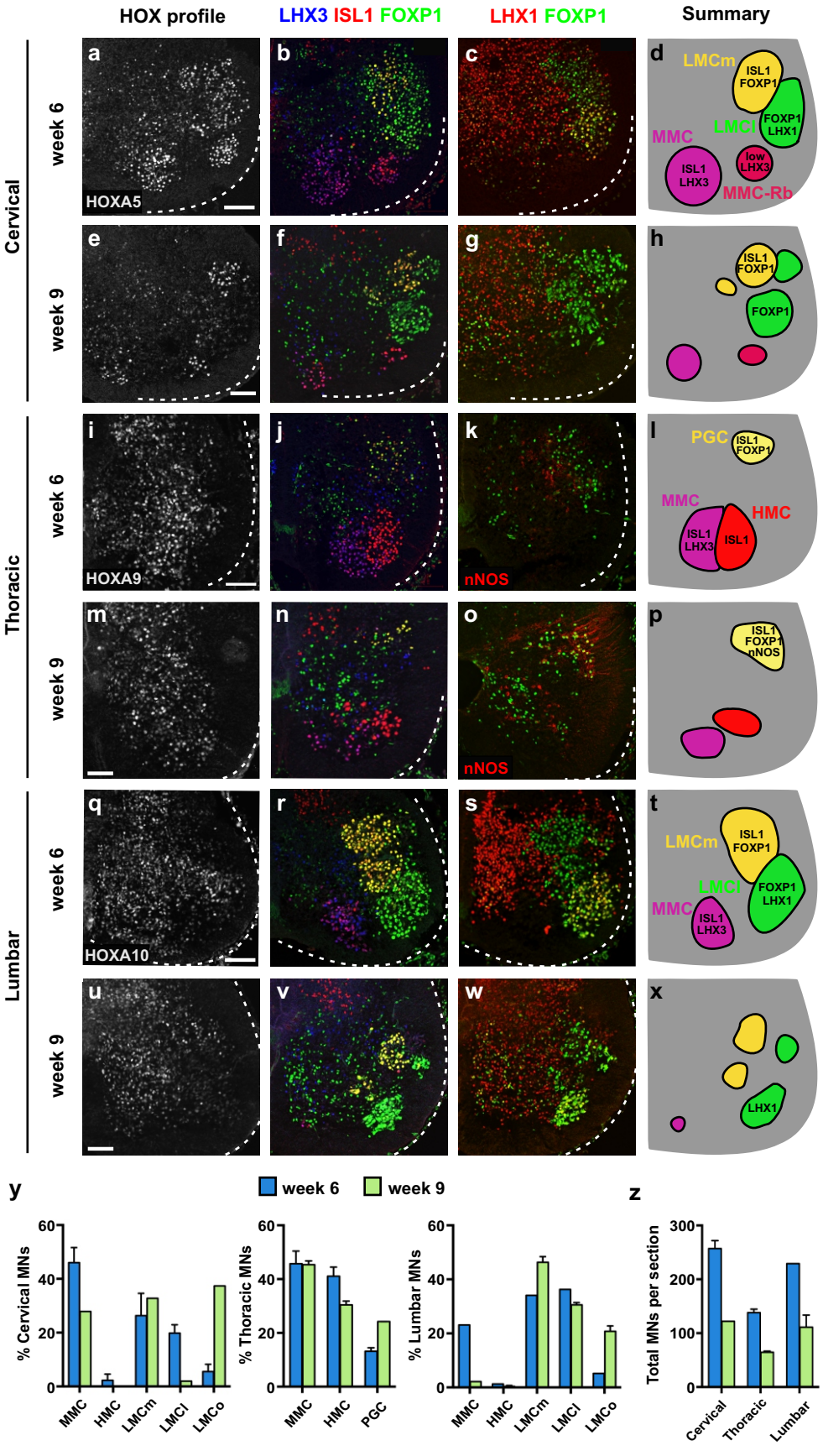
HOX profile
LHX3 ISL1 FOXP1
LHX1 FOXP1
Summary
Cervical
Thoracic
Lumbar
week 6
week 9
HOXA5
HOXA9
HOXA10
nNOS
LMCm
LMCl
MMC
HMC
PGC
MMC-Rb
ISL1 FOXP1
FOXP1 LHX1
ISL1 LHX3
low LHX3
ISL1
FOXP1
nNOS
LHX1
week 6
week 9
% Cervical MNs
% Thoracic MNs
% Lumbar MNs
Total MNs per section
MMC
HMC
LMCm
LMCl
LMCo
PGC
Cervical
Thoracic
Lumbar

Figure 2-2 Human embryonic MNs are organized into 5 distinct columns in the developing spinal cord.

Human embryonic MN populations were analyzed at cervical, thoracic, and lumbar levels of the spinal cord at weeks 6 and 9. Images are transverse sections of the spinal cord ventral horn. Scale bars = 100 μm.

(**a-h**) At cervical levels, identified by $HOXA5^+$ cells, MNs were organized into MMC and LMC columns based on their expression profile and cell soma position. LHX1 expression in LMCl MNs was turned off by week 9 (g).

(**i-p**) At thoracic levels, identified by $HOXA9^+$ cells, MNs were organized into MMC, HMC, and PGC columns. nNOS levels greatly increased in PGC MNs between weeks 6 and 9 (o).

(**q-x**) At lumbar levels, identified by $HOXA10^+$ cells, MNs were organized into MMC and LMC columns. A percentage of LMCl MNs maintained expression of LHX1 at week 9 (w).

(**y**) Quantification of the percentage of each MN column at cervical, thoracic, and lumbar regions of the spinal cord (mean ± SEM; n = 1-3 samples per age and region). MMC MNs defined as $ISL1^+/LHX3^+$. HMC MNs defined as $ISL1^+/LHX3^-/FOXP1^-$. LMCm MNs defined as $ISL1^+/FOXP1^+$. LMCl MNs defined as $FOXP1^+/LHX1^+$. LMCo (other LMC) MNs defined as $FOXP1^+/ISL1^-/LHX1^-$. PGC MNs defined as $ISL1^+/FOXP1^+$.

(**z**) Quantification of the number of total MNs per section (mean ± SEM; n = 1-3 samples per age and region).

Figure 2-3

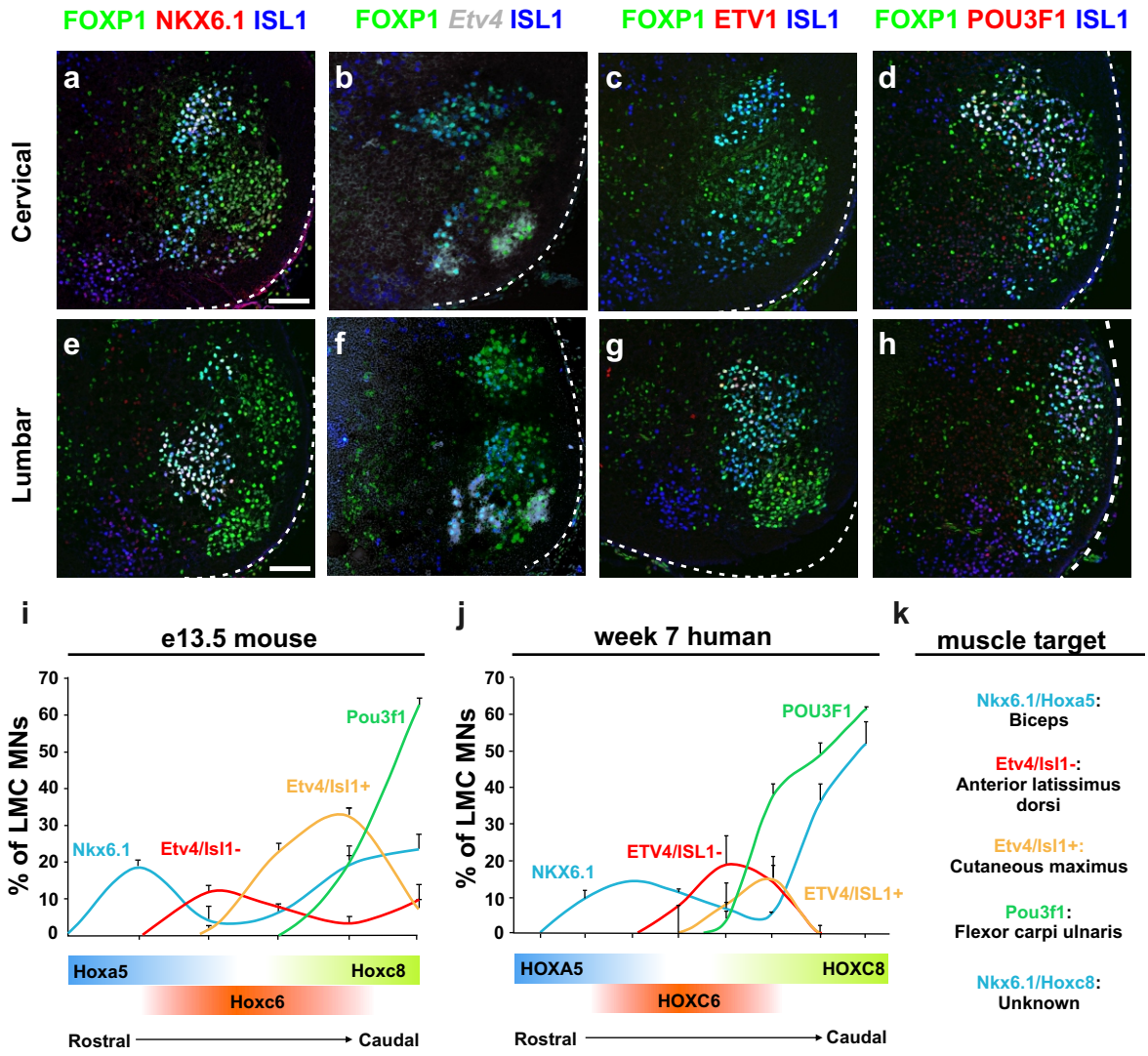
FOXP1 NKX6.1 ISL1
FOXP1 Etv4 ISL1
FOXP1 ETV1 ISL1
FOXP1 POU3F1 ISL1
Cervical
Lumbar
a
b
c
d
e
f
g
h
i
e13.5 mouse
% of LMC MNs
Nkx6.1
Etv4/Isl1-
Etv4/Isl1+
Pou3f1
Hoxa5
Hoxc8
Hoxc6
Rostral
Caudal
j
week 7 human
NKX6.1
ETV4/ISL1-
ETV4/ISL1+
POU3F1
HOXA5
HOXC8
HOXC6
k
muscle target
Nkx6.1/Hoxa5:
Biceps
Etv4/Isl1-:
Anterior latissimus dorsi
Etv4/Isl1+:
Cutaneous maximus
Pou3f1:
Flexor carpi ulnaris
Nkx6.1/Hoxc8:
Unknown

Figure 2-3 Human embryonic LMC MNs are organized into the same motor pools found in mouse embryos and show specific differences in motor pool size.

Cervical and lumbar human LMC MNs were analyzed at week 7 for known motor pool markers. Images are transverse sections of the spinal cord ventral horn. Scale bars = 50 μm.

(**a-d**) Cervical LMC MNs expressed NKX6.1, *Etv4*, and POU3F1, but did not express ETV1.

(e-h) Lumbar LMC MNs expressed NKX6.1, *Etv4*, ETV1, and POU3F1.

(**i**) Quantification of cervical LMC motor pools in E13.5 mouse spinal cords (mean ± SEM; n = 3 embryos).

(**j**) Quantification of cervical LMC motor pools in week 7 human spinal cords (mean ± SEM; n = 3 spinal cords).

(**k**) Known muscle targets of each motor pool in mouse embryos. The Nkx6.1/Hoxc8 pool has not been previously described, but likely innervates distal forelimb muscles.

Figure 2-4

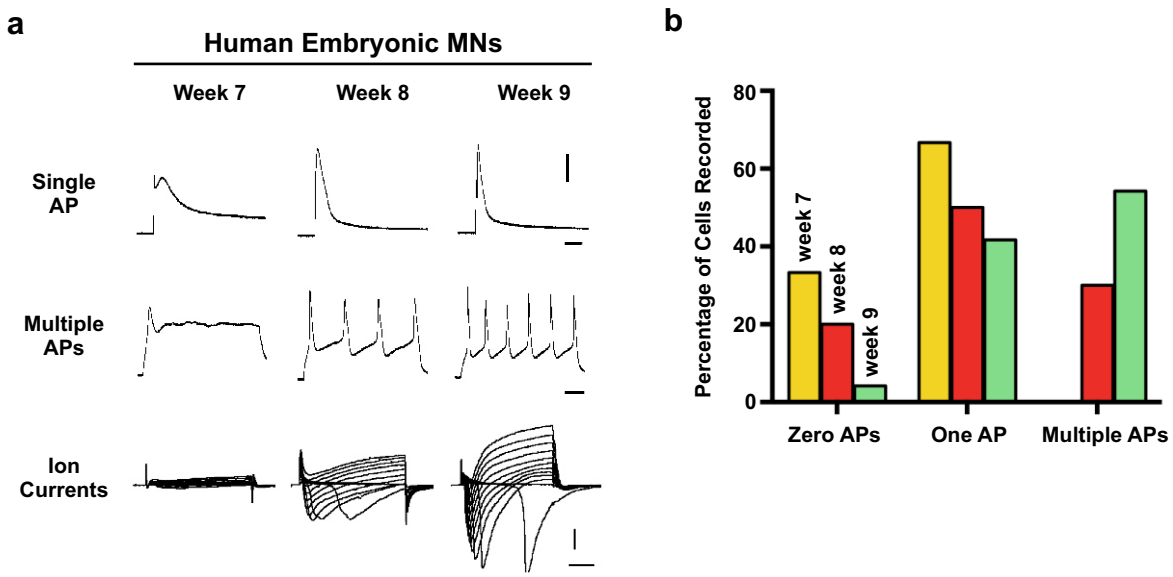

Figure 2-4 Human embryonic MNs mature functionally from weeks 7 to 9 of development. (**a**) Representative recordings of single action potentials (AP), multiple APs, and ion currents exhibited by human embryonic MNs. Single APs were elicited by 0.5 msec current pulses of +2.5 nA. Around week 8 of development, human embryonic MNs fired multiple APs in response to a +100 pA, 250 msec current pulse. For single and multiple AP recordings, cells were held at -70 mV under current clamp conditions. The third row depicts the ion currents in response to 10 msec voltage steps of 10 mV increments between -50 to +60 mV from a holding potential of -60 mV. Once cells were able to fire multiple APs, inward and outward components were clearly distinguishable. Vertical scale bar for APs = 40 mV. Vertical scale bar for ion currents = 1 nA. Horizontal scale bar for single AP = 10 msec. Horizontal scale bar for multiple APs = 20 msec. Horizontal scale bar for ion currents = 5 msec. For each age, AP recordings and ion currents are from the same cell.

(**b**) Quantification of the number of APs fired by human embryonic MNs from week 7 to week 9 of development (n = 6 cells for week 7, 10 cells for week 8, and 24 cells for week 9).

Figure 2-5

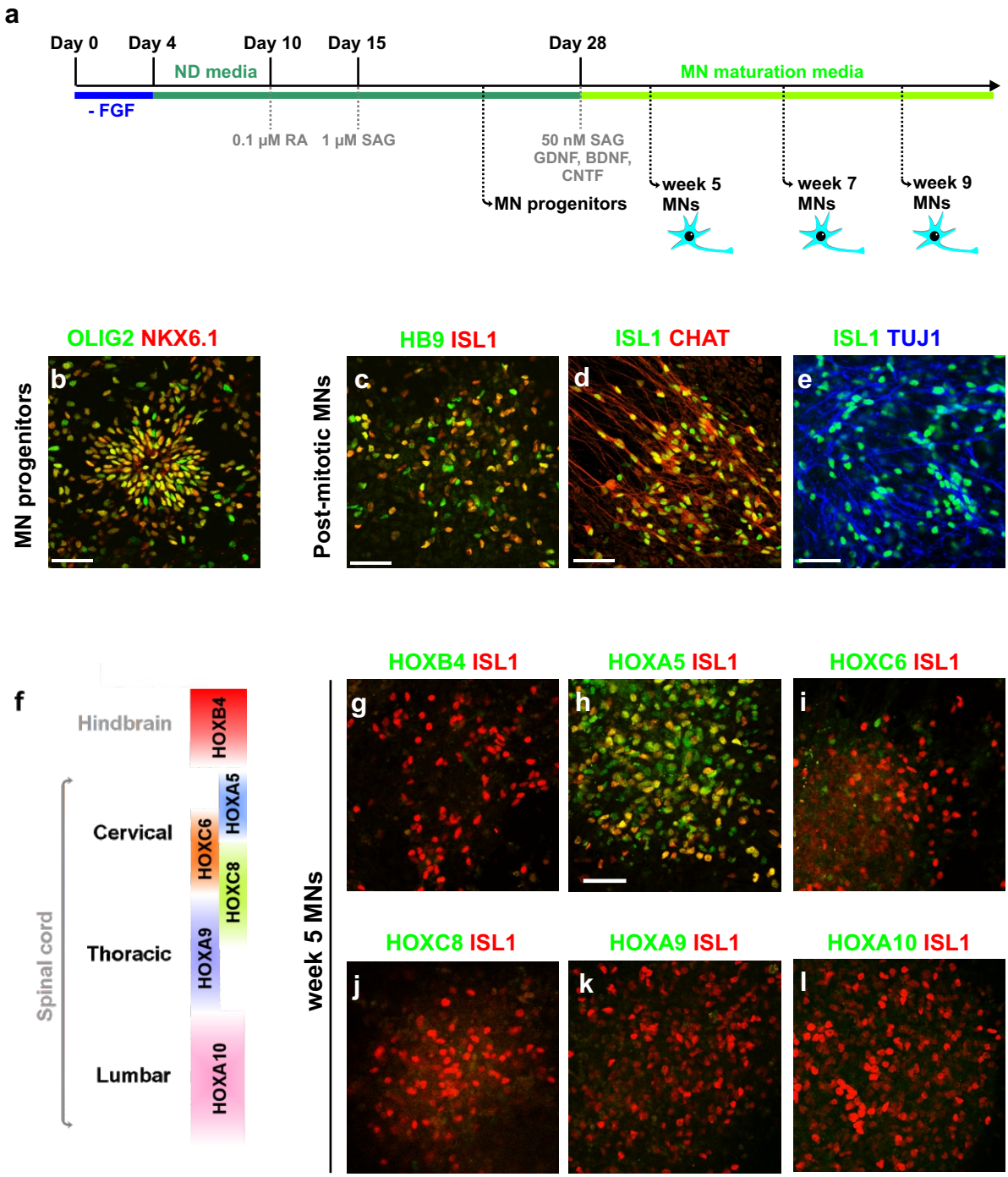
a
Day 0
Day 4
Day 10
Day 15
Day 28
ND media
MN maturation media
- FGF
0.1 μM RA
1 μM SAG
50 nM SAG
GDNF, BDNF,
CNTF
MN progenitors
week 5
MNs
week 7
MNs
week 9
MNs
OLIG2 NKX6.1
HB9 ISL1
ISL1 CHAT
ISL1 TUJ1
MN progenitors
Post-mitotic MNs
b
c
d
e
f
Hindbrain
HOXB4
Cervical
HOXA5
HOXC6
HOXC8
Thoracic
HOXA9
Lumbar
HOXA10
Spinal cord
week 5 MNs
HOXB4 ISL1
HOXA5 ISL1
HOXC6 ISL1
g
h
i
HOXC8 ISL1
HOXA9 ISL1
HOXA10 ISL1
j
k
l

Figure 2-5 hESC-derived MNs express rostral cervical HOX proteins.

(**a**) Differentiation scheme.

(**b**) MN progenitors were identified by co-expression of OLIG2 and NKX6.1 at 3 weeks after the start of differentiation. Scale bar = 50 μm.

(**c-e**) hESC-derived MNs expressed known markers HB9, ISL1, CHAT, and TUJ1. Scale bars = 50 μm.

(**f**) Schematic illustrating HOX protein expression along the rostrocaudal axis (not drawn to scale).

(**g-l**) The majority of hESC-derived MNs expressed HOXA5 (b), and did not express more caudal HOX proteins. Scale bars = 50 μm.

Figure 2-6

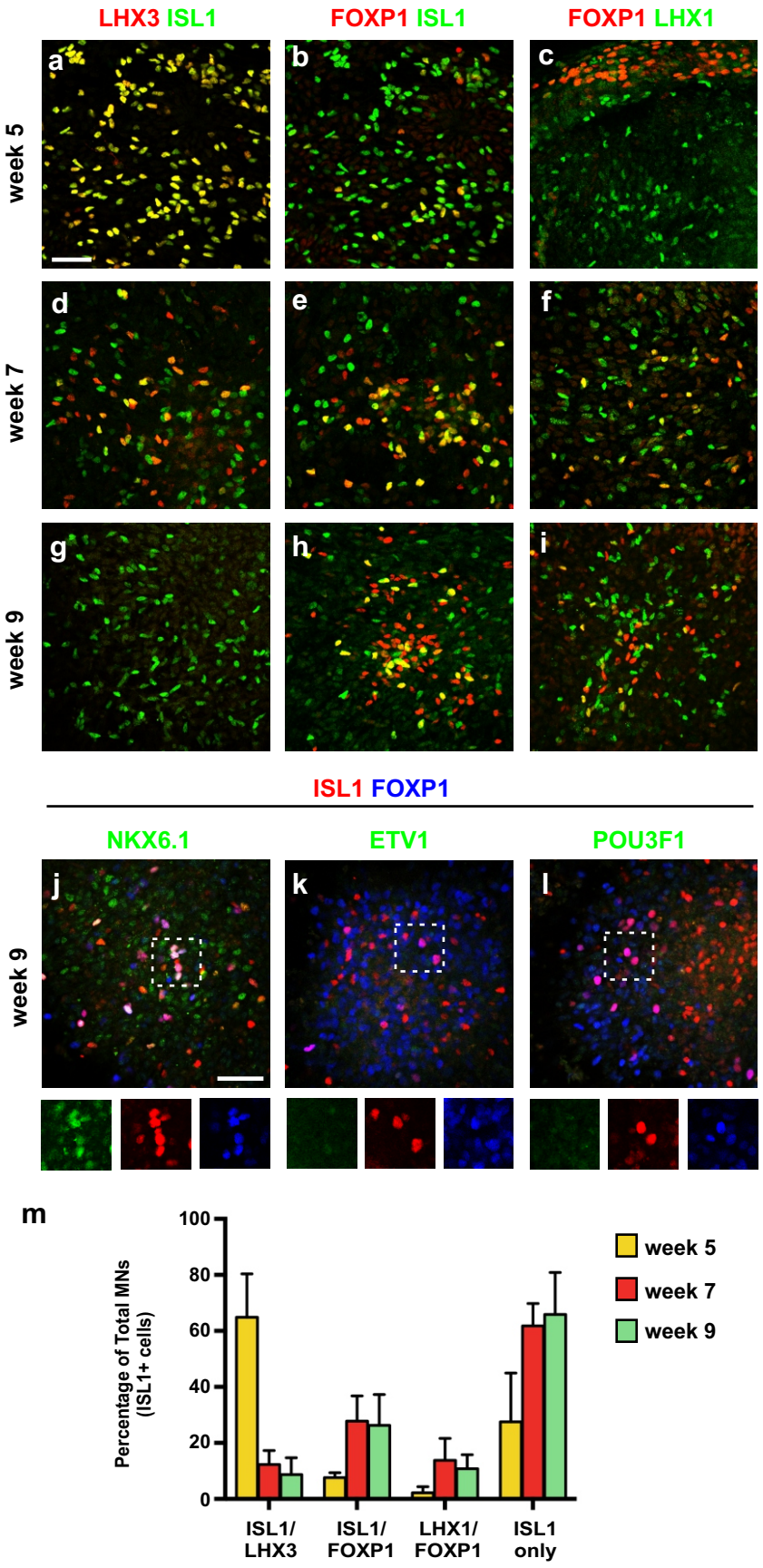
LHX3 ISL1
FOXP1 ISL1
FOXP1 LHX1
week 5
week 7
week 9
a
b
c
d
e
f
g
h
i
ISL1 FOXP1
NKX6.1
ETV1
POU3F1
week 9
j
k
l
m
Percentage of Total MNs (ISL1+ cells)
100
80
60
40
20
0
week 5
week 7
week 9
ISL1/ LHX3
ISL1/ FOXP1
LHX1/ FOXP1
ISL1 only

Figure 2-6 Diversity of hESC-derived MNs alters throughout differentiation.

hESC-derived MNs were analyzed for the expression of MN subtype markers at 3 time points (week 5, week 7, week 9) after the start of differentiation. Scale bar = 50 μm.

(**a-c**) At 5 weeks, the majority of hESC-derived MNs ($ISL1^+$ cells) expressed LHX3, and very few MNs expressed LMC MN markers FOXP1 and LHX1.

(**d-f**) At 7 weeks, LHX3 expression had decreased and FOXP1 and LHX1 expression had increased in hESC-derived MNs.

(**g-i**) At 9 weeks, very few $ISL1^+$ hESC-derived MNs expressed LHX3. A small percentage of hESC-derived MNs maintained expression of FOXP1 and LHX1.

(**j-l**) LMC-like MNs derived from hESCs did not express LMC motor pool markers ETV1 and POU3F1. A small percentage of $ISL1^+/FOXP1^+$ MNs expressed NKX6.1 (j). Boxed areas are depicted as single channel images below.

(**m**) Quantification of MN subtypes generated by hESCs (mean ± SEM; n = 2 independent experiments for weeks 5 and 7, and 3 independent experiments for week 9).

Figure 2-7

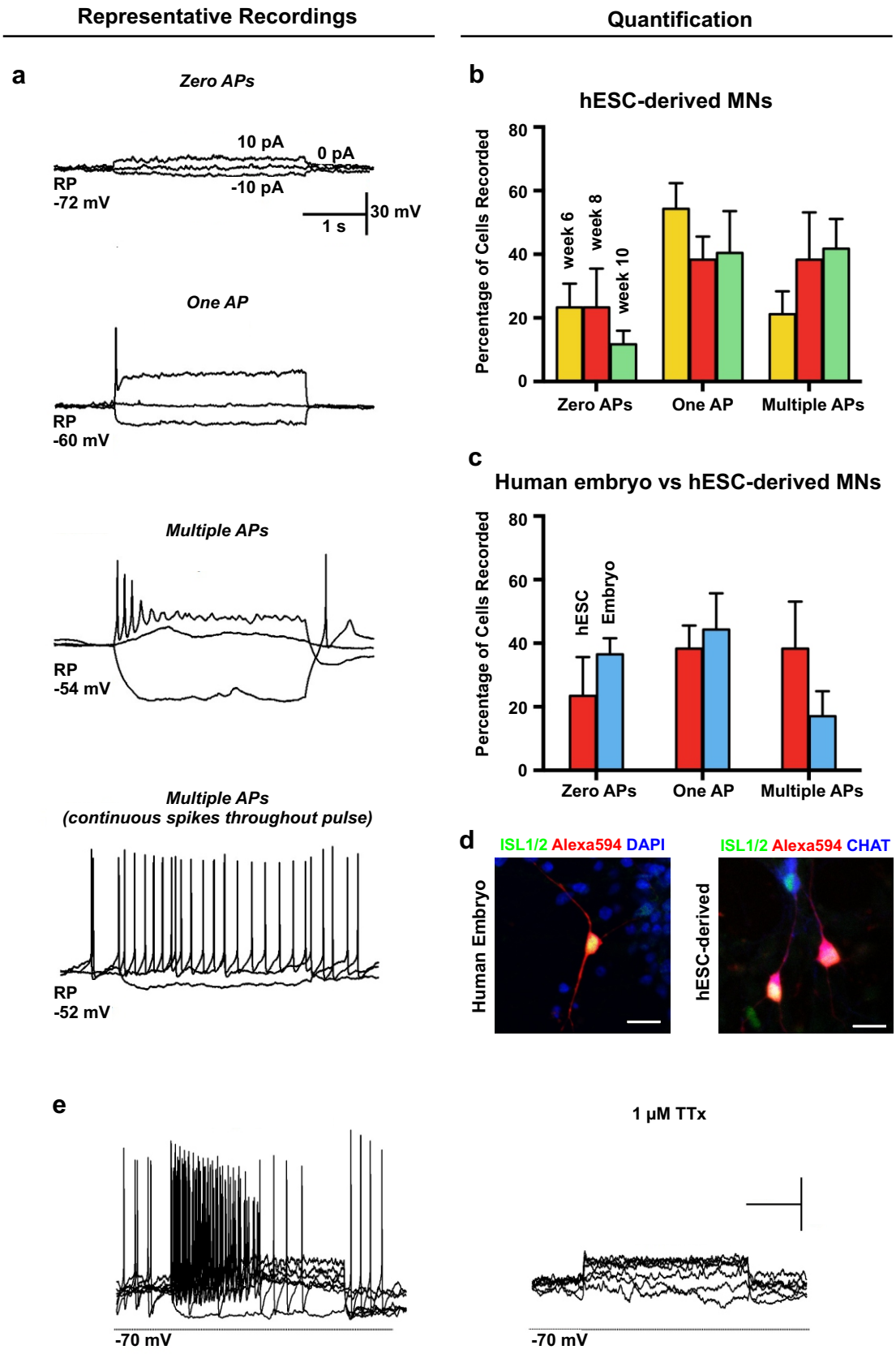
Representative Recordings
Quantification
a
Zero APs
10 pA
0 pA
-10 pA
RP
-72 mV
30 mV
1 s
One AP
RP
-60 mV
Multiple APs
RP
-54 mV
Multiple APs
(continuous spikes throughout pulse)
RP
-52 mV
b
hESC-derived MNs
Percentage of Cells Recorded
week 6
week 8
week 10
Zero APs
One AP
Multiple APs
c
Human embryo vs hESC-derived MNs
Percentage of Cells Recorded
hESC
Embryo
Zero APs
One AP
Multiple APs
d
ISL1/2 Alexa594 DAPI
ISL1/2 Alexa594 CHAT
Human Embryo
hESC-derived
e
-70 mV
1 µM TTx
-70 mV

Figure 2-7 Functional maturation of hESC-derived MNs and comparison to human embryonic MNs.

(**a**) Representative recordings of hESC-derived MNs, showing the different types of responses to current injections of -10 pA, 0 pA, and +10 pA. “AP” = action potential.

(**b**) Quantification of the number of APs fired by hESC-derived MNs from week 6 to 10 of differentiation (n = 5 independent experiments for week 6, 4 for week 8, and 3 for week 10)

(**c**) Quantification of the number of APs fired by hESC-derived MNs and human embryonic MNs around week 8 of differentiation/development (n = 4 independent experiments for hESC-derived MNs and 6 for human embryonic MNs).

(**d**) Recorded human embryonic MNs and hESC-derived MNs were filled with Alexa594 dye and stained for MN markers ISL1/2 and CHAT. Scale bars = 10 μm.

(**e**) Application of 1 μm Tetrototoxin (TTX) to hESC-derived MNs abolished action potential firings. Horizontal scale bar = 1 second. Vertical scale bar = 30 mV.

Supplementary Figure 2-S1

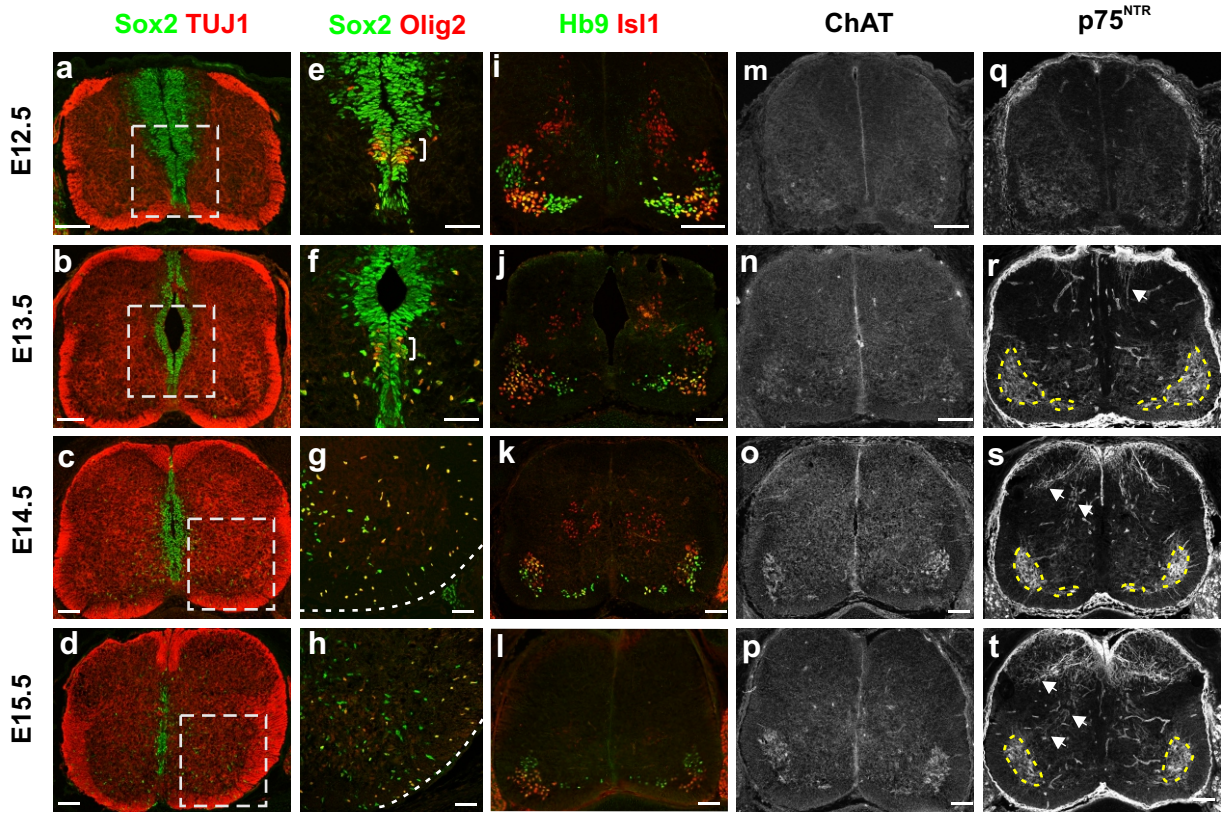

Supplementary Figure 2-S1 Mouse embryonic spinal cord development from E13.5 to E15.5 mirrors human development from weeks 6 to 9.

Images depict transverse sections of cervical regions of mouse embryonic spinal cord.

(**a-d**) Postmitotic neurons (identified by TUJ1) populated the majority of the ventral spinal cord at E12.5. By E13.5, dorsal neuronal populations had been born. By E15.5, very few $Sox2^{+}$ progenitors remained in the ventricular zone. Scale bars = 100 μm. Boxes represent areas shown in e-h.

(**e-h**) $Olig2^{+}$ progenitors were present in the pMN domain of the ventricular zone at E12.5-E13.5. Migrating $Olig2^{+}$ oligodendrocyte progenitors were first identified at E13.5. By E14.5, all $Olig2^{+}$ cells were found in the mantle zone. Scale bars = 50 μm.

(**i-l**) All postmitotic MN populations had been born by E12.5. MNs maintained expression of Hb9 and Isl1 up to E15.5, but the total number of MNs decreased with time.

(**m-p**) ChAT levels increased in MN populations around E14.5. Scale bars = 100μm.

(**q-t**) $p75^{NTR}$ levels increased in MNs around E13.5 (outlined in yellow). $p75^{NTR+}$ sensory axons extended into the dorsal spinal cord around E13.5 and reached MNs around E15.5 (arrows). Scale bars = 100 μm.

Supplementary Figure 2-S2

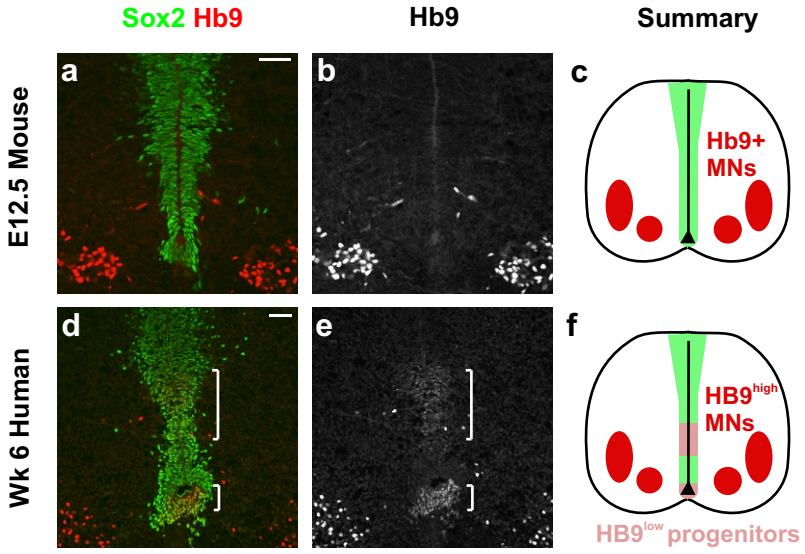

Supplementary Figure 2-S2 Ventral progenitor populations in the human spinal cord express low levels of HB9, unlike mouse progenitors.

Images depict transverse sections of mouse and human cervical spinal cord, focusing on the ventral portion of the ventricular zone.

(**a-c**) Hb9 was only expressed by postmitotic mouse MNs. Scale bar = 50 um.

(**d-f**) HB9 was expressed by both postmitotic human MNs and some $SOX2^{+}$ progenitors in the ventricular zone, at reduced levels (brackets). Scale bar = 50 um.

Supplementary Figure 2-S3

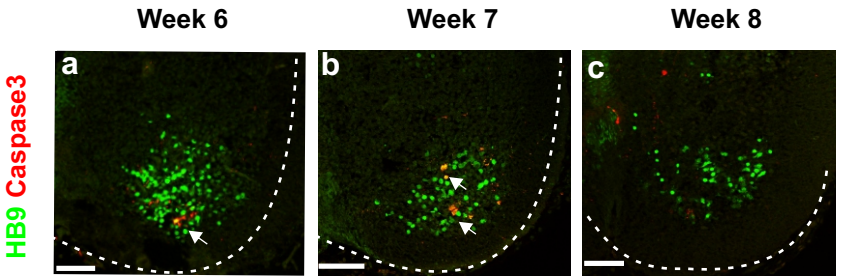

Supplementary Figure 2-S3 Programmed MN cell death can be observed in human embryonic spinal cords at weeks 6 and 7.

Images show transverse sections of human thoracic spinal cord ventral horns. Scale bars = 100 um.

(**a-b**) At weeks 6 and 7, Caspase3^{+} MNs were identified, indicating MN cell death (arrows).

(**c**) At week 8, very few numbers of Caspase3^{+} MNs were identified.

Supplementary Figure 2-S4

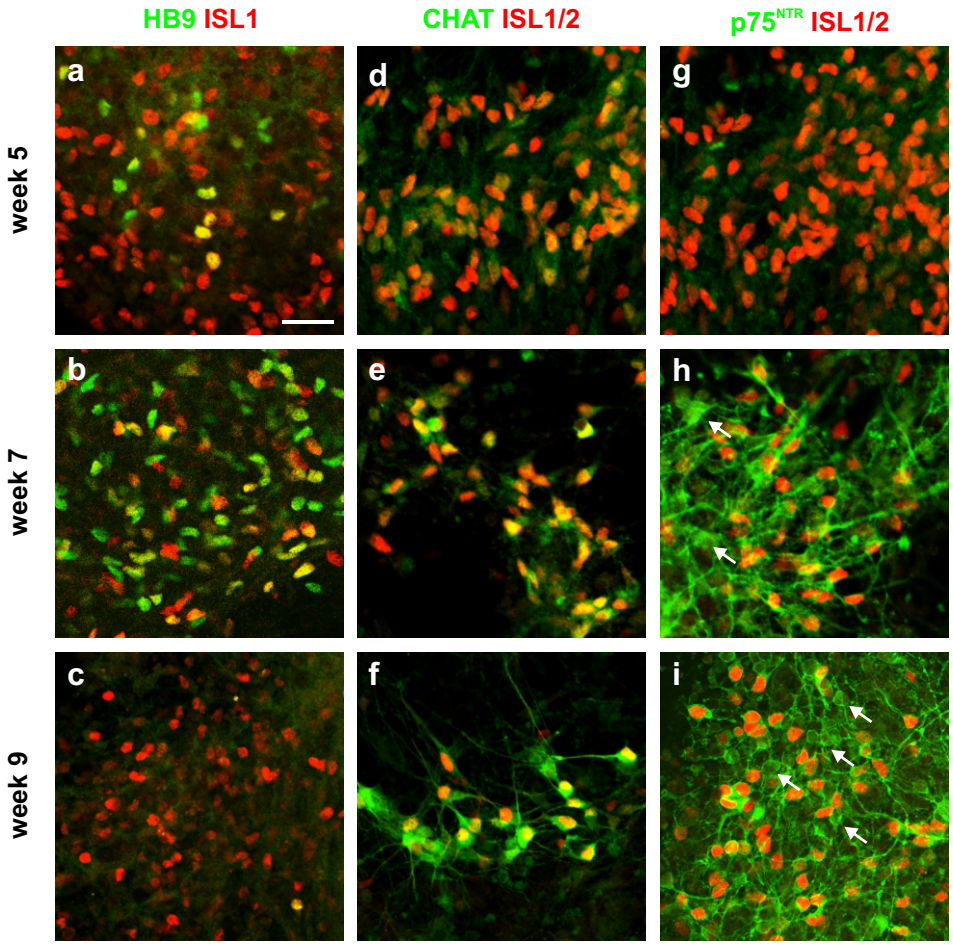

Supplementary Figure 2-S4. hESC-derived MNs express HB9, ISL1, CHAT, and $p75^{NTR}$ at specific times of differentiation.

hESC-derived MNs were analyzed for the expression of mature MN markers at 3 time points (week 5, week 7, week 9) after the start of differentiation. Scale bar = 25 μm.

(**a-c**) ISL1 expression remained constant throughout hESC-derived MN maturation, while HB9 expression peaked around week 7.

(**d-f**) CHAT expression gradually increased from week 5 to 9 of differentiation.

(**g-i**) $p75^{NTR}$ expression increased significantly around week 7 of differentiation. Non-ISL1/2^{+} cells also expressed $p75^{NTR}$ (arrows).

BIBLIOGRAPHY

1. Ebert, A.D.*, et al.* Induced pluripotent stem cells from a spinal muscular atrophy patient. *Nature* **457**, 277-280 (2009).

2. Corti, S.*, et al.* Genetic correction of human induced pluripotent stem cells from patients with spinal muscular atrophy. *Sci Transl Med* **4**, 165ra162 (2012).

3. Dimos, J.T.*, et al.* Induced pluripotent stem cells generated from patients with ALS can be differentiated into motor neurons. *Science* **321**, 1218-1221 (2008).

4. Egawa, N.*, et al.* Drug screening for ALS using patient-specific induced pluripotent stem cells. *Sci Transl Med* **4**, 145ra104 (2012).

5. Sareen, D.*, et al.* Targeting RNA foci in iPSC-derived motor neurons from ALS patients with a C9ORF72 repeat expansion. *Sci Transl Med* **5**, 208ra149 (2013).

6. Di Giorgio, F.P., Boulting, G.L., Bobrowicz, S. & Eggan, K.C. Human embryonic stem cell-derived motor neurons are sensitive to the toxic effect of glial cells carrying an ALS-causing mutation. *Cell Stem Cell* **3**, 637-648 (2008).

7. Briscoe, J. & Novitch, B.G. Regulatory pathways linking progenitor patterning, cell fates and neurogenesis in the ventral neural tube. *Philos. Trans. R. Soc. Lond. B. Biol. Sci.* **363**, 57-70 (2008).

8. Novitch, B.G., Chen, A.I. & Jessell, T.M. Coordinate regulation of motor neuron subtype identity and pan-neuronal properties by the bHLH repressor Olig2. *Neuron* **31**, 773-789 (2001).

9. Arber, S.*, et al.* Requirement for the homeobox gene Hb9 in the consolidation of motor neuron identity. *Neuron* **23**, 659-674 (1999).

10. Davis-Dusenbery, B.N., Williams, L.A., Klim, J.R. & Eggan, K. How to make spinal motor neurons. *Development* **141**, 491-501 (2014).

11. Rousso, D.L., Gaber, Z.B., Wellik, D., Morrisey, E.E. & Novitch, B.G. Coordinated actions of the forkhead protein Foxp1 and Hox proteins in the columnar organization of spinal motor neurons. *Neuron* **59**, 226-240 (2008).

12. Dasen, J.S., De Camilli, A., Wang, B., Tucker, P.W. & Jessell, T.M. Hox repertoires for motor neuron diversity and connectivity gated by a single accessory factor, FoxP1. *Cell* **134**, 304-316 (2008).

13. Hu, B.Y. & Zhang, S.C. Differentiation of spinal motor neurons from pluripotent human stem cells. *Nat Protoc* **4**, 1295-1304 (2009).

14. Chambers, S.M.*, et al.* Highly efficient neural conversion of human ES and iPS cells by dual inhibition of SMAD signaling. *Nat. Biotechnol.* **27**, 275-280 (2009).

15. Karumbayaram, S.*, et al.* Directed differentiation of human-induced pluripotent stem cells generates active motor neurons. *Stem Cells* **27**, 806-811 (2009).

16. Saraga-Babic, M., Stefanovic, V., Wartiovaara, J. & Lehtonen, E. Spinal cord-notochord relationship in normal human embryos and in a human embryo with double spinal cord. *Acta Neuropathol* **86**, 509-514 (1993).

17. Marklund, U.*, et al.* Detailed expression analysis of regulatory genes in the early developing human neural tube. *Stem Cells Dev* **23**, 5-15 (2014).

18. Dechant, G. & Barde, Y.A. The neurotrophin receptor p75(NTR): novel functions and implications for diseases of the nervous system. *Nat. Neurosci.* **5**, 1131-1136 (2002).

19. Sendtner, M., Pei, G., Beck, M., Schweizer, U. & Wiese, S. Developmental motoneuron cell death and neurotrophic factors. *Cell Tissue Res.* **301**, 71-84 (2000).

20. Livet, J.*, et al.* ETS gene Pea3 controls the central position and terminal arborization of specific motor neuron pools. *Neuron* **35**, 877-892 (2002).

21. De Marco Garcia, N.V. & Jessell, T.M. Early motor neuron pool identity and muscle nerve trajectory defined by postmitotic restrictions in Nkx6.1 activity. *Neuron* **57**, 217-231 (2008).

22. Lacombe, J.*, et al.* Genetic and functional modularity of Hox activities in the specification of limb-innervating motor neurons. *PLoS Genet* **9**, e1003184 (2013).

23. Dasen, J.S., Tice, B.C., Brenner-Morton, S. & Jessell, T.M. A Hox regulatory network establishes motor neuron pool identity and target-muscle connectivity. *Cell* **123**, 477-491 (2005).

24. Vrieseling, E. & Arber, S. Target-induced transcriptional control of dendritic patterning and connectivity in motor neurons by the ETS gene Pea3. *Cell* **127**, 1439-1452 (2006).

25. Pan, B.*, et al.* The lateral thoracic nerve and the cutaneous maximus muscle--a novel in vivo model system for nerve degeneration and regeneration studies. *Exp. Neurol.* **236**, 6-18 (2012).

26. Hester, M.E.*, et al.* Rapid and efficient generation of functional motor neurons from human pluripotent stem cells using gene delivered transcription factor codes. *Mol Ther* **19**, 1905-1912 (2011).

27. Amoroso, M.W.*, et al.* Accelerated high-yield generation of limb-innervating motor neurons from human stem cells. *J. Neurosci.* **33**, 574-586 (2013).

28. Takazawa, T.*, et al.* Maturation of spinal motor neurons derived from human embryonic stem cells. *PLoS One* **7**, e40154 (2012).

29. Hansen, D.V., Lui, J.H., Parker, P.R. & Kriegstein, A.R. Neurogenic radial glia in the outer subventricular zone of human neocortex. *Nature* **464**, 554-561 (2010).

30. Lui, J.H., Hansen, D.V. & Kriegstein, A.R. Development and evolution of the human neocortex. *Cell* **146**, 18-36 (2011).

31. Sharma, K.*, et al.* LIM homeodomain factors Lhx3 and Lhx4 assign subtype identities for motor neurons. *Cell* **95**, 817-828 (1998).

32. Kanning, K.C., Kaplan, A. & Henderson, C.E. Motor neuron diversity in development and disease. *Annu. Rev. Neurosci.* **33**, 409-440 (2010).

CHAPTER 3 – Foxp1-mediated programming of limb-innervating motor neurons from embryonic stem cells

ABSTRACT

Spinal motor neurons (MNs) are a specialized and diverse group of neurons that innervate and control muscles to permit respiration, posture, and locomotion. Methods to direct MN differentiation from stem cells have been developed enabling disease modeling *in vitro*. However, most differentiation protocols produce only a limited subset of endogenous MN subtypes. Here, we demonstrate that large numbers of limb-innervating lateral motor column (LMC) MNs can be generated from stem cells through genetic manipulation of the transcription factor Foxp1. Foxp1-programmed MNs express markers of medial and lateral LMC MNs, as well as specific motor pool markers and LMC axon guidance receptors. Importantly, they preferentially project axons towards limb muscle explants *in vitro* and innervate distal limb muscles *in vivo* upon transplantation –hallmarks of *bona fide* LMC MNs. These results present a new approach for generating specific MN populations from stem cells for use in studying MN development and disease processes.

This chapter is modified from:

Adams KL, Rousso DL, Umbach JA, and Novitch BG. (2014) Foxp1-mediated programming of limb-innervating motor neurons from embryonic stem cells. *In review (Nature Neuroscience).*

K.L.A. and B.G.N. conceived and designed the experiments and wrote the manuscript. K.L.A. performed and analyzed most of the experiments. D.L.R. generated the *Hb9::Foxp1* transgenic mice. J.A.U. performed the electrophysiology experiments.

INTRODUCTION

The ability to derive specialized cell types from pluripotent stem cells has allowed for novel insights into development and disease, particularly in the case of neurodegenerative diseases where specific neuronal populations are affected. However, in order to accurately model development and disease, stem cell-derived populations must fully recapitulate endogenous cell populations – both in the diversity of cell types generated and their functional behavior. A prime example includes the differentiation of spinal motor neurons (MNs) from mouse and human embryonic stem cells (ESCs) and induced pluripotent stem cells (iPSCs), which has provided an unprecedented opportunity to model the pathogenesis of MN diseases such as Amyotrophic Lateral Sclerosis (ALS) and Spinal Muscular Atrophy (SMA). However, despite these advances, standard differentiation protocols for generating MNs produce only a limited subset of endogenous MN populations[1].

In the developing mouse embryo, spinal MNs are organized into motor columns that innervate distinct muscle targets along the length of the body. In addition to their muscle targets, motor columns can be distinguished by their differential and combinatorial expression of LIM-homeodomain proteins, Hox proteins, and other transcription factors[2-5]. The medial motor column (MMC) innervates axial muscles along the entire rostrocaudal axis. The lateral motor column (LMC) innervates limb muscles at cervical and lumbar levels. LMC MNs are further subdivided into medial (LMCm) and lateral (LMCl) populations that innervate the ventral and dorsal limb muscles, respectively. The hypaxial motor column (HMC) innervates respiratory muscles, including the diaphragm, intercostals, and abdominal muscles at different levels of the spinal cord. Lastly, the preganglionic motor column (PGC) innervates the sympathetic ganglia and is only present at thoracic levels. The generation of these different types of MNs, which are essential for the correct formation of motor circuitry, depends on the expression and function of key fate determinants in the differentiating MNs[2-5].

Most ESC to MN differentiation protocols rely on the use of retinoic acid (RA) and Sonic hedgehog (Shh) or Shh pathway agonists to mimic the natural process of MN formation in vivo[6-9]. However, these protocols have been observed to introduce significant bias in the formation of only select MN subtypes, particularly MMC MNs and few LMC-like MNs[1, 7]. Spontaneous differentiation of ESCs has been shown to increase the diversity of MNs generated to an extent, but the efficiency of MN production is severely reduced[10]. An alternative approach is to directly program MN subtypes, taking advantage of our knowledge of the transcriptional programs that specify different MN fates. One of the major fate determinants of LMC MNs *in vivo* is the Forkhead domain transcription factor Foxp1. All LMC and PGC MNs in the developing spinal cord express Foxp1, and *Foxp1* mutant animals have severely reduced innervation and motor control of limb muscles[4, 5, 11]. We thus examined whether Foxp1 function could be used to direct the differentiation of limb-innervating MNs from ESCs, without compromising differentiation efficiency.

In this study, we demonstrate that misexpression of Foxp1 in differentiating MNs is sufficient to generate *bona fide* LMC MNs in both the mouse spinal cord and mouse ESC-derived MNs *in vitro*. These Foxp1-programmed ESC-derived MNs express molecular markers of both LMCm and LMCl MNs, as well as specific LMC motor pools, indicating conversion from an MMC to an LMC fate. Furthermore, we show that these Foxp1-programmed MNs express LMC axon guidance receptors and preferentially project axons towards limb muscle explants *in vitro*, as well as distal limb muscles in chick embryos after transplantation. Lastly, we show that these Foxp1-programmed MNs preferentially form synapses with limb muscles *in vitro* and *in vivo*, in contrast to control MMC-like MNs that preferentially innervate axial muscles. Together, these results illustrate the feasibility of generating specific subtypes of MNs from ESCs using a transcriptional programming approach, and the importance of generating ESC-derived MNs that display distinct functional behaviors.

MATERIALS AND METHODS

Mouse husbandry. *Hb9::GFP*, *Hb9::Foxp1*, and *Foxp1*$^{+/-}$ heterozygous mice were maintained as previously described[5, 7, 12]. *Hb9::Foxp1* heterozygous mice were crossed with *Foxp1*$^{+/-}$ mice to generate *Hb9::Foxp1; Foxp1*$^{+/-}$ mice. These mice were then interbred with *Foxp1*$^{+/-}$ mice to produce *Hb9::Foxp1; Foxp1*$^{-/-}$ embryos. The *Hb9::Foxp1* transgene contains an IRES-GFP sequence but GFP expression levels were very low in ESC-derived MNs. All mice were maintained and tissue collected in accordance with guidelines set forth by the UCLA Institutional Animal Care and Use Committee.

***Hb9::Foxp1* mouse ESC line generation and characterization**. Superovulation was induced in *Hb9::GFP* heterozygous female mice by sequential injections of Pregnant Mares Serum Gonadotropin (PMSG; 5 IU) followed by human Chorionic Gonadotropin (hCG; 50 IU) 48 hours later per female. These mice were paired overnight with *Hb9::Foxp1* transgenic male mice. E0.5 pre-implantation embryos were isolated the next morning and incubated in hyaluronidase (0.3 mg/ml; Sigma) until cumulus cells were removed from the embryos. 24 embryos were collected in total and cultured in KSOM media (Millipore) until the blastocyst stage[13]. 15/24 embryos developed into blastocysts and were plated on mitomycin-treated mouse embryonic fibroblasts (MEFs) in mouse ESC media [DMEM high glucose, 10% ES-qualified FBS, 1% Penicillin/Streptomycin, 1% Glutamax, 1% non essential amino acids, Primocin (50 µg/ml; Invivogen), 2-mercaptoethanol (560 nM), and Leukemia Inhibitory Factor (ESGRO; Millipore)] plus MEK1 inhibitor (50 µM; PD98059; Cell Signaling Technologies). Except as noted, media components were obtained from Invitrogen. Four days after plating, 12/15 blastocysts had hatched and attached to MEFs. Attached inner cell masses were monitored and passaged after 3-4 days of growth. MEK1 inhibitor was removed from the media after the appearance of ES colonies. Mouse ESC colonies appeared within 1 week and were expanded on MEFs until confluent[14]. Ten final mouse ESC lines were genotyped for presence of the two transgenes.

Four lines contained both the *Hb9::Foxp1* and *Hb9::GFP* transgenes and three lines contained only the *Hb9::GFP* transgene. All mouse ESCs were maintained in mouse ESC media on MEFs.

Mouse ESC differentiation to MNs. HBG3 *Hb9::EGFP* mouse ESCs (gift from Hynek Wichterle) and newly generated *Hb9::GFP* and *Hb9::Foxp1*; *Hb9::GFP* mouse ESCs were maintained and differentiated into MNs as previously described[8, 15]. Briefly, mouse ESCs were first plated on gelatin to remove MEFs prior to differentiation, and then plated in 60mm bacterial petri dishes in core MN medium to induce embryoid body (EB) formation. Core MN medium consisted of a 1:1 mixture of Dulbecco's Modified Eagle's Medium/F12 (DMEM/F12) and Neurobasal Medium supplemented with 10% Knockout Serum Replacement, 1% Glutamax, 2-mercaptoethanol (560 nM), 1% Penicillin/Streptomycin, and Primocin (50 μg/ml; Invivogen). Except as noted, media components were obtained from Invitrogen. Two days later, N2 supplement (1x, Invitrogen), Retinoic Acid (RA; 1 μM; Sigma), and Smoothened agonist (SAG; 1 μM; Calbiochem) were added to the EBs. After 5-6 days, the EBs were either dissociated and plated on matrigel-coated coverslips for immunostaining or used for transplantation and muscle assays. For culturing the MNs past day 6, RA and SAG were removed from the medium and replaced with Glia-Derived Neurotrophic Factor (10 ng/ml; Peprotech), Brain-Derived Neurotrophic Factor (10 ng/ml; Peprotech), and Ciliary Neurotrophic Factor (10 ng/ml; Peprotech).

Cell sorting of stem cell-derived MNs and RNA isolation. *Hb9::GFP* and *Hb9::Foxp1* EBs were collected 5-7 days after RA and SAG addition. EBs were dissociated using ice-cold Trypsin-EDTA (0.25%; Invitrogen) for 6 minutes at room temperature, followed by trituration in L-15 Leibovitz media (Thermo Scientific)[16]. The dissociated cells were pipetted through 40 μm cell strainers and live GFP^+ MNs (identified as lacking staining for 7AAD) were sorted and

collected using a BD ARIA II FACS machine in the UCLA Broad Stem cell center core facility. Total RNA was isolated from GFP$^+$ MNs using an RNAeasy MiniKit (Qiagen).

Quantitative PCR. Quantitative PCR analysis of MN populations was performed as previously described[17]. The following primer pairs were used: mouse *Foxp1 3'UTR*, forward 5'-cagccacgaaagaaacagaag-3' and reverse 5'-ggtcctggtcacctgattata-3'; mouse *Aldh1a2*, forward 5'-catggtatcctccgcaatg-3' and reverse 5'-gcgcatttaaggcattgtaac-3'; mouse *EphA4*, forward 5'-ctgagccagtaccgaataga-3' and reverse 5'-gagggcgaagacaaagtaaa-3'; mouse *EphB1*, forward 5'-gaagaaaggaaggaggtggaa-3' and reverse 5'-agggaggagtaagaaaggagaa-3'; mouse *c-Ret*, forward 5'-ctgactgaggtgagagaacaag-3' and reverse 5'-acacgtaccatagcagcataaa-3'; mouse *c-Met*, forward 5'- tcagccatcccaatgttctc-3' and reverse 5'-cgcagatctccatgcttcata-3'; mouse *Fgfr1,* forward 5'- aggttagccagagggtagaa-3'and reverse 5'-aggagaggaatatgaggagtagg-3'; mouse *β-Actin*, forward 5'-gccaaccgtgaaaagatgac-3' and reverse 5'-gaggcatacagggacagcac-3'. Relative mRNA expression levels were determined by normalizing crossing points for each gene to *β-Actin* and calculating fold-changes of Foxp1 misexpression over control *Hb9::GFP* MNs.

Immunostaining. All embryos and cell cultures were fixed in 4% Paraformaldehyde (Fisher). Antibody staining of cryosections and vibratome sections were performed as previously described[5]. Fixed adherent cell cultures were washed in block solution (PB, 1% heat-inactivated horse serum, 0.1% Triton X100) for 10 minutes, followed by incubation with primary antibodies overnight at 4°C. The following primary antibodies were used: guinea pig anti-Aldh1a2 (1:20,000)[18], rabbit anti-EphA4 (1:500; Santa Cruz Sc-291)[5], rabbit anti-Etv4 (1:1000)[19], guinea pig anti-Foxp1 (1:16,000)[5], sheep anti-GFP (1:800; AbD Serotec 4745-1051), rabbit anti-GFP (1:3,000; Life Technologies A6455)[20], chick anti-GFP (1:1,000; Aves Labs GFP-1020), rabbit anti-Hb9 (1:8000)[21]; guinea pig anti-Hoxa5 (1:8000)[22], goat anti-Hoxa9 (1:1000; Santa Cruz SC-17155)[5], rabbit anti-Hoxc6 (1:1000; Santa Cruz SC-66925)[5], mouse anti-Hoxc8 (1:2,000;

Covance MMS-266R)[5], goat anti-Isl1 (1:8,000, R&D Systems AF1837)[5], mouse anti-Isl1/2 (39.4D5; 1:100; Developmental Studies Hybridoma Bank)[23], mouse anti-Lhx1 (4F2; 1:100; Developmental Studies Hybridoma Bank)[24], rabbit anti-Lhx3 (1:1000; Abcam Ab14555), mouse anti-Lhx3 (67.4E12; 1:100; Developmental Studies Hybridoma Bank)[23], mouse anti-MHC (MF20; 1:100; Developmental Studies Hybridoma Bank)[25], rabbit anti-Nkx6.1 (1:2,500)[26]; rabbit anti-nNOS (1:10,000; ImmunoStar 24287)[5], rabbit anti-Pou3f1 (1:2,000)[27]; mouse anti-Pou5f1 (1:1,000; Santa Cruz SC-5279), goat anti-Sox2 (1:2,000, Santa Cruz SC-17320)[17, 20], mouse anti-Synaptotagmin (mAb 30; 1:100; Developmental Studies Hybridoma Bank)[28], mouse anti-Synaptotagmin 2 (znp-1; 1:100; Developmental Studies Hybridoma Bank)[29, 30], rabbit anti-βIII Tubulin (1:3,000; Covance MRB-435P), and mouse anti-βIII Tubulin (1:3,000; Covance MMS-435P). Monoclonal antibodies obtained from the DSHB were developed under the auspices of the NICHD and maintained by the University of Iowa, Department of Biology, Iowa City, IA 52242. Cells were washed and then incubated with Alexa^{488}-, FITC-, Cy3-, Cy5-, and DyLight^{649}-conjugated secondary antibodies (Jackson Immunoresearch) for 1 hour at room temperature the following day, and coverslips were mounted with Prolong Gold (Invitrogen). Representative images shown for antibody staining were successfully repeated at least 2-3 times.

Image analysis. DIC images were collected using a Zeiss Axioobserver microscope equipped with the Apotome optical imaging system. Fluorescent images were collected using either a Zeiss LSM5 Exciter or Zeiss LSM780 confocal imaging system. Images were processed using Adobe Photoshop and CorelDraw Software. Cell number quantification was performed using the NIH ImageJ software suite with an ITCN add-in for automated cell counting.

Muscle and EB co-cultures. *Hb9::GFP* and *Hb9::Foxp1* ESC-derived EBs with high levels of GFP expression were manually collected 5-6 days after RA/SAG addition. Axial, dorsal limb muscle, and ventral limb muscle was dissected from Hamburger Hamilton (HH) stage 35 chick

embryos. For adherent muscle co-cultures: dissected muscle was dissociated and plated onto matrigel-coated glass bottom dishes (MatTek Corporation). *Hb9::GFP* and *Hb9::Foxp1* EBs were plated on top of the dissociated muscle and cultured for 3 days. Synapse formation was assayed using Alexa647-conjugated alpha-bungarotoxin (1:300; Invitrogen). For three-dimensional collagen cultures: muscle explants were placed on either side of a single EB in a collagen bed (rat tail collagen IV, Calbiochem) and cultured for 24 hours. ~80% of muscle explants showed >70% myosin heavy chain (MHC) positive staining and ~90% of muscle explants showed axon growth. Data was extracted from this latter group. In both assays, muscle and MN co-cultures were incubated in core MN medium with N2 supplement and Heparin (10 µg/ml; Sigma).

Electrophysiology. *Hb9::GFP* and *Hb9::Foxp1* EBs were dissociated using papain (0.5 U/ml; Worthington) and plated at low density on Matrigel-coated 35mm culture dishes [1.2 x 10^4 cells/dish] in core MN medium with neurotrophic factors and cultured for an additional 2-3 d. Recordings were made from GFP^+ cells using standard whole-cell, current-clamp techniques at 20-22^{o}C. The recording bath solution contained [in mM]: NaCl (120), KCl (1.9), KH_2PO_4 (1.2), Na-bicarbonate (20), $CaCl_2$ (2.2), $MgCl_2$ (1.4), D-Glucose (10), Hepes (7.5). Patch pipettes [resistance 3-5MΩ] were filled with internal recording solution containing [in mM]: K-gluconate (140), Hepes (10), EGTA (1), Mg-ATP (4), Na-GTP (0.3). The pH of both solutions was adjusted to 7.2. Cells with resting potentials < -30mV were discarded. Patched MNs [maintained in current clamp mode at approximately -70 mV] were stimulated with 0.1 nA depolarizing current pulses of 250 msec duration. For each MN, this stimulus pulse was applied at least 3 times [with intervals $\geq$ 30 sec]. Only data from cells in which the long stimulus pulse elicited the same number of action potentials were included in this study. Data were collected using Axopatch 2B patch clamp amplifiers with 4-pole Bessel filtering at 5 kHz. Signals were digitized, stored and

analyzed using pClamp software (Axon Instruments). AP amplitude was measured as the voltage change from the threshold to the peak of the first AP in a train.

Chick transplantations. Fertilized chicken eggs (McIntyre Poultry and Fertile Eggs) were incubated at 38ºC for ~60 hours to HH stage 14-17 prior to use. *Hb9::GFP* and *Hb9::Foxp1* ESC-derived MNs were transplanted into the lumen of the spinal cord, as described previously[16]. Briefly, GFP^+ EBs were manually collected 5-6 days after RA/SAG addition and cut into 4-6 pieces. A glass needle was inserted through a small nick in the neural tube of the embryo and a small portion of the neural tube was removed at brachial levels. GFP^+ EBs were injected into this lesion site. Embryos were allowed to develop for 2-5 days post-transplantation and then collected, fixed, and prepared for cryosections or vibratome sections.

Lentiviral infections. The coding sequence of the human Hoxc10 gene was cloned into a FU-CRW lentiviral vector, using plasmid HsCD00002630 as a template (PlasmID Database, DF/HCC DNA Resource Core). Control FU-CRW (RFP) lentivirus and FU-CRW-Hoxc10 lentivirus were generated using standard 3rd generation protocols, and concentrated viral aliquots were stored at -80°C. 25 µl of concentrated lentivirus was used to infect 1 well of hESC-derived MNs in a 24-well plate, in a total volume of 500 µl per well. Medium was changed the morning after infection. RFP^+ cells were identified 3-5 days after infection. hESC-derived MNs were infected ~5 weeks of differentiation and analyzed 2 weeks later.

Quantification. For analysis of MN populations in E12.5 mouse embryos: mean ± SEM values were calculated by pooling at least 3 sections at both cervical and thoracic levels, collected from at least three embryos of each genotype. For analysis of ESC-derived MNs: 3-5 field images containing ~100 cells per field were counted for each antibody stain per differentiation batch.

Values from three separate differentiation batches were averaged to generate mean ± SEM values shown in the figures.

Statistics. No statistical methods were used to predetermine sample sizes, but our sample sizes are similar to those reported in previous publications[5, 10]. All quantification of *in vitro* MN-muscle co-cultures and explants was performed blind. Blinding of other experiments and randomization were not performed. Data were not tested for normality and compared using either the Student's t-test, a paired two-tail t-test, or one or two-way ANOVAs with Bonferroni adjustments for multiple comparisons. Variance was similar between groups being compared. The test used for each experiment is noted in the figure legends. All statistics and graphs were generated using Prism6 Graphpad software.

RESULTS

In vivo misexpression of Foxp1 in MNs restores LMC production in Foxp1 mutants

Previous work in our laboratory and others has shown that Foxp1 is necessary and sufficient for the correct generation and function of LMC and PGC MNs in the developing mouse spinal cord[4, 5, 11]. In *Foxp1* mutants, the majority of LMC and PGC MNs convert into MMC and HMC MNs, illustrated by their change in molecular markers, settling position within the ventral horn of the spinal cord, and axon projections[4, 5]. Accordingly, *Olig2::Cre; Foxp1$^{fl/fl}$* mutants, in which Foxp1 is removed from MN progenitors, are unable to move their forelimb and hindlimb muscles due to the inability of MNs to coalesce into functional motor pools resulting in defects in sensory-motor connectivity[11]. In contrast, *Hb9::Foxp1* transgenic mice, in which Foxp1 is misexpressed in most spinal MNs under the Hb9 promoter, display an increased generation of LMC and PGC MNs, and a corresponding decrease in MMC and HMC populations[4, 5].

To test whether the *Hb9::Foxp1* transgene has the capacity to generate LMC MNs d*e novo*, we interbred *Hb9::Foxp1* mice with *Foxp1$^{-/-}$* mice and analyzed the status of MN formation

in different mutant and transgenic allele combinations (**Fig. 3-1**). At E12.5, control *Foxp1*$^{+/+}$ and *Foxp1*$^{+/-}$ embryos had MMC, HMC, and LMC MN subtypes present at cervical levels in the spinal cord (**Fig. 3-1a**). *Foxp1*$^{-/-}$ embryos displayed prominent MN defects as previously described[4, 5]. At cervical levels, *Foxp1*$^{-/-}$ embryos showed an almost complete loss of LMC MNs, resulting in a large expansion of Hb9^{+}/Isl1^{+}/Lhx3^{-} HMC MNs and a smaller, but significant, expansion of Isl1^{+}/Lhx3^{+} MMC-like MNs (**Fig. 3-1a**). *Hb9::Foxp1*; *Foxp1*$^{-/-}$ embryos showed an ~11% increase in LMCm MNs and a ~20% increase in LMCl MNs, compared to *Foxp1*$^{-/-}$ embryos (**Fig. 3-1a,c**). In addition, crossing *Hb9::Foxp1* mice with *Foxp1*$^{-/-}$ mice resulted in a ~25% reduction of the ectopic HMC and a ~40% reduction of the ectopic MMC MNs found in *Foxp1*$^{-/-}$ embryos (**Fig. 3-1a,c**). Interestingly, MMC MNs in *Hb9::Foxp1*; *Foxp1*$^{-/-}$ embryos were reduced back to the levels seen in wild-type embryos, but LMCm and LMCl MNs remained below normal levels (**Fig. 3-1c**). This trend was also observed in the thoracic spinal cord (**Fig. 3-1b**). PGC MNs – another Foxp1-dependent population – were largely restored in *Hb9::Foxp1*; *Foxp1*$^{-/-}$ embryos (15.6 ± 1.7%) compared to *Foxp1*$^{-/-}$ embryos (2.3 ± 0.4%), coincident with a nearly complete suppression of ectopic HMC MNs seen in *Foxp1* mutants (**Fig. 3-1d**). There was no significant difference in total MN number between all three genotypes, indicating that changes in MN subtypes were likely a result of fate conversion rather than variations in cell death and survival (**Fig. 3-1e**). Overall, these results indicate that ectopic expression of Foxp1 is sufficient to generate LMC MNs and suppress ectopic MMC and HMC MN formation in a *Foxp1* null background *in vivo.*

Hb9::Foxp1 ESC-derived MNs express markers of both LMCm and LMCl MNs

The ability of the *Hb9::Foxp1* transgene to rescue *Foxp1*$^{-/-}$ MN phenotypes *in vivo* led us to hypothesize that Foxp1 misexpression during ESC differentiation would be sufficient to generate LMC MNs *in vitro*. Foxp1 overexpression in neural progenitors disrupts MN differentiation, mimicking Foxp4 overexpression phenotypes[17]; highlighting the importance of overexpressing

Foxp1 only in postmitotic MNs. Therefore, we derived mouse ESC lines from *Hb9::Foxp1; Hb9::GFP* blastocysts. Four *Hb9::Foxp1; Hb9::GFP* (hereafter termed *Hb9::Foxp1*) ESC lines were generated and exhibited characteristic ESC colony appearance and expression of pluripotency markers (**Fig. 3-2a**). The widely used HBG3 *Hb9::GFP* ESC line[7], as well as newly created isogenic *Hb9::GFP* ESC lines, were used as controls for comparison throughout this study. All *Hb9::GFP* ESC lines behaved equivalently (data not shown). Foxp1 misexpression did not affect the efficiency of MN production, since both control *Hb9::GFP* and *Hb9::Foxp1* ESC lines generated similar numbers of $GFP^+/Hb9^+$ MNs (**Fig. 3-2a**). Approximately 40% of all ESC-derived cultures expressed GFP (data not shown). *Hb9::Foxp1* ESC-derived MNs expressed 15-20 fold higher levels of *Foxp1a* coding mRNA, compared to all *Hb9::GFP* control MNs (data not shown). Using primers designed against the 3'UTR region of *Foxp1a* mRNA, we also analyzed ESC-derived MNs and embryonic spinal MNs for endogenous *Foxp1* mRNA levels (**Fig. 3-2e**). *Hb9::Foxp1* ESC-derived MNs showed a nearly 3-fold increase in levels of *Foxp1* 3'UTR mRNA expression compared to *Hb9::GFP* ESC-derived MNs, indicating activation of the endogenous *Foxp1* locus. Interestingly, *Foxp1* 3'UTR mRNA levels were also reduced in $Foxp1^{-/-}$ embryonic MNs compared to $Foxp1^{+/-}$ embryos (**Fig. 3-2e**). These data together suggest that Foxp1 promotes its own expression through a positive feedback loop.

We next analyzed the ESC-derived MNs for specific MN subtype markers to determine whether Foxp1 misexpression alters MN subtype formation *in vitro*. In agreement with previously published results[1], the majority of control *Hb9::GFP* ESC-derived MNs expressed Lhx3, a marker of MMC MNs (**Fig. 3-2b**). Only ~5% of *Hb9::GFP* MNs expressed LMC markers (Foxp1, Lhx1, Aldh1a2) 7 days after addition of RA and Smoothened agonist (SAG) (**Fig. 3-2b,c**). In contrast, *Hb9::Foxp1* ESC-derived MNs displayed significantly reduced numbers of cells expressing Lhx3 and increased numbers of cells positive for LMCm (Isl1/Foxp1) and LMCl (Hb9/Lhx1) MN markers (**Fig. 3-2b,c**). Interestingly, ~18% of *Hb9::Foxp1* ESC-derived MNs expressed both Lhx3 and Foxp1, a cell population that is rarely found *in vivo*. However, this

population disappeared with additional time in culture, likely due to resolution in cell fates associated with the cross-repressive activities of Lhx3 and Foxp1 (**Supplementary Fig. 3-S1**)[4, 5]. We also examined the ESC-derived MNs for expression of Aldh1a2, an RA-synthesizing enzyme expressed by LMC MNs *in vivo*[31]. *Aldh1a2* mRNA levels were ~6 fold higher in *Hb9::Foxp1* ESC-derived MNs compared to *Hb9::GFP* controls (**Fig. 3-2b,f**). Within the LMC-like MNs produced by the *Hb9::Foxp1* ESCs, ~57% expressed Lhx1, suggesting a slight bias in the formation of LMCl over LMCm MNs (**Fig. 3-2d**). This could reflect the presence of RA in the differentiation media, seeing as LMCl formation *in vivo* is strongly influenced by retinoid signaling[31]. Consistent with this possibility, we found that altering RA levels in the differentiation protocol lead to corresponding changes in the percentage of $Lhx1^+$ *Hb9::Foxp1* MNs (**Supplementary Fig. 3-S2**). Together, these results indicate that Foxp1 misexpression is sufficient to transform the molecular identity of ESC-derived MNs from an MMC-like phenotype to an LMC-like phenotype.

Foxp1 misexpression promotes the expression of specific LMC motor pool markers *in vivo* and *in vitro*

In the embryo, LMC MNs are further divided into individual motor pools consisting of MN groups that innervate the same muscle. At cervical regions, these pools include the $Etv4^+$ (also known as Pea3) pools that innervate the latissimus dorsi and cutaneous maximus muscles[32, 33]; the $Nkx6.1^+$ pool that innervates the biceps muscle (data not shown); and the $Pou3f1^+$ (also known as SCIP) pool that innervates the flexor carpi ulnaris muscle of the lower forearm (**Fig. 3-3a**)[22, 33]. *In vivo*, the expression of these pool markers is initiated by exposure of MN axon growth cones to signals emanating from the surrounding peripheral tissue and developing muscles. For example, Etv4 is expressed in LMC MNs upon exposure to GDNF as LMC MN axons approach the developing limbs[34]. In $Foxp1^{-/-}$ embryos, there is a complete loss of $Etv4^+$ and $Nkx6.1^+$ LMC motor pools at cervical levels, and a conversion of $Pou3f1^+$ LMC MNs to $Pou3f1^+$ HMC MNs

(**Fig. 3-3a**)[4, 5]. To test whether Foxp1 misexpression in MNs could rescue these lost LMC motor pools, we analyzed *Hb9::Foxp1; Foxp1*$^{-/-}$ embryos for expression of pool markers. Interestingly, the Etv4^{+} motor pool was significantly restored, while the Nkx6.1^{+} and Pou3f1^{+} LMC motor pools were not (**Fig. 3-3a**). This deficiency may be attributed to the fact that both Nkx6.1^{+} and Pou3f1^{+} LMC motor pools are associated with the LMCm, which was only partially restored in *Hb9::Foxp1; Foxp1*$^{-/-}$ embryos.

To determine whether Foxp1 misexpression results in LMC motor pool formation *in vitro*, we analyzed *Hb9::GFP* and *Hb9::Foxp1* ESC-derived MNs for these same pool markers. Control *Hb9::GFP* ESC-derived MNs did not express Nkx6.1, Etv4, or Pou3f1 on day 7 of differentiation, despite addition of GDNF to the culture medium on day 5 (**Fig. 3-3b**). Conversely, *Hb9::Foxp1* ESC-derived MNs expressed both Etv4 and Pou3f1 (32.4 ± 3.1% and 23.5 ± 0.14% of GFP^{+} MNs, respectively), but did not express Nkx6.1 despite the clear presence of LMCm MNs in the culture (**Fig. 3-3b**). The factor(s) required for the establishment of the Nkx6.1^{+} LMC motor pool are not known and we surmise that such factors are most likely missing from the culture media. To determine whether the addition of neurotrophic factors to the MN cultures biases the types of motor pools generated, we analyzed *Hb9::Foxp1* ESC-derived MNs that were cultured with and without GDNF (**Supplementary Fig. 3-S3**). As expected, only the Etv4 motor pool showed altered numbers when GDNF was removed from the media (**Supplementary Fig. 3-S3a,b**). We also confirmed that Pou3f1^{+}/Foxp1^{+} MNs did not express Lhx1, in agreement with an LMCm phenotype; while Etv4^{+}/Foxp1^{+} MNs did express Lhx1, consistent with an LMCl phenotype (**Supplementary Fig. 3-S3c**). A low number of Pou3f1^{+}/Foxp1^{-} GFP^{+} MNs were also identified in both *Hb9::GFP* and *Hb9::Foxp1* ESC-derived MN cultures, which likely represent HMC MNs (**Fig. 3-3d**)[5, 35, 36].

Lastly, we examined whether Foxp1 misexpression had an impact on Hox protein expression, which is implicated in both columnar and pool identities[22, 37], but did not observe any significant differences in the cultures. The majority of both *Hb9::GFP* and *Hb9::Foxp1* ESC-

derived MNs expressed Hoxa5 and Hoxc6, which are characteristic of rostral forelimb MNs, and did not express Hoxc8 or Hoxa9 associated with more caudal MN subtypes (**Supplementary Fig. 3-S4**). These data indicate that the ability of Foxp1 misexpression to convey LMC motor pool identities is most likely independent of changes in Hox protein activity.

Hb9::Foxp1* ESC-derived MNs preferentially project axons towards limb muscle *in vitro

It has been previously shown that ESC-derived MNs do not stably innervate developing limb muscle likely due to their lack of LMC character[1]. To determine whether Foxp1 misexpression in ESC-derived MNs alters axon projections, we embedded GFP^+ embryoid bodies (EBs) in three dimensional (3D) collagen beds between explants of different groups of chick embryo muscle and analyzed axon outgrowth (**Fig. 3-4a**). When *Hb9::GFP* and *Hb9::Foxp1* EBs were cultured alone, very few axons projected into the surrounding collagen and the majority of axons were very short in length (**Fig. 3-4a**). However, when *Hb9::GFP* EBs were cultured between axial and dorsal limb muscle explants, the majority of axons projected towards the axial muscle (56.4 ± 1.8% axial versus 43.6 ± 1.8% dorsal limb) (**Fig. 3-4b,c**). This trend was also seen when *Hb9::GFP* EBs were cultured between axial and ventral limb muscle explants (60.9 ± 6.2% axial versus 39.1 ± 6.2% ventral limb) (**Fig. 3-4b,c**). In contrast, a significant percentage of *Hb9::Foxp1* EB axons projected towards dorsal limb muscle (26.8 ± 2.7% axial versus 73.2 ± 2.7% dorsal limb) or ventral limb muscle (39.3 ± 5.8% axial versus 60.7 ± 5.8% ventral limb) when cultured together with axial muscle explants (**Fig. 3-4a-d**).

These differences in axon projections suggest changes in the ability of the motor axons to detect guidance and/or outgrowth cues present in the muscle explants. We therefore analyzed control *Hb9::GFP* and *Hb9::Foxp1* ESC-derived MNs for expression of known LMC axon guidance receptors. *Hb9::Foxp1* ESC-derived MNs expressed increased levels of the EphA4 and *c-Ret* receptors, which are highly expressed by LMCl MNs and critical for correct innervation of the dorsal limb *in vivo* (**Fig. 3-4e-f**)[38-40]. *Hb9::Foxp1* ESC-derived MNs also

expressed increased levels of the *EphB1* receptor, which is expressed by endogenous LMCm MNs and important for ventral limb innervation (**Fig. 3-4e**)[41]. In addition, *Hb9::Foxp1* ESC-derived MNs expressed increased levels of *c-Met,* which is critical for both dorsal and ventral limb innervation (**Fig. 3-4e**)[42, 43]. However, there was no significant difference in the levels of *Fgfr1*, which is important for MMC MN axon projections towards developing axial muscle[44]*,* possibly due to the residual population of $Lhx3^+$ MNs present in *Hb9::Foxp1* MN cultures (**Fig. 3-4e**). Together, these results provide evidence that Foxp1 misexpression in ESC-derived MNs alters axon projections *in vitro* to favor innervation of limb muscles over axial muscles, most likely due to increased expression of LMC axon guidance receptors.

Hb9::Foxp1 ESC-derived MNs form synapses with limb-derived myotubes *in vitro*

To determine whether these changes in muscle preference were also observed at the neuromuscular junction level, we generated ESC-derived MN and muscle co-cultures. Axial and dorsal limb muscle from chick embryos were dissociated and cultured as single myotubes for several days prior to addition of ESC-derived MNs. Cultures were analyzed for synapse formation using $Alexa^{647}$-conjugated alpha-bungarotoxin (αBTX) to label neuromuscular junctions (**Fig. 3-5a**). $GFP^+/\alpha BTX^+$ synapses were identified in all cultures, regardless of muscle type. To analyze the frequency of synapse formation with different muscle types, we calculated the percentage of myotubes with at least one $GFP^+/\alpha BTX^+$ synapse, over the total number of myotubes contacted by GFP^+ axons. Control *Hb9::GFP*-derived MNs plated on axial myotubes resulted in a higher percentage (53.7 ± 0.3%) of myotubes with $GFP^+/\alpha BTX^+$ synapses, compared to limb myotube co-cultures (40.4 ± 2.3%) (**Fig. 3-5b**). The opposite trend was seen with *Hb9::Foxp1*-derived MNs (41.7 ± 3.6% axial versus 58.9 ± 2.8% limb) (**Fig. 3-5a-b**). Furthermore, we observed a significant increase in size of the neuromuscular junctions when *Hb9::Foxp1* ESC-derived MNs were cultured with limb muscle, compared to *Hb9::GFP* MNs

(**Fig. 3-5c**). However, there was no difference in synapse area between the two cell lines when they were cultured with axial muscle (data not shown).

Lastly, we performed whole-cell patch clamp recordings of the *Hb9::GFP* and *Hb9::Foxp1* ESC-derived MNs to assess whether they displayed any differences in functional maturation (**Fig. 3-5d-e**). Both *Hb9::GFP* and *Hb9::Foxp1* ESC-derived MNs robustly fired multiple action potentials (APs) upon depolarizing current injection as expected for mature MNs, without any disparities in AP frequency or amplitude (63 ± 1.5 mV *Hb9::GFP*; 60 ± 2.5 mV *Hb9::Foxp1*) between the cell lines. These results indicate that Foxp1 misexpression in ESC-derived MNs produces functionally mature MNs with enhanced capacity to innervate limb muscles *in vitro*.

Hb9::Foxp1 ESC-derived MNs innervate limb muscles *in vivo* after transplantation

Hb9::GFP MNs have previously been shown to preferentially project axons towards axial muscle upon transplantation into developing chick embryos[1]. A more recent study found that spontaneously differentiated mouse ESC-derived MNs projected axons towards limb muscles upon transplantation, but did not show whether they innervated and formed synapses with the limb muscles[10]. We injected GFP^+ EBs into the neural tube of st.14-17 chick embryos at brachial regions and collected the embryos 3-5 days later (**Fig. 3-6a**). First, we confirmed that the molecular profile of the ESC-derived MNs did not change upon transplantation. The majority of transplanted *Hb9::GFP* ESC-derived MNs expressed Lhx3 and Hoxa5, despite injection into $Hoxc8^+$ brachial regions of the chick neural tube (**Supplementary Fig. 3-S5**). In contrast, transplanted *Hb9::Foxp1* ESC-derived EBs contained a mixture of $Lhx3^+$ (~20%), $Lhx1^+/Foxp1^+$ (~30%), and $Foxp1^+$ only (~30%) MNs, which matched the distribution of MN subtypes characterized *in vitro* (**Supplementary Fig. 3-S5b**). Transplanted *Hb9::GFP* MNs that migrated into the ventral horn of the spinal cord typically settled in a medial position where endogenous

MMC MNs are located, while transplanted *Hb9::Foxp1* MNs migrated more laterally towards endogenous LMC MNs (**Fig. 3-6b**).

We first analyzed axon projections 3 days post transplantation, when both endogenous and transplanted MN axons have reached their target muscles (**Fig. 3-6c**). We found that in control *Hb9::GFP* transplantations, significantly more GFP^+ axons projected dorsally towards axial muscles than laterally towards limb muscles (57.3 ± 3.6% axial vs. 42.7 ± 3.6% limb). In comparison, in *Hb9::Foxp1* transplantations, significantly more GFP^+ axons projected laterally towards limb muscles (40.2 ± 4.7% axial vs. 59.8 ± 4.7% limb) (**Fig. 3-6d**). At later stages in development, neural circuit refinement occurs as inappropriate or non-functional connections are removed by axon pruning and programmed MN cell death[45]. To see whether increased muscle specificity of transplanted ESC-derived MNs could be observed during this process, we analyzed embryos 4 days after transplantation. 100% of control *Hb9::GFP* transplants maintained their axial muscle-innervating projections, but none contained GFP^+ projections into the forelimbs (**Fig. 3-6c,e**). ~75% of *Hb9::Foxp1* transplants had GFP^+ axial projections, which is not unexpected since ~30% of transplanted *Hb9::Foxp1* MNs expressed Lhx3. However, ~50% of *Hb9::Foxp1* transplants also contained GFP^+ limb projections (**Fig. 3-6c,e**). Of these limb projections, the majority of axons (>60%) innervated the distal dorsal limb, likely due to their robust expression of EphA4, *c-Ret*, and Lhx1, with the remainder extending ventrally (data not shown).

We lastly analyzed transplanted ESC-derived MNs for presence of synaptic proteins and formation of neuromuscular junctions *in vivo* (**Fig. 3-7**). At HH stages 30-32, transplanted *Hb9::GFP* axons appeared to innervate axial muscles, demonstrated by presence of GFP^+ boutons that contained the presynaptic protein, Synaptotagmin 2 (**Fig. 3-7a**). These boutons overlapped with a high number of postsynaptic acetylcholine receptors on chick axial muscles (marked by punctate labeling of $Alexa^{647}$-cconjugated αBTX), suggesting formation of neuromuscular junctions. In contrast, *Hb9::Foxp1* axons that innervated axial muscles showed

rather less co-localization of Synaptotagmin 2 and αBTX, indicating fewer synapses (**Fig. 3-7a**). To quantify this difference, we counted the number of Synaptotagmin $2^+/\alpha BTX^+$ synapses and normalized it to the number of GFP^+ axons (**Fig. 3-7c,d**). Indeed, we found that *Hb9::GFP* ESC-derived MNs formed significantly more synapses with axial muscle than *Hb9::Foxp1* ESC-derived MNs (**Fig. 3-7c**). We then analyzed transplanted *Hb9::Foxp1* MNs for evidence of synapse formation with distal forelimb muscles, and found co-localization of Synaptotagmin 2 and αBTX clusters at the terminals of GFP^+ axons in dorsal limb regions (**Fig. 3-7b**). In contrast, *Hb9::GFP* ESC-derived MNs did not innervate any limb muscles (**Fig. 3-7d**). Finally, using an antibody known to label pre-motor synaptic terminals in chick spinal cord[46], we found bright $Synaptotagmin^+$ puncta clustered around the cell bodies and dendrites of transplanted *Hb9::GFP* and *Hb9::Foxp1* ESC-derived MNs (**Fig. 3-7e**), suggesting that these stem cell-derived MNs are capable of receiving presynaptic inputs from the host spinal cord. Collectively, these data show that Foxp1 misexpression during MN differentiation generates *bona fide* LMC MNs that successfully integrate into the spinal neural circuitry and innervate distal limb muscles *in vivo*, unlike control ESC-derived MNs.

Hoxc10 overexpression alters the diversity of MNs generated from human ESCs

From previous characterization, we knew that the majority of human ESC-derived MNs also expressed characteristics of cervical MMC MNs[47] (unpublished data). We next wanted to determine whether overexpression of other MN fate determinants in differentiating human ESCs also resulted in increased MN diversity. Hoxc10 is normally expressed by lumbar LMC MN populations in mouse embryos, and *Hoxc10*/*Hoxd10* double mutant mice have decreased hindlimb mobility[48]. Using a lentiviral overexpression system, we overexpressed Hoxc10 with an RFP reporter during week 5 of human ESC differentiation and analyzed the resulting MN populations 2 weeks later. Overexpression of Hoxc10 resulted in a ~30% decrease in the number of $HOXA5^+/RFP^+$ cells, compared to RFP only controls (**Supplementary Fig. 3-S6**

a,b,e). This indicates that Hoxc10 has the ability to suppress rostral Hox protein expression. Interestingly, Hoxc10 overexpression also resulted in a significant increase of $ISL1^+/FOXP1^+$ MNs from ~20% to ~60% of RFP^+ cells (**Supplementary Fig. 3-S6 c-e**), suggesting that MN subtype diversity is restricted by the endogenous Hox protein activities in human ESC-derived MN cultures. Together, these results illustrate that misexpression of other MN fate determinants, such as Hox proteins, allows formation of more caudal MN populations from pluripotent stem cells.

DISCUSSION

MNs are essential for all voluntary and involuntary muscle movements as well as visceral organ functions, illustrated by the catastrophic and often fatal loss of motor control associated with MN disease[49]. Considerable effort has been accordingly directed towards generating MNs from stem cells for use in modeling MN disease pathologies, and potentially as cellular therapies[50, 51]. In most stem cell studies, little attention is given to the fact that MNs *in vivo* are not a single cell type, but rather a collection of functionally distinct cells. In the developing mouse spinal cord, MNs are segregated into distinct columns and pools that are organized topographically along rostrocaudal, mediolateral, and dorsoventral axes, largely controlled by the expression of unique combinations of transcription factors (**Fig. 3-8a**)[49, 52]. This complex organization allows MNs to correctly innervate the different muscles of the body and receive the correct presynaptic inputs from sensory neurons, spinal interneurons, and descending pathways needed to form stable and functional motor circuits[53]. In agreement with previous reports[1, 10], we have found that differentiation of control mouse ESCs with RA and SAG, a protocol that is widely used in MN differentiation studies, predominantly produces MMC-like MNs that preferentially innervate and form synapses with axial but not limb muscles (**Fig. 3-8b**). Our results show that it is possible to expand the molecular and functional diversity of these stem cell-derived motor neurons through the programmed expression of Foxp1, which is

sufficient to transform newly born MNs towards an LMC fate reflected by changes in both molecular and functional profiles (**Fig. 3-8b**). Importantly, we show that *Hb9::Foxp1* ESC-derived MNs innervate and form synapses with distal limb muscle – the defining property of LMC MNs.

Foxp1 has been previously shown to be required for LMC MN generation *in vivo*[4, 5, 11]; however, the mechanisms of Foxp1 action in MNs remain largely unknown. *Hb9::Foxp1* ESCs therefore provide a unique model system for analyzing Foxp1 downstream events. Interestingly, *Hb9::Foxp1* ESCs appeared to preferentially produce LMCl-like rather than LMCm-like MNs, reflected in high levels of Lhx1, Etv4, EphA4, and *c-Ret* expression in the cultures. These MNs also displayed dramatically altered axon projections *in vitro* and *in vivo*, with both assays showing a preference for dorsal limb muscle over axial muscle. In addition, in *Hb9::Foxp1; Foxp1*$^{-/-}$ embryos, LMCl MNs were better restored to wild-type levels than LMCm or HMC MNs. While the bias seen *in vitro* could be partially explained by the inclusion of RA in the MN differentiation procedure, as RA is known to promote LMCl formation[31], it doesn't easily account for the bias seen *in vivo*. Another factor that could potentially influence LMC subdivision is the differential activity of the Hb9 promoter used to drive ectopic Foxp1 expression in different MN subtypes. While Hb9 is expressed by all somatic MNs, it is notably elevated in LMCl MNs and low in LMCm MNs[4, 7]. Consequently, LMCl cells may contain more ectopically expressed Foxp1 than their LMCm counterparts, which could increase the efficiency and/or completeness of their transformation away from the MMC state exhibited by most ESC-derived MNs.

Despite these biases, *Hb9::Foxp1* ESC-derived MNs still produced substantial numbers of Foxp1^{+}/Lhx1^{-}/Pou3f1^{+} MNs, which likely represent an LMCm-associated motor pool[22], and were also capable of innervating ventral limb muscles upon transplantation. We further found that Foxp1 misexpression did not alter Hox protein expression, which agrees with previous reports of Foxp1 acting downstream and/or in combination with cervical Hox proteins to direct LMC motor pool formation in the embryonic spinal cord[4, 5, 33]. The signals required for the

formation of most cervical LMC motor pools remain unknown; however, seeing as *Foxp1*$^{-/-}$ embryos lack all known LMC motor pool markers[4, 5], it seems likely that Foxp1 plays a central role in the assignment of pool identities. In this regard, Foxp1 overexpression during ESC MN differentiation could be a useful tool for identifying novel Foxp1 gene targets in spinal MNs.

One of the current bottlenecks to achieving MN diversity *in vitro* is our limited understanding of how this process occurs *in vivo*, particularly the nature of the environmental signals that are involved. It is notable that removal of exogenous growth factors has been shown to broaden the types of MNs that can be generated *in vitro*, but the efficiency of MN production is greatly diminished[10]. Interestingly, it has recently been observed that addition of two types of Shh agonists (Purmorphamine and SAG) in addition to RA, results in accelerated generation of Foxp1^{+} MNs from human pluripotent stem cells[54]. It will be insightful to determine how these culture conditions related to the endogenous signaling events that drive MN specification *in vivo*, and to explore the innervation capacities of these cells.

At the opposite end of the spectrum, others have begun using transcriptional programming approaches to directly generate MNs from ESCs[55] and fibroblasts[56]. The types of MNs generated from these procedures remain unclear; however, they most likely represent MMC-like MNs because Lhx3 overexpression is required for MN conversion[55, 56]. Interestingly, MNs directly converted from fibroblasts cluster separately from embryonic and ESC-derived MNs in microarray analyses[56], suggesting that directly converted MNs retain some epigenetic differences related to their fibroblast origin. In our study, we present a hybrid approach incorporating both developmental signaling molecules and transcriptional programming to generate LMC MNs efficiently *in vitro*. The advantages of this method are that it maintains normal differentiation efficiencies, could be applied to both mouse and human systems, and can be adapted to produce other types of MNs, such as thoracic and lumbar populations, as long as candidate transcription factors are known. We found that Hoxc10 overexpression in human ESC-derived MNs was sufficient to increase the number of caudal Foxp1^{+} MNs. In principle, it

should be possible to combine the approach of misexpressing Foxp1 in combination with different Hox proteins to create PGC MNs from ESCs, which have never been effectively generated *in vitro*.

Finally, our studies stress the importance of knowing what type of MNs are being produced within the stem cell cultures for the purposes of disease modeling and cellular therapies. Limb-innervating MNs are thought to be among the earliest affected in ALS, while MMC and HMC MNs are predominantly affected in SMA[49, 57]. It is thus possible that *Hb9::Foxp1* ESC-derived MNs might exhibit enhanced sensitivity to ALS-associated mutations, compared to the MMC-like MNs typically produced from other ESCs.. These differences in MN identity are also paramount for the successful use of stem cell-derived MNs in regenerative contexts. Our results show that different classes of ESC-derived MNs exhibit distinct axon growth potentials and preferences in forming synaptic contacts. It is notable that transplanted *Hb9::Foxp1* ESC-derived MNs successfully innervated and formed synapses with limb muscles *in vivo*, an activity that was not seen with control *Hb9::GFP* MNs. These latter cells were nevertheless capable of innervating axial muscles consistent with their MMC-like identity. These results are reminiscent of experiments in which thoracic spinal cord segments were transplanted into lumbar levels of chick embryos. The transplanted thoracic MNs initially innervated hindlimb muscles, but at later ages, both the MNs and muscles degenerated, resulting in impaired hindlimb motor functions [58, 59]. Together, these studies suggest that correct matching of MN and muscle subtypes may be critical for optimal synapse formation and function. This detail is incredibly important in the context of MN diseases – both for modeling disease pathology *in vitro* with MN-muscle co-cultures and for transplantation into the spinal cord to replace damaged cells. It is very likely that generating specific MN subtypes from stem cells and matching them with appropriate and inappropriate muscle types will reveal novel and significant discoveries into MN development and neurodegenerative disease pathologies.

Figure 3-1

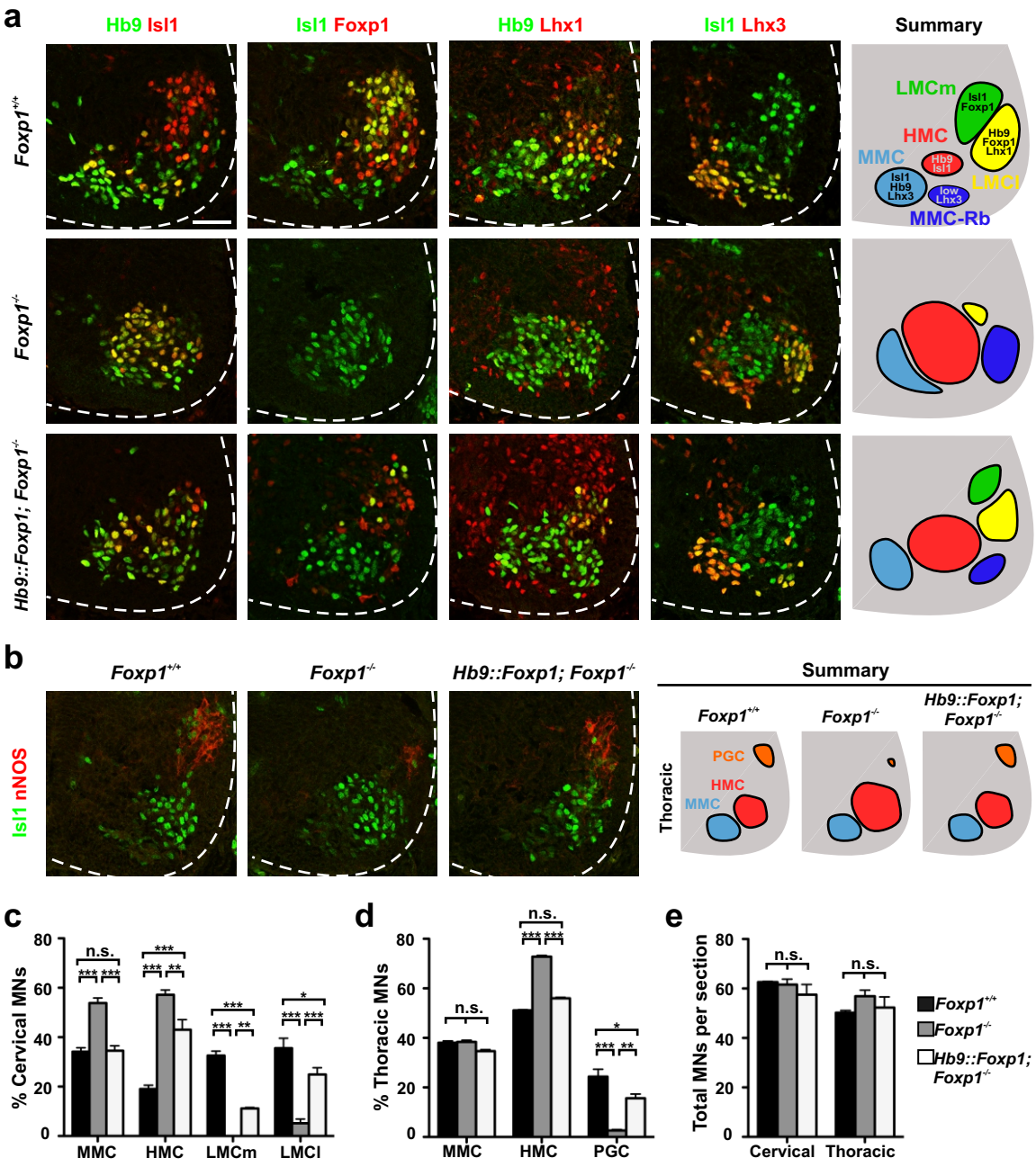
a
Hb9 Isl1
Isl1 Foxp1
Hb9 Lhx1
Isl1 Lhx3
Summary
Foxp1+/+
Foxp1-/-
Hb9::Foxp1; Foxp1-/-
LMCm
HMC
MMC
LMCl
MMC-Rb
b
Foxp1+/+
Foxp1-/-
Hb9::Foxp1; Foxp1-/-
Isl1 nNOS
Summary
Thoracic
PGC
HMC
MMC
c
% Cervical MNs
MMC
HMC
LMCm
LMCl
d
% Thoracic MNs
MMC
HMC
PGC
e
Total MNs per section
Cervical
Thoracic
n.s.

Figure 3-1 *In vivo* misexpression of Foxp1 in MNs rescues the *Foxp1* mutant phenotype. Analysis of MN subtypes in the ventral horn of E12.5 *Foxp*$^{+/+}$, *Foxp*$^{-/-}$, and *Hb9::Foxp1; Foxp1*$^{-/-}$ littermate embryo spinal cords. Scale bar = 50 μm.

(**a**) MN subtypes at cervical levels. *Foxp1*$^{-/-}$ embryos had reduced numbers of LMCm (Isl1^{+}/Foxp1^{+}) and LMCl (Hb9^{+}/Lhx1^{+}) MNs, while HMC (Hb9^{+}/Isl1^{+}) and MMC-Rhomboideus (Isl1^{+}/Lhx3^{low}) MNs[5] were expanded, compared to *Foxp1*$^{+/+}$ embryos. *Hb9::Foxp1; Foxp1*$^{-/-}$ embryos had partially restored LMCm and LMCl MNs that resided at the correct lateral positions, and reduced numbers of ectopic HMC and MMC-Rb MNs, compared to *Foxp1*$^{-/-}$ embryos. Rb = rhomboideus.

(**b**) MN subtypes at thoracic levels. The loss of PGC (Isl1^{+}/nNOS^{+}) MNs in *Foxp1*$^{-/-}$ embryos was rescued in *Hb9::Foxp1; Foxp1*$^{-/-}$ embryos.

(**c**) Quantification of MN percentages at cervical levels (mean ± SEM; n = 3 sections averaged per embryo, 3 embryos per genotype; two-way ANOVA with Bonferroni adjustment). MMC MNs: ***p-values = <0.0001. HMC MNs: ***p-value = <0.0001 and **p-value = 0.001. LMCm MNs: ***p-values = <0.0001 and **p-value = 0.006. LMCl MNs: ***p-values = <0.0001 and *p-value = 0.01. “n.s.” = not significant.

(**d**) Quantification of MN percentages at thoracic levels (mean ± SEM; n = 3 sections averaged per embryo, 3 embryos per genotype; two-way ANOVA with Bonferroni adjustment). HMC MNs: ***p-value = <0.0001. PGC MNs: ***p-values = <0.0001, **p-value = 0.0001, and *p-value = 0.0023.

(**e**) Quantification of total number of MNs per section (mean ± SEM; n = 3 sections averaged per embryo, 3 embryos per genotype; two-way ANOVA with Bonferroni adjustment).

Figure 3-2

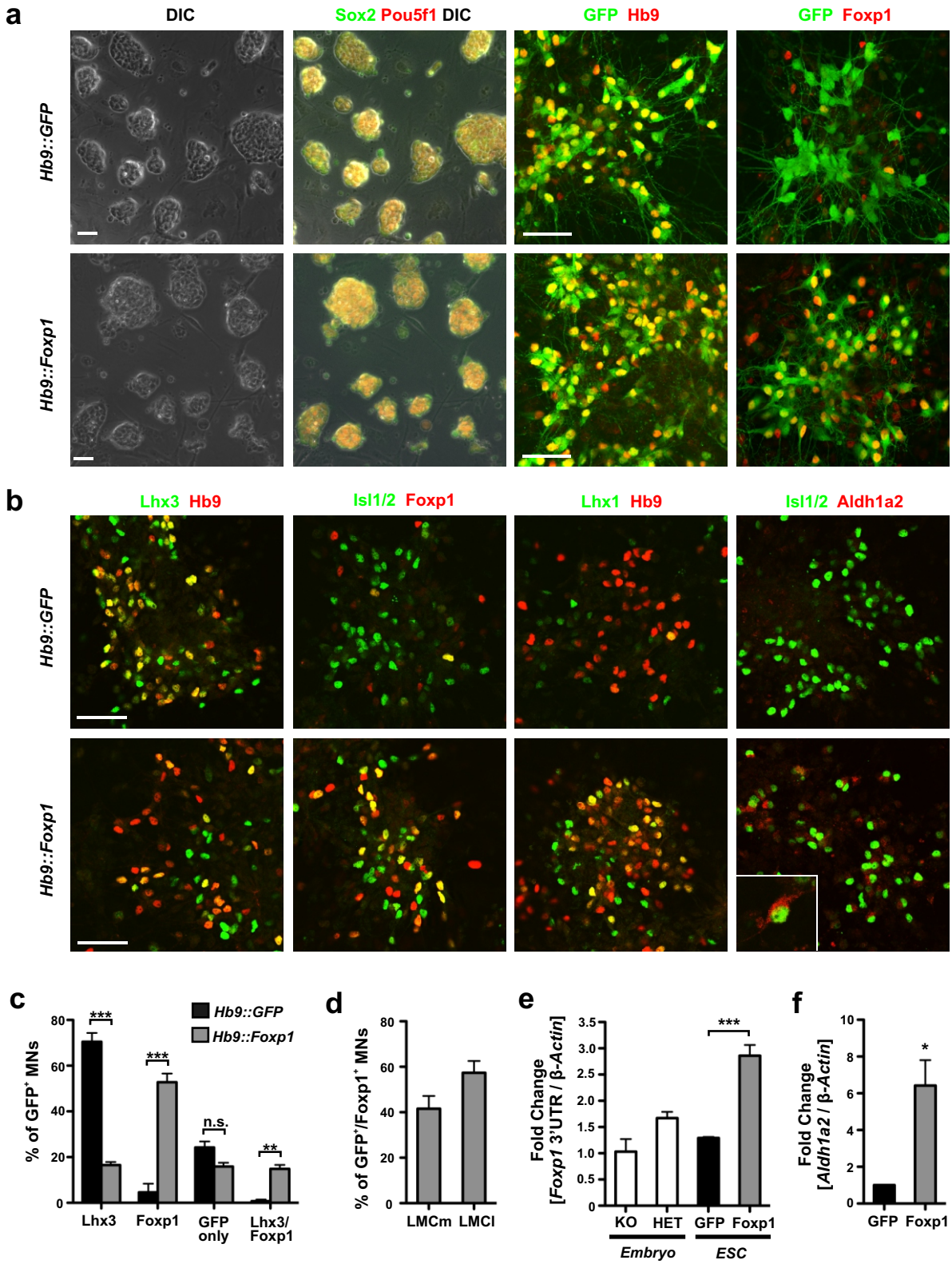
a
DIC
Sox2 Pou5f1 DIC
GFP Hb9
GFP Foxp1
Hb9::GFP
Hb9::Foxp1
b
Lhx3 Hb9
Isl1/2 Foxp1
Lhx1 Hb9
Isl1/2 Aldh1a2
Hb9::GFP
Hb9::Foxp1
c
Hb9::GFP
Hb9::Foxp1
% of GFP+ MNs
***
***
n.s.
**
Lhx3
Foxp1
GFP only
Lhx3/ Foxp1
d
% of GFP+/Foxp1+ MNs
LMCm
LMCl
e
Fold Change [Foxp1 3'UTR / β-Actin]
***
KO
HET
GFP
Foxp1
Embryo
ESC
f
Fold Change [Aldh1a2 / β-Actin]
*
GFP
Foxp1

Figure 3-2 *Hb9::Foxp1* ESCs generate MNs that express markers of LMCm and LMCl MNs.

(**a**) Newly derived ESC lines displayed characteristic ESC morphology and expressed pluripotency markers. Both *Hb9::GFP* and *Hb9::Foxp1* ESC lines differentiated into $GFP^+/Hb9^+$ MNs, but only *Hb9::Foxp1* ESC-derived MNs expressed high levels of Foxp1 protein. Scale bars = 50 μm.

(**b**) Analysis of MN columnar marker expression in ESC-derived MNs. The majority of control *Hb9::GFP* ESC-derived MNs expressed Lhx3 and low levels of Foxp1, Lhx1, and Aldh1a2. *Hb9::Foxp1* ESC-derived MNs expressed reduced levels of Lhx3, and increased levels of LMCm ($Isl1^+/Foxp1^+$) and LMCl ($Hb9^+/Lhx1^+$) MN markers. Inset shows a single $Aldh1a2^+$ MN. Scale bars = 50 μm.

(**c**) Quantification of MN subtypes generated by each ESC line (mean ± SEM; n = 3 independent experiments, 373 *Hb9::GFP* MNs and 403 *Hb9::Foxp1* MNs total; Student's t-test). ***p-value for Lhx3 = 0.0002. ***p-value for Foxp1 = 0.0008. **p-value for Lhx3/Foxp1 = 0.002. "n.s." = not significant.

(**d**) Quantification of the percentages of *Hb9::Foxp1* ESC-derived $Foxp1^+$ MNs that express markers of LMCm ($GFP^+/Foxp1^+$) and LMCl ($GFP^+/Foxp1^+/Lhx1^+$) MNs (mean ± SEM; n = 3 independent experiments, 222 *Hb9::Foxp1* MNs total).

(**e**) Endogenous Foxp1 mRNA was expressed ~3-fold higher in *Hb9::Foxp1* ESC-derived MNs, compared to *Hb9::GFP* ESC-derived MNs. E11.5 $Foxp1^{+/-}$ and $Foxp1^{-/-}$ purified MNs were used as controls (mean ± SEM; n = 3 $Foxp1^{+/-}$ embryos, 3 $Foxp1^{-/-}$ embryos, 3 independent RNA collections of *Hb9::GFP* and *Hb9::Foxp1* MNs; one-way ANOVA with Bonferroni adjustment). ***p-value = 0.001.

(**f**) *Aldh1a2* mRNA levels were elevated ~6-fold higher in *Hb9::Foxp1* ESC-derived MNs, compared to *Hb9::GFP* controls (mean ± SEM; n = 5 independent RNA collections of *Hb9::GFP* and *Hb9::Foxp1* MNs; paired two-tailed t-test). *p-value = 0.017.

Figure 3-3

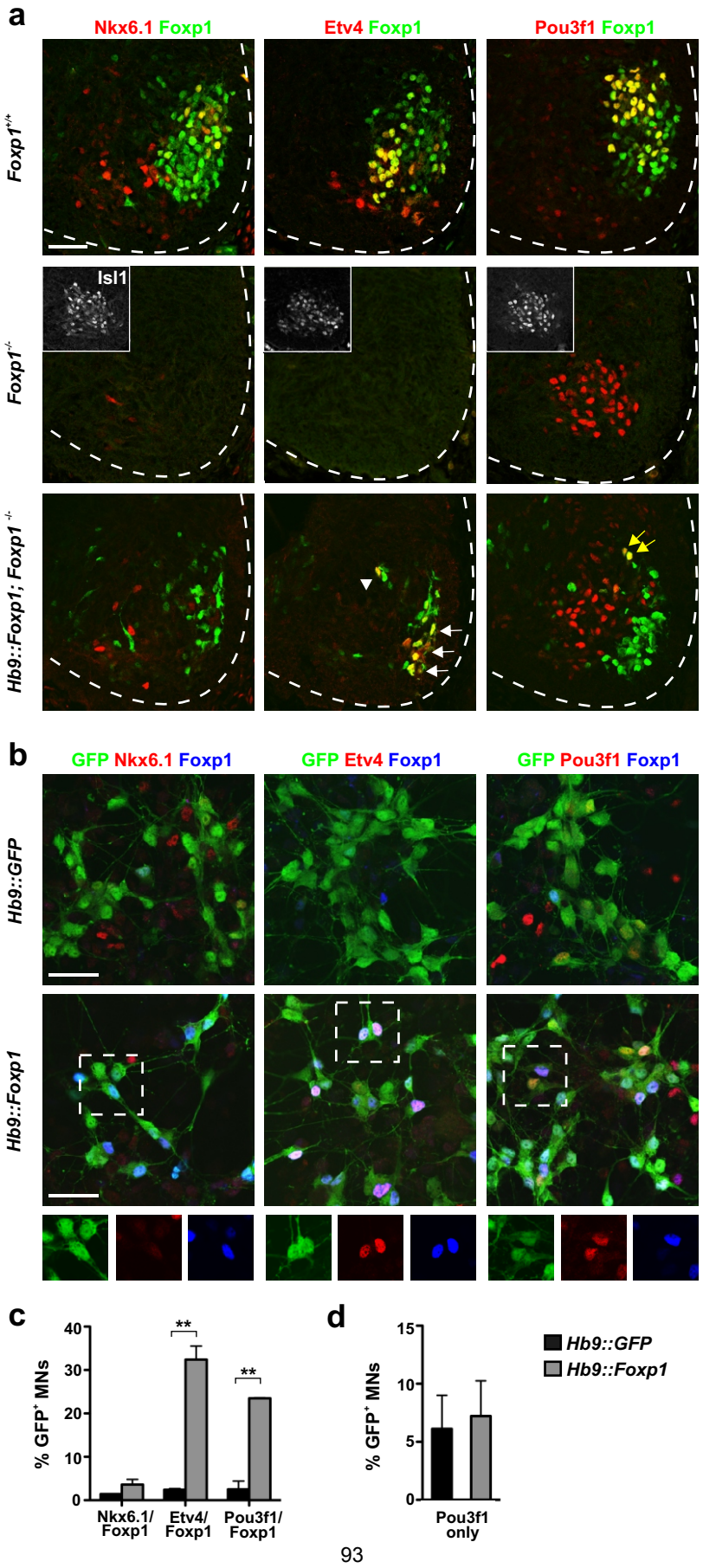
a
Nkx6.1 Foxp1
Etv4 Foxp1
Pou3f1 Foxp1
Foxp1+/+
Foxp1-/-
Isl1
Hb9::Foxp1; Foxp1-/-
b
GFP Nkx6.1 Foxp1
GFP Etv4 Foxp1
GFP Pou3f1 Foxp1
Hb9::GFP
Hb9::Foxp1
c
% GFP+ MNs
40
30
20
10
0
**
**
Nkx6.1/ Foxp1
Etv4/ Foxp1
Pou3f1/ Foxp1
d
% GFP+ MNs
15
10
5
0
Pou3f1 only
Hb9::GFP
Hb9::Foxp1

Figure 3-3 Foxp1 misexpression promotes the expression of LMC motor pool markers *in vivo* and *in vitro*.

(**a**) Analysis of cervical LMC motor pools in E12.5 *Foxp1*$^{+/+}$, *Foxp1*$^{-/-}$, and *Hb9::Foxp1*; *Foxp1*$^{-/-}$ embryos. All LMC motor pools were lost in *Foxp1*$^{-/-}$ embryos. The Pou3f1^{+} MNs in *Foxp1*$^{-/-}$ embryos represent the expanded HMC MN population (identified by their medial position). Insets depict Islet1 co-staining of the same section. The Etv4 motor pool was restored in *Hb9::Foxp1; Foxp1*$^{-/-}$ embryos (white arrows), with some Foxp1^{+}/Etv4^{+} MNs located more dorsally (arrowhead). The Nkx6.1 and Pou3f1 motor pools were not restored in *Hb9::Foxp1; Foxp1*$^{-/-}$ embryos, although a small number of Foxp1^{+}/Pou3f1^{+} MNs were identified (yellow arrows). Scale bar = 50 μm.

(**b**) Control *Hb9::GFP* ESC-derived MNs did not express any LMC motor pool markers. *Hb9::Foxp1* ESC-derived MNs expressed Etv4 and Pou3f1 at high levels, but did not express Nkx6.1. Boxed regions are depicted as single-color images below each image. Scale bars = 50 μm.

(**c**) Quantification of motor pool markers in ESC-derived MNs (mean ± SEM; n = 2 independent experiments, 938 *Hb9::GFP* MNs and 723 *Hb9::Foxp1* MNs total; Student's t-test). Etv4 **p-value = 0.009. Pou3f1 **p-value = 0.008.

(**d**) Foxp1 misexpression did not alter the percentage of Pou3f1^{+}/Foxp1^{-} ESC-derived HMC-like MNs (mean ± SEM; n = 3 independent experiments, 390 *Hb9::GFP* MNs and 255 *Hb9::Foxp1* MNs total).

Figure 3-4

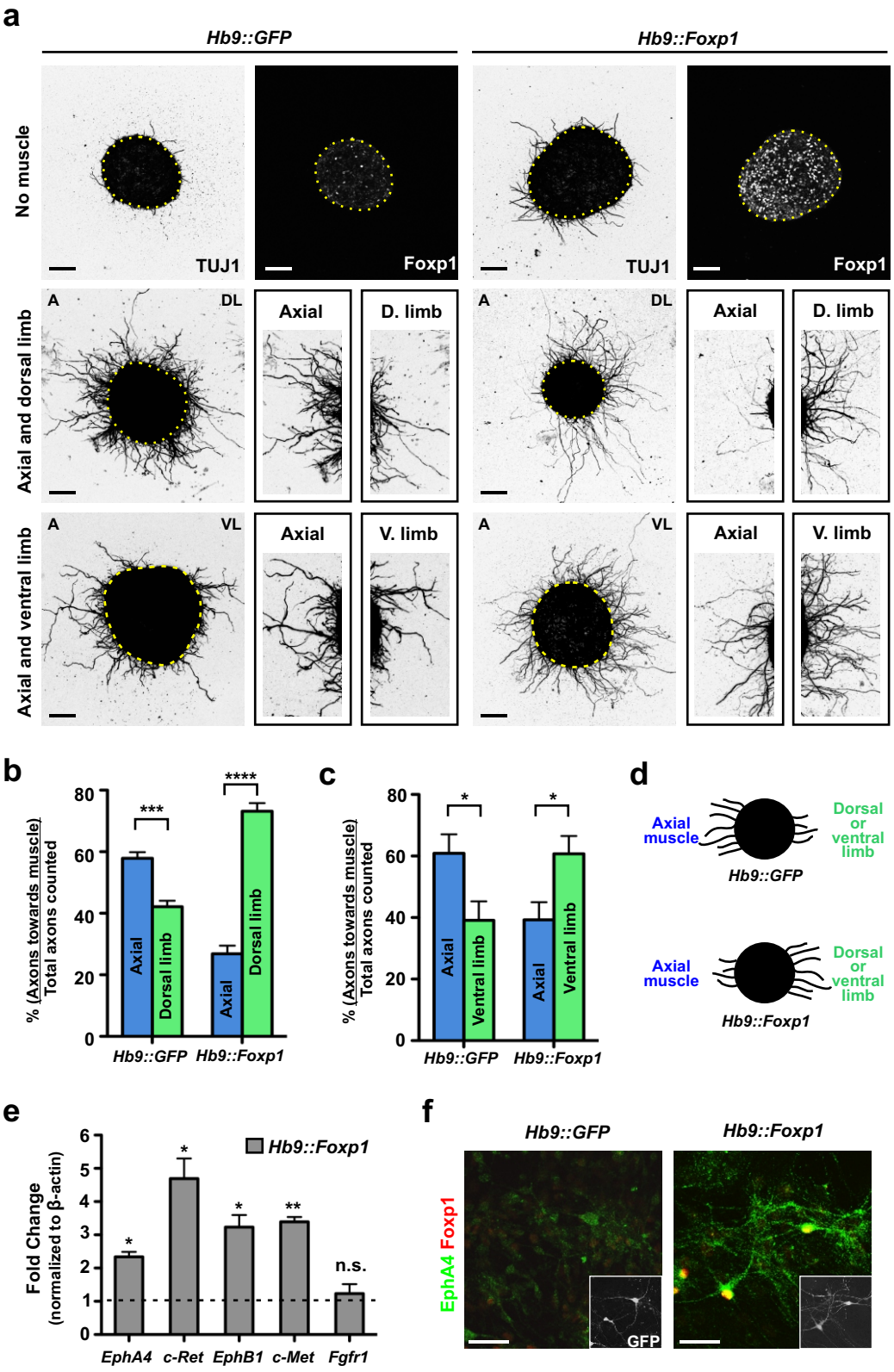
a
Hb9::GFP
Hb9::Foxp1
No muscle
TUJ1
Foxp1
Axial and dorsal limb
A
DL
Axial
D. limb
Axial and ventral limb
VL
V. limb
b
% (Axons towards muscle) / Total axons counted
Axial
Dorsal limb
Ventral limb
Hb9::GFP
Hb9::Foxp1
c
d
Axial muscle
Dorsal or ventral limb
e
Fold Change (normalized to β-actin)
EphA4
c-Ret
EphB1
c-Met
Fgfr1
n.s.
f
EphA4 Foxp1
GFP

Figure 3-4 *Hb9::Foxp1* ESC-derived MNs project axons towards limb muscle explants *in vitro*.

(**a**) 3D collagen cultures of EBs and different chick muscle explants. *Hb9::GFP* EBs projected more axons towards axial muscle than dorsal or ventral limb muscle. *Hb9::Foxp1* EBs projected more axons towards dorsal and ventral limb muscle than axial muscle explants. Scale bars = 100 μm. “A” = axial muscle. “DL” and “D. limb” = dorsal limb muscle. “VL” and “V. limb” = ventral limb muscle.

(**b**) Quantification of *Hb9::GFP* and *Hb9::Foxp1* axon projections when cultured between axial and dorsal limb explants (mean ± SEM; n = 5 cultures per cell line; Student’s t-test).***p-value = 0.0005. ****p-value = <0.0001.

(**c**) Quantification of *Hb9::GFP* and *Hb9::Foxp1* axon projections when cultured between axial and ventral limb explants (mean ± SEM; n = 5 cultures per cell line; Student’s t-test). *p-value = 0.0465 for *Hb9::GFP* and *p-value = 0.0386 for *Hb9::Foxp1*.

(**d**) Schematic summary of muscle explant results.

(**e**) *Hb9::Foxp1* ESC-derived MNs expressed increased levels of *EphA4*, *c-Ret*, *EphB1*, and *c-Met* mRNA, compared to *Hb9::GFP* ESC-derived MNs. There was no change in *Fgfr1* expression (mean ± SEM; n = 3 independent RNA collections of *Hb9::GFP* and *Hb9::Foxp1* MNs; paired two-tailed t-test). *p-value = 0.0115 for *EphA4*, *p-value = 0.0264 for *EphB1*, *p-value = 0.0258 for *c-Ret*, **p-value = 0.0037 for *c-Met*.

(**f**) *Hb9::Foxp1* ESC-derived MNs expressed higher levels of EphA4 compared to control *Hb9::GFP* ESC-derived MNs. Insets depict GFP staining of ESC-derived MNs. Scale bars = 50 μm.

Figure 3-5

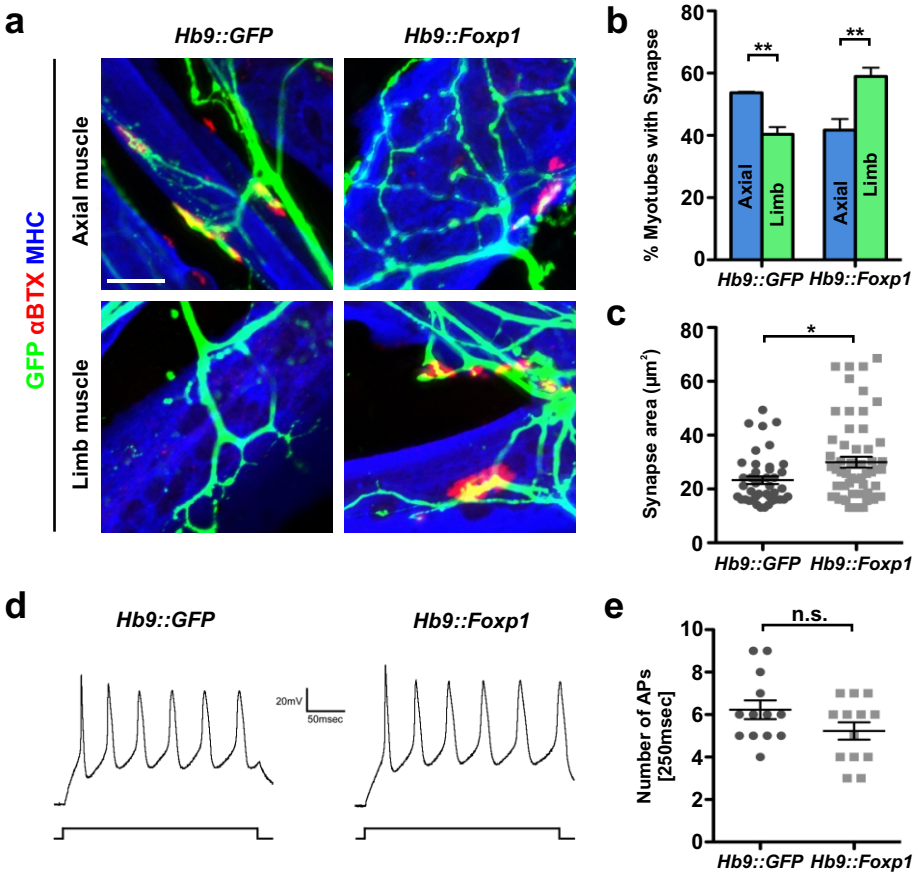
a
Hb9::GFP
Hb9::Foxp1
Axial muscle
Limb muscle
GFP αBTX MHC
b
% Myotubes with Synapse
80
60
40
20
0
**
**
Axial
Limb
Axial
Limb
Hb9::GFP Hb9::Foxp1
c
Synapse area (μm²)
80
60
40
20
0
*
Hb9::GFP Hb9::Foxp1
d
Hb9::GFP
Hb9::Foxp1
20mV
50msec
e
Number of APs [250msec]
10
8
6
4
2
0
n.s.
Hb9::GFP Hb9::Foxp1

Figure 3-5 *Hb9::Foxp1* ESC-derived MNs preferentially form neuromuscular junctions with limb myotubes *in vitro*.

(**a**) *Hb9::GFP* MNs formed synapses ($GFP^+/\alpha BTX^+$) with axial myotubes more frequently than with limb myotubes. *Hb9::Foxp1* MNs formed synapses with limb-derived myotubes more frequently than with axial myotubes. Scale bar = 20 μm.

(**b**) Quantification of the frequency of synapse formation with primary myotubes in vitro. The percentage of myotubes with $GFP^+/\alpha BTX^+$ synapses over the total number of myotubes with GFP^+ axon contacts was calculated for each cell line/muscle pairing (mean ± SEM; n = 3 independent experiments, 20 images per experiment; Student's t-test). **p-value = 0.0046 for *Hb9::GFP* and **p-value = 0.0081 for *Hb9::Foxp1*.

(**c**) *Hb9::Foxp1* MNs formed significantly larger neuromuscular junctions with limb muscle than *Hb9::GFP* MNs, as determined by measuring the area of $GFP^+/\alpha BTX^+$ synapses (mean ± SEM; n = 5 images per cell line, 117 total synapses; Student's t-test). *p-value = 0.0143.

(**d**) Representative recordings of *Hb9::GFP* and *Hb9::Foxp1* ESC-derived MNs. Both cell types responded to a +0.1 nA long duration [250 msec] current pulse with multiple action potentials.

(**e**) Quantification of the number of action potentials (APs) fired by ESC-derived MNs during a +0.1nA, 250 msec current pulse (mean ± SEM; n = 13 cells per cell line; Student's t-test). “n.s” = not significant.

Figure 3-6

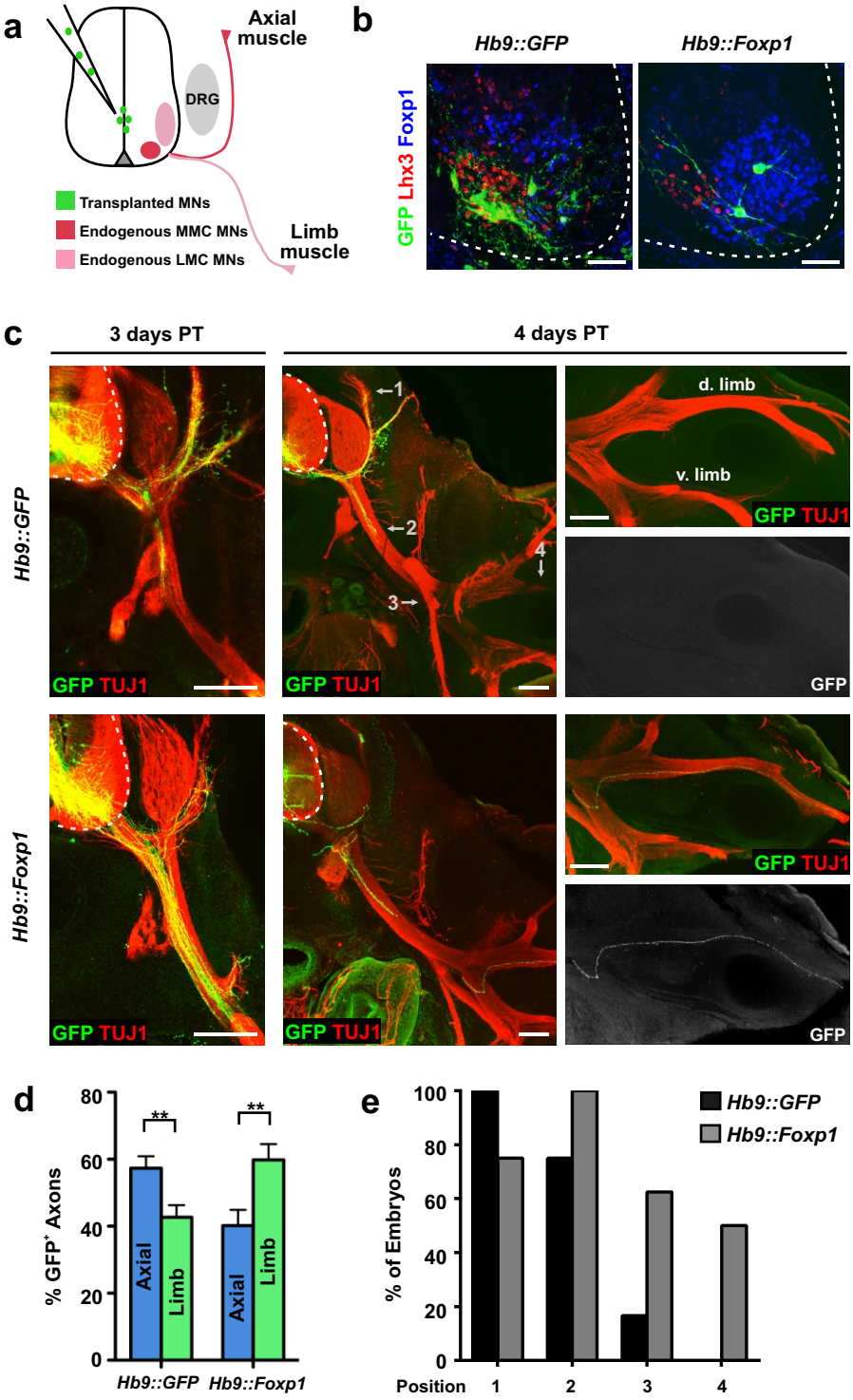
a
Axial muscle
DRG
Transplanted MNs
Endogenous MMC MNs
Endogenous LMC MNs
Limb muscle
b
Hb9::GFP
Hb9::Foxp1
GFP Lhx3 Foxp1
c
3 days PT
4 days PT
Hb9::GFP
Hb9::Foxp1
GFP TUJ1
d. limb
v. limb
GFP
1
2
3
4
d
% GFP+ Axons
Axial
Limb
Hb9::GFP
Hb9::Foxp1
e
% of Embryos
Position
Hb9::GFP
Hb9::Foxp1

Figure 3-6 *Hb9::Foxp1* ESC-derived MNs innervate distal limb muscles *in vivo*.

(**a**) Transplantation scheme. DRG = dorsal root ganglion.

(**b**) Transverse sections of the ventral horn chick spinal cords showing GFP^+ transplanted MNs. *Hb9::GFP* MNs settled at a medial position associated with endogenous $Lhx3^+$ MMC MNs. *Hb9::Foxp1* MNs settled at lateral positions associated with endogenous $Foxp1^+$ LMC MNs. Scale bars = 50 μm.

(**c**) Transverse vibratome sections of transplantations. *Hb9::GFP* ESC-derived MNs projected axons towards dorsal axial muscles both 3 and 4 days post transplantation (PT). *Hb9::GFP* axons that projected laterally did not extend into the limb. The majority of *Hb9::Foxp1* ESC-derived MNs projected axons laterally towards the limbs 3 days PT and limb projections were maintained at 4 days PT. “d. limb” = dorsal limb. “v. limb” = ventral limb. “DRG” = dorsal root ganglion. Scale bars = 200 μm.

(**d**) Quantification of the percentage of transplanted GFP^+ MN axons that projected towards axial and limb muscles at 3 days PT (mean ± SEM; n = 10 transplants per cell line; Student’s t-test). **p-values = 0.008.

(**e**) Quantification of transplanted GFP^+ axons at 4 days PT. Graph shows the percentage of chick embryos that had GFP^+ axons at positions 1-4. Position 1 = axial muscle. Position 2 = halfway to brachial plexus. Position 3 = brachial plexus. Position 4 = distal limb (these are marked in **c**). n = 8 transplants per cell line.

Figure 3-7

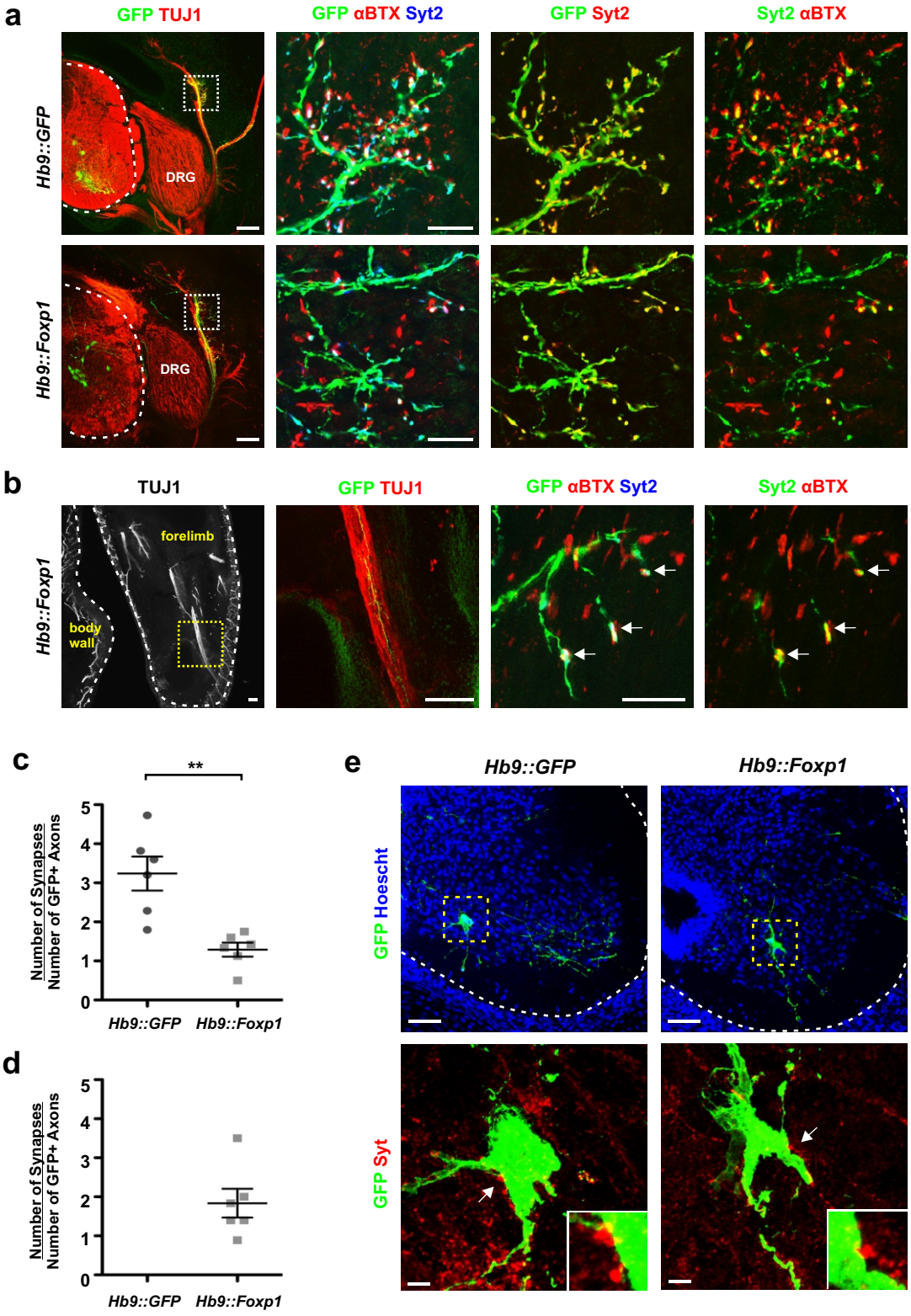
a
GFP TUJ1
GFP αBTX Syt2
GFP Syt2
Syt2 αBTX
Hb9::GFP
Hb9::Foxp1
DRG
DRG
b
TUJ1
GFP TUJ1
GFP αBTX Syt2
Syt2 αBTX
Hb9::Foxp1
forelimb
body wall
c
**
Number of Synapses
Number of GFP+ Axons
0
1
2
3
4
5
Hb9::GFP
Hb9::Foxp1
d
Number of Synapses
Number of GFP+ Axons
0
1
2
3
4
5
Hb9::GFP
Hb9::Foxp1
e
Hb9::GFP
Hb9::Foxp1
GFP Hoescht
GFP Syt

Figure 3-7 Transplanted ESC-derived MN axons form neuromuscular junctions with appropriate muscle targets *in vivo*.

Analysis of synapse formation 5 days after transplantation of *Hb9::GFP* and *Hb9::Foxp1* ESC-derived MNs. Scale bars = 100 μm for TUJ1 images and 20 μm for αBTX images.

(**a**) Transplanted GFP^+ axons innervating axial muscle. *Hb9::GFP* axons co-localized with a high density of presynaptic (mouse specific Synaptotagmin 2 [Syt2]) and postsynaptic (αBTX) markers. *Hb9::Foxp1* axons displayed fewer synaptic boutons. Boxes represent the areas imaged for synapse markers. "DRG" = dorsal root ganglion.

(**b**) Transplanted GFP^+ axons innervating limb muscle. *Hb9::Foxp1* axons in the distal limb co-localized with Synaptotagmin 2 and αBTX (arrows). *Hb9::GFP* ESC-derived MNs did not project axons into the limbs. Yellow box represents the area shown in GFP/TUJ1 image where GFP^+ axons were analyzed for synapse markers.

(**c**) Quantification of the number of synapses formed by each cell line with axial muscle *in vivo* (mean ± SEM; n = 6 images per cell line; Student's t-test). **p-value = 0.002.

(**d**) Quantification of the number of synapses formed by each cell line with limb muscles *in vivo* (mean ± SEM; n = 6 images per cell line; Student's). *Hb9::GFP* control cells showed no synapses in this assay.

(**e**) Transplanted ESC-derived MNs in the ventral horns of chick spinal cords (outlined in boxes) had bright Synaptotagmin $(Syt)^+$ punctae surrounding their cell body and dendrites. Scale bars = 50 μm in top row and 5 μm in bottom row. Arrows point to regions shown in insets.

Figure 3-8

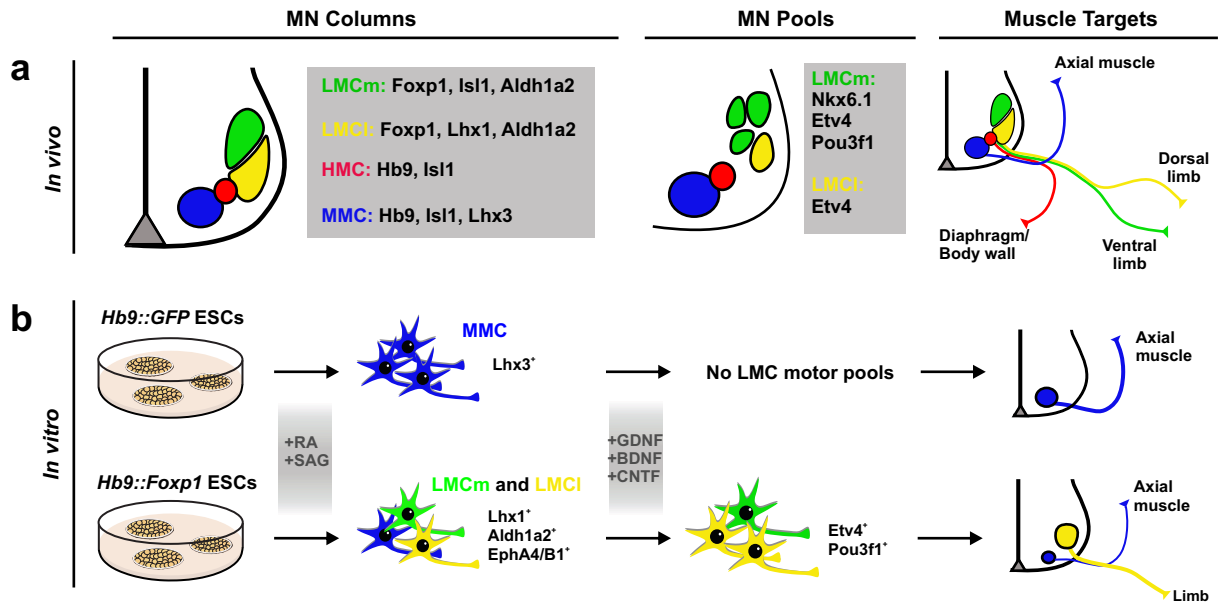

Figure 3-8 Summary of spinal MN diversity generated *in vivo* and from ESCs.

(**a**) At cervical levels in the developing spinal cord, MNs are segregated into different columns that express different transcription factors and proteins. These columns are further organized into motor pools, or groups of MNs that innervate the same muscle. These different MN subtypes innervate and form synapses with distinct muscles.

(**b**) Under standard differentiation conditions with retinoic acid (RA) and Smoothened agonist (SAG), the majority of control *Hb9::GFP* ESC-derived MNs expressed Lhx3 – a marker of MMC MNs, and did not express markers of LMC MNs. *Hb9::GFP* ESC-derived MNs preferentially projected axons towards and formed synapses with axial muscle both *in vitro* and *in vivo*. Conversely, Foxp1 misexpression resulted in large numbers of bona fide LMC MNs that expressed multiple LMCm and LMCl molecular markers and preferentially innervated and formed synapses with limb muscle both *in vitro* and *in vivo*.

Supplementary Figure 3-S1

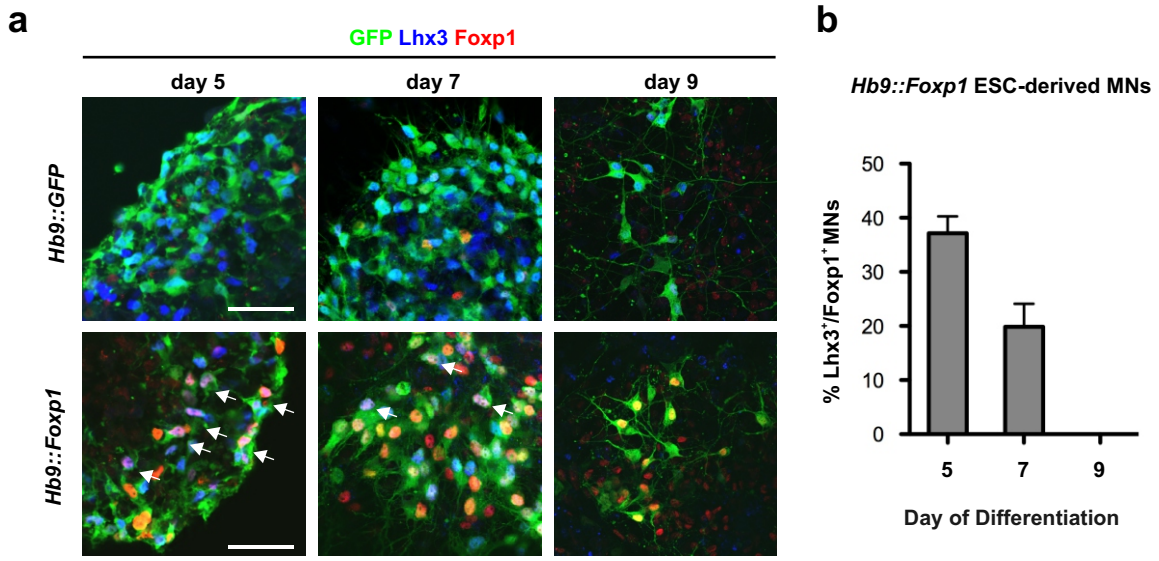

Supplementary Figure 3-S1 Lhx3$^+$/Foxp1$^+$ *Hb9::Foxp1* MNs are resolved with additional time in culture.

Hb9::GFP and *Hb9::Foxp1* ESC-derived MNs were analyzed by antibody staining for the presence of Lhx3$^+$/Foxp1$^+$ MNs at three time-points after RA/SAG addition.

(**a**) *Hb9::GFP* ESC-derived MNs maintained expression of Lhx3 and did not express Foxp1. A large number of *Hb9::Foxp1* ESC-derived MNs co-expressed Lhx3 and Foxp1 early in differentiation (arrows), but by day 9, Lhx3 expression had turned off in Foxp1$^+$ MNs. Scale bars = 50 μm.

(**b**) Quantification of the percentage of Lhx3$^+$/Foxp1$^+$ MNs generated from *Hb9::Foxp1* ESCs over time (mean ± SEM; n = 5-7 images per day, 520 total MNs for day 5, 478 total MNs for day 7, 264 total MNs for day 9).

Supplementary Figure 3-S2

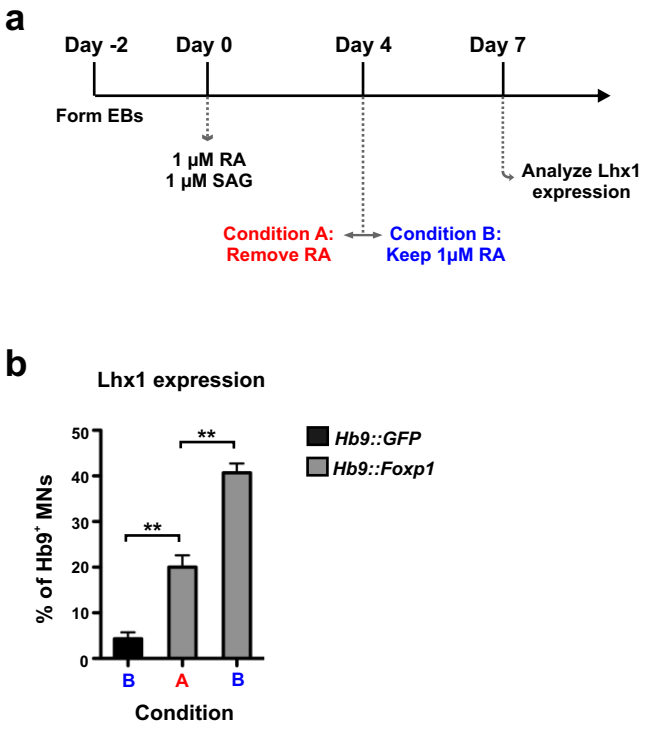

Supplementary Figure 3-S2 Altering RA levels during ESC differentiation affects the percentage of Lhx1^{+} MNs generated by *Hb9::Foxp1* ESC-derived Mns.

(**a**) Schematic diagram of differentiation protocol used to analyze effects of RA concentration. ESC-derived cultures either received RA only up to day 4 (Condition A) or throughout the entire protocol (Condition B). All cultures were analyzed on day 7.

(**b**) Quantification of the percentage of Lhx1^{+} LMCl MNs generated by *Hb9::GFP* and *Hb9::Foxp1* ESC-derived MNs in conditions A and B (mean ± SEM; n = 3 independent experiments, 387 *Hb9::GFP* and 1106 *Hb9::Foxp1* MNs total; one-way ANOVA with Bonferroni adjustments). Left to right: **p-value = 0.0051 and **p-value = 0.0014.

Supplementary Figure 3-S3

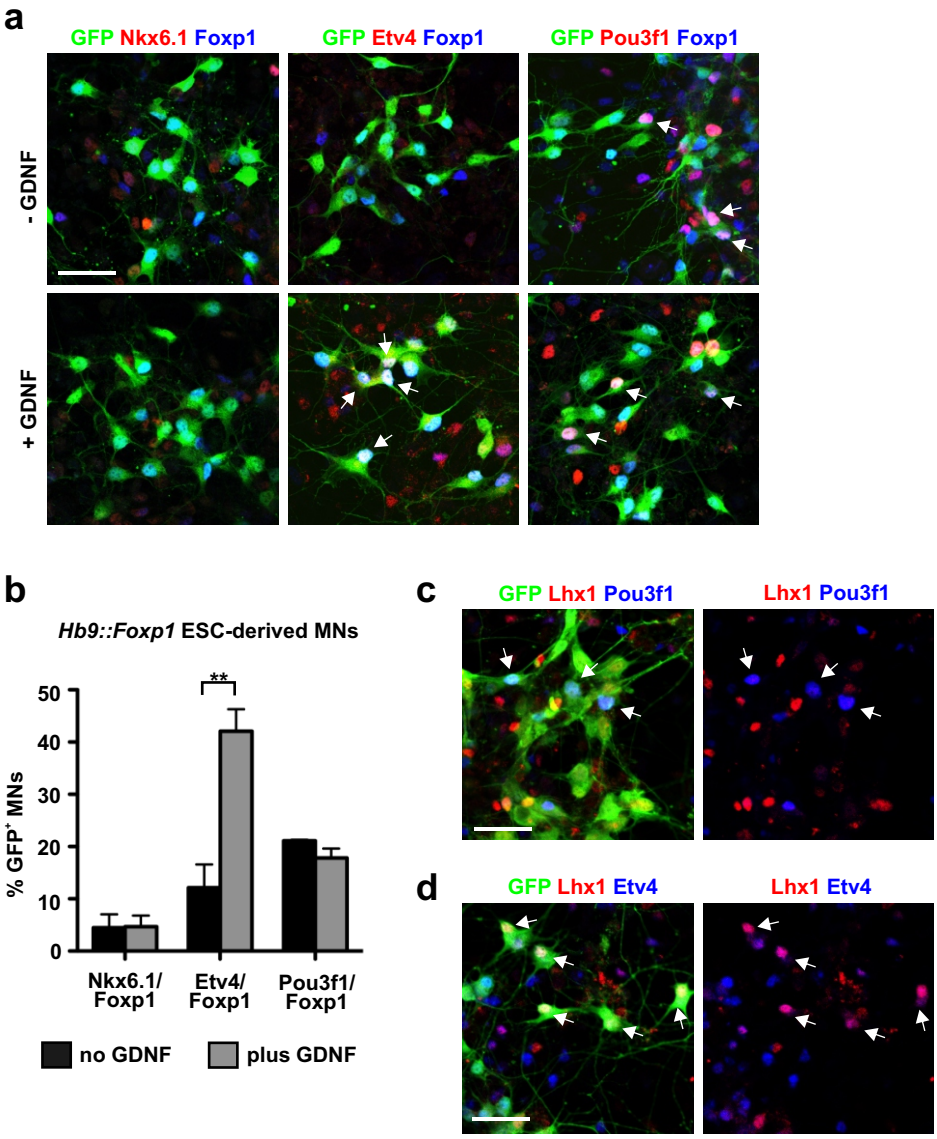

Supplementary Figure 3-3S Etv4, but not Pou3f1, expression by *Hb9::Foxp1* ESC-derived MNs is dependent on GDNF exposure.

(**a**) In the absence of GDNF (-GDNF) *Hb9::Foxp1* MNs expressed low levels of Etv4, but maintained expression of Pou3f1 (arrows). In the presence of GDNF (+GDNF), *Hb9::Foxp1* MNs expressed high levels of both Etv4 and Pou3f1 (arrows). $Foxp1^+$ MNs did not express Nkx6.1 in either condition. Scale bars = 50 μm.

(**b**) Quantification of the percentage of GFP^+ MNs that expressed cervical LMC motor pool markers in the absence and presence of GDNF (mean + SEM; n = 3 independent experiments; Student's t-test). **p-value = 0.008.

(**c**) $Pou3f1^+$ *Hb9::Foxp1* MNs did not express Lhx1 (arrows). Scale bar = 50 μm.

(**d**) $Etv4^+$ *Hb9::Foxp1* MNs also expressed Lhx1 (arrows). Scale bar = 50 μm.

Supplementary Figure 3-S4

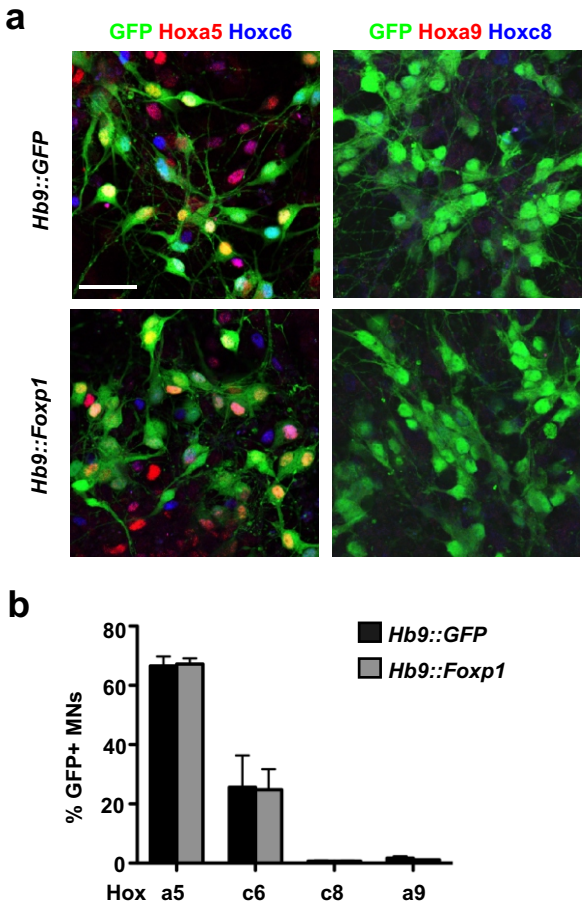

Supplementary Figure 3-S4 Foxp1 misexpression does not alter the Hox expression profile of ESC-derived MNs.

(**a**) Both *Hb9::GFP* and *Hb9::Foxp1* ESC-derived MNs expressed rostral forelimb Hox proteins Hoxa5 and Hoxc6, but did not express more caudal Hox proteins Hoxc8 and Hoxa9. Scale bar = 50 μm.

(**b**) Quantification of the percentage of GFP^+ MNs that expressed each Hox protein (mean ± SEM; n = 3 independent experiments, 1404 *Hb9::GFP* and 891 *Hb9::Foxp1* MNs total).

Supplementary Figure 3-S5

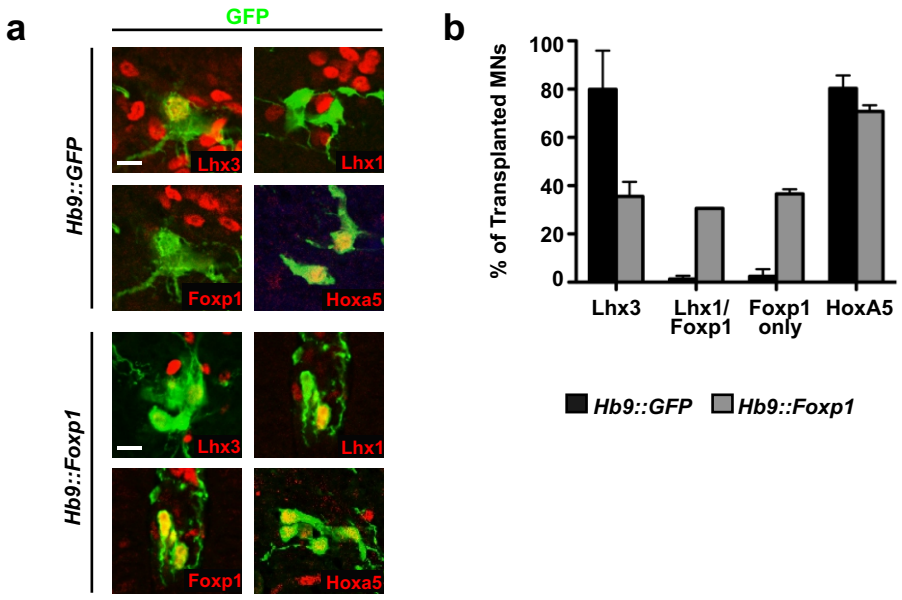

Supplementary Figure 3-S5 ESC-derived MNs do not change their molecular profile upon transplantation into the chick neural tube.

(**a**) Transplanted *Hb9::GFP* MNs maintained expression of Lhx3 and Hoxa5. *Hb9::Foxp1* transplanted MNs expressed reduced levels of Lhx3 and increased levels of Foxp1 and Lhx1. All Lhx1^{+}MNs co-expressed Foxp1. Scale bars = 10 µm.

(**b**) Quantification of the percentage of transplanted ESC-derived MNs that express different MN subtype markers (mean ± SEM; n = 85 *Hb9::GFP* transplanted cells and 79 *Hb9::Foxp1* transplanted cells).

Supplementary Figure 3-S6

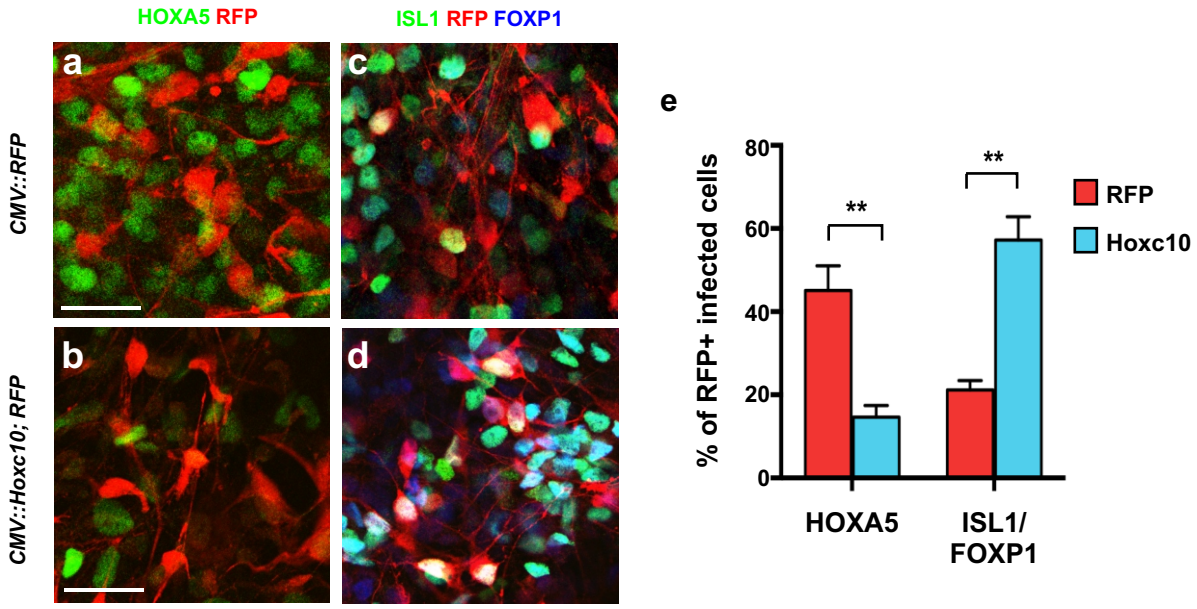

Supplementary Figure 3-S6 Hoxc10 overexpression alters the diversity of MNs generated from human ESCs

(**a-b**) The majority of human ESC-derived MNs expressed HOXA5 after infection with RFP virus. Hoxc10 overexpression reduced the number of RFP+/HOXA5+ human ESC-derived MNs. Scale bars = 25 µm.

(**c-d**) Few RFP+ human ESC-derived MNs expressed ISL1 and FOXP1 under normal conditions. Hoxc10 overexpression increased the number of ISL1+/FOXP1+ human ESC-derived MNs.

(**e**) Quantification of the percentage of RFP+ cells that expressed HOXA5 or ISL1/FOXP1 after infection with RFP lentivirus or Hoxc10 lentivirus (mean ± SEM; n = 3 images per stain; Student's t-test). **p-value = 0.0018 and **p-value = 0.0039 from left to right.

BIBLIOGRAPHY

1. Soundararajan, P., Miles, G.B., Rubin, L.L., Brownstone, R.M. & Rafuse, V.F. Motoneurons derived from embryonic stem cells express transcription factors and develop phenotypes characteristic of medial motor column neurons. *The Journal of neuroscience : the official journal of the Society for Neuroscience* **26**, 3256-3268 (2006).

2. Francius, C. & Clotman, F. Generating spinal motor neuron diversity: a long quest for neuronal identity. *Cell. Mol. Life Sci.* **71**, 813-829 (2014).

3. Davis-Dusenbery, B.N., Williams, L.A., Klim, J.R. & Eggan, K. How to make spinal motor neurons. *Development* **141**, 491-501 (2014).

4. Dasen, J.S., De Camilli, A., Wang, B., Tucker, P.W. & Jessell, T.M. Hox repertoires for motor neuron diversity and connectivity gated by a single accessory factor, FoxP1. *Cell* **134**, 304-316 (2008).

5. Rousso, D.L., Gaber, Z.B., Wellik, D., Morrisey, E.E. & Novitch, B.G. Coordinated actions of the forkhead protein Foxp1 and Hox proteins in the columnar organization of spinal motor neurons. *Neuron* **59**, 226-240 (2008).

6. Hu, B.Y. & Zhang, S.C. Differentiation of spinal motor neurons from pluripotent human stem cells. *Nature protocols* **4**, 1295-1304 (2009).

7. Wichterle, H., Lieberam, I., Porter, J.A. & Jessell, T.M. Directed differentiation of embryonic stem cells into motor neurons. *Cell* **110**, 385-397 (2002).

8. Wichterle, H. & Peljto, M. Differentiation of mouse embryonic stem cells to spinal motor neurons. *Curr Protoc Stem Cell Biol* **Chapter 1**, Unit 1H 1 1-1H 1 9 (2008).

9. Qu, Q.*, et al.* High-efficiency motor neuron differentiation from human pluripotent stem cells and the function of Islet-1. *Nat Commun* **5**, 3449 (2014).

10. Peljto, M., Dasen, J.S., Mazzoni, E.O., Jessell, T.M. & Wichterle, H. Functional diversity of ESC-derived motor neuron subtypes revealed through intraspinal transplantation. *Cell Stem Cell* **7**, 355-366 (2010).

11. Surmeli, G., Akay, T., Ippolito, G.C., Tucker, P.W. & Jessell, T.M. Patterns of spinal sensory-motor connectivity prescribed by a dorsoventral positional template. *Cell* **147**, 653-665 (2011).

12. Wang, B.*, et al.* Foxp1 regulates cardiac outflow tract, endocardial cushion morphogenesis and myocyte proliferation and maturation. *Development* **131**, 4477-4487 (2004).

13. Nagy, A., Gertsenstein, M., Vintersten, K. & Behringer, R. Collecting zygotes and removing cumulus cells with hyaluronidase. *CSH Protoc* **2006** (2006).

14. Nagy, A., Gertsenstein, M., Vintersten, K. & Behringer, R. De Novo Isolation of Embryonic Stem (ES) Cell Lines from Blastocysts. *CSH Protoc* **2006** (2006).

15. Umbach, J.A., Adams, K.L., Gundersen, C.B. & Novitch, B.G. Functional neuromuscular junctions formed by embryonic stem cell-derived motor neurons. *PLoS One* **7**, e36049 (2012).

16. Wichterle, H., Peljto, M. & Nedelec, S. Xenotransplantation of embryonic stem cell-derived motor neurons into the developing chick spinal cord. *Methods Mol Biol* **482**, 171-183 (2009).

17. Rousso, D.L.*, et al.* Foxp-mediated suppression of N-cadherin regulates neuroepithelial character and progenitor maintenance in the CNS. *Neuron* **74**, 314-330 (2012).

18. Ji, S.J., *et al.* Mesodermal and neuronal retinoids regulate the induction and maintenance of limb innervating spinal motor neurons. *Dev Biol* **297**, 249-261 (2006).

19. Arber, S., Ladle, D.R., Lin, J.H., Frank, E. & Jessell, T.M. ETS gene Er81 controls the formation of functional connections between group Ia sensory afferents and motor neurons. *Cell* **101**, 485-498 (2000).

20. Gaber, Z.B., Butler, S.J. & Novitch, B.G. PLZF regulates fibroblast growth factor responsiveness and maintenance of neural progenitors. *PLoS Biol* **11**, e1001676 (2013).

21. Arber, S., *et al.* Requirement for the homeobox gene Hb9 in the consolidation of motor neuron identity. *Neuron* **23**, 659-674 (1999).

22. Dasen, J.S., Tice, B.C., Brenner-Morton, S. & Jessell, T.M. A Hox regulatory network establishes motor neuron pool identity and target-muscle connectivity. *Cell* **123**, 477-491 (2005).

23. Ericson, J., Briscoe, J., Rashbass, P., van Heyningen, V. & Jessell, T.M. Graded sonic hedgehog signaling and the specification of cell fate in the ventral neural tube. *Cold Spring Harb Symp Quant Biol* **62**, 451-466 (1997).

24. Tsuchida, T., *et al.* Topographic organization of embryonic motor neurons defined by expression of LIM homeobox genes. *Cell* **79**, 957-970 (1994).

25. Bader, D., Masaki, T. & Fischman, D.A. Immunochemical analysis of myosin heavy chain during avian myogenesis in vivo and in vitro. *The Journal of cell biology* **95**, 763-770 (1982).

26. De Marco Garcia, N.V. & Jessell, T.M. Early motor neuron pool identity and muscle nerve trajectory defined by postmitotic restrictions in Nkx6.1 activity. *Neuron* **57**, 217-231 (2008).

27. Ilia, M.*, et al.* Expression of Oct-6, a POU III domain transcription factor, in schizophrenia. *Am J Psychiatry* **159**, 1174-1182 (2002).

28. Matthew, W.D., Tsavaler, L. & Reichardt, L.F. Identification of a synaptic vesicle-specific membrane protein with a wide distribution in neuronal and neurosecretory tissue. *The Journal of cell biology* **91**, 257-269 (1981).

29. Trevarrow, B., Marks, D.L. & Kimmel, C.B. Organization of hindbrain segments in the zebrafish embryo. *Neuron* **4**, 669-679 (1990).

30. Beurg, M.*, et al.* Control of exocytosis by synaptotagmins and otoferlin in auditory hair cells. *The Journal of neuroscience : the official journal of the Society for Neuroscience* **30**, 13281-13290 (2010).

31. Sockanathan, S. & Jessell, T.M. Motor neuron-derived retinoid signaling specifies the subtype identity of spinal motor neurons. *Cell* **94**, 503-514 (1998).

32. Vrieseling, E. & Arber, S. Target-induced transcriptional control of dendritic patterning and connectivity in motor neurons by the ETS gene Pea3. *Cell* **127**, 1439-1452 (2006).

33. Lacombe, J.*, et al.* Genetic and functional modularity of Hox activities in the specification of limb-innervating motor neurons. *PLoS Genet* **9**, e1003184 (2013).

34. Haase, G.*, et al.* GDNF acts through PEA3 to regulate cell body positioning and muscle innervation of specific motor neuron pools. *Neuron* **35**, 893-905 (2002).

35. Machado, C.B.*, et al.* Reconstruction of phrenic neuron identity in embryonic stem cell-derived motor neurons. *Development* **141**, 784-794 (2014).

36. Philippidou, P., Walsh, C.M., Aubin, J., Jeannotte, L. & Dasen, J.S. Sustained Hox5 gene activity is required for respiratory motor neuron development. *Nature neuroscience* **15**, 1636-1644 (2012).

37. Dasen, J.S., Liu, J.P. & Jessell, T.M. Motor neuron columnar fate imposed by sequential phases of Hox-c activity. *Nature* **425**, 926-933 (2003).

38. Kania, A. & Jessell, T.M. Topographic motor projections in the limb imposed by LIM homeodomain protein regulation of ephrin-A:EphA interactions. *Neuron* **38**, 581-596 (2003).

39. Helmbacher, F., Schneider-Maunoury, S., Topilko, P., Tiret, L. & Charnay, P. Targeting of the EphA4 tyrosine kinase receptor affects dorsal/ventral pathfinding of limb motor axons. *Development* **127**, 3313-3324 (2000).

40. Kramer, E.R.*, et al.* Cooperation between GDNF/Ret and ephrinA/EphA4 signals for motor-axon pathway selection in the limb. *Neuron* **50**, 35-47 (2006).

41. Luria, V., Krawchuk, D., Jessell, T.M., Laufer, E. & Kania, A. Specification of motor axon trajectory by ephrin-B:EphB signaling: symmetrical control of axonal patterning in the developing limb. *Neuron* **60**, 1039-1053 (2008).

42. Ebens, A.*, et al.* Hepatocyte growth factor/scatter factor is an axonal chemoattractant and a neurotrophic factor for spinal motor neurons. *Neuron* **17**, 1157-1172 (1996).

43. Yamamoto, Y.*, et al.* Hepatocyte growth factor (HGF/SF) is a muscle-derived survival factor for a subpopulation of embryonic motoneurons. *Development* **124**, 2903-2913 (1997).

44. Shirasaki, R., Lewcock, J.W., Lettieri, K. & Pfaff, S.L. FGF as a target-derived chemoattractant for developing motor axons genetically programmed by the LIM code. *Neuron* **50**, 841-853 (2006).

45. Sendtner, M., Pei, G., Beck, M., Schweizer, U. & Wiese, S. Developmental motoneuron cell death and neurotrophic factors. *Cell Tissue Res.* **301**, 71-84 (2000).

46. Hadas, Y.*, et al.* A 'tool box' for deciphering neuronal circuits in the developing chick spinal cord. *Nucleic Acids Res* (2014).

47. Amoroso, M.W.*, et al.* Accelerated high-yield generation of limb-innervating motor neurons from human stem cells. *J. Neurosci.* **33**, 574-586 (2013).

48. Wu, Y., Wang, G., Scott, S.A. & Capecchi, M.R. Hoxc10 and Hoxd10 regulate mouse columnar, divisional and motor pool identity of lumbar motoneurons. *Development* **135**, 171-182 (2008).

49. Kanning, K.C., Kaplan, A. & Henderson, C.E. Motor neuron diversity in development and disease. *Annu Rev Neurosci* **33**, 409-440 (2010).

50. Winner, B., Marchetto, M.C., Winkler, J. & Gage, F.H. Human-induced pluripotent stem cells pave the road for a better understanding of motor neuron disease. *Hum Mol Genet* (2014).

51. Sandoe, J. & Eggan, K. Opportunities and challenges of pluripotent stem cell neurodegenerative disease models. *Nature neuroscience* **16**, 780-789 (2013).

52. Dalla Torre di Sanguinetto, S.A., Dasen, J.S. & Arber, S. Transcriptional mechanisms controlling motor neuron diversity and connectivity. *Current opinion in neurobiology* **18**, 36-43 (2008).

53. Arber, S. Motor circuits in action: specification, connectivity, and function. *Neuron* **74**, 975-989 (2012).

54. Amoroso, M.W.*, et al.* Accelerated high-yield generation of limb-innervating motor neurons from human stem cells. *The Journal of neuroscience : the official journal of the Society for Neuroscience* **33**, 574-586 (2013).

55. Hester, M.E.*, et al.* Rapid and efficient generation of functional motor neurons from human pluripotent stem cells using gene delivered transcription factor codes. *Mol Ther* **19**, 1905-1912 (2011).

56. Son, E.Y.*, et al.* Conversion of mouse and human fibroblasts into functional spinal motor neurons. *Cell Stem Cell* **9**, 205-218 (2011).

57. Theys, P.A., Peeters, E. & Robberecht, W. Evolution of motor and sensory deficits in amyotrophic lateral sclerosis estimated by neurophysiological techniques. *J Neurol* **246**, 438-442 (1999).

58. O'Brien, M.K., Landmesser, L. & Oppenheim, R.W. Development and survival of thoracic motoneurons and hindlimb musculature following transplantation of the thoracic neural tube to the lumbar region in the chick embryo: functional aspects. *J Neurobiol* **21**, 341-355 (1990).

59. O'Brien, M.K. & Oppenheim, R.W. Development and survival of thoracic motoneurons and hindlimb musculature following transplantation of the thoracic neural tube to the lumbar region in the chick embryo: anatomical aspects. *J Neurobiol* **21**, 313-340 (1990).

CHAPTER 4 – Functional Neuromuscular Junctions Formed by Embryonic Stem Cell-Derived Motor Neurons

ABSTRACT

A key objective of stem cell biology is to create physiologically relevant cells suitable for modeling disease pathologies *in vitro*. Much progress towards this goal has been made in the area of motor neuron (MN) disease through the development of methods to direct spinal MN formation from both embryonic and induced pluripotent stem cells. Previous studies have characterized these neurons with respect to their molecular and intrinsic functional properties. However, the synaptic activity of stem cell-derived MNs remains less well defined. In this study, we report the development of low-density co-culture conditions that encourage the formation of active neuromuscular synapses between stem cell-derived MNs and muscle cells *in vitro*. Fluorescence microscopy reveals the expression of numerous synaptic proteins at these contacts, while dual patch clamp recording detects both spontaneous and multi-quantal evoked synaptic responses similar to those observed *in vivo*. Together, these findings demonstrate that stem cell-derived MNs innervate muscle cells in a functionally relevant manner. This dual recording approach further offers a sensitive and quantitative assay platform to probe disorders of synaptic dysfunction associated with MN disease.

This chapter is modified from:

Umbach JA, Adams KL, Gunderson CB, and Novitch BG. (2012) Functional neuromuscular junctions formed by embryonic stem cell-derived motor neurons. *PLoS One 7, e36049*.

JAU performed the electrophysiology. KLA generated the motor neurons. JAU, KLA, CBG, and BGN wrote the paper.

INTRODUCTION

All motor functions from locomotion to respiration depend on the communication between motor neurons (MNs) in the spinal cord and muscle cells in different regions of the body. This vital activity is susceptible to many neurodegenerative diseases, most notably Amyotrophic lateral sclerosis (ALS) and Spinal muscular atrophy (SMA), resulting in MN dysfunction and ultimately death [1, 2]. While progress has been made in identifying genes associated with MN degeneration [3-5], the molecular and cellular processes underlying disease onset and progression remain unclear.

Over the past decade, considerable attention has been focused on using stem cell-derived MNs to model disease pathogenesis, driven by demonstrations that mouse and human embryonic stem cells (mESCs and hESCs) can be directed to form MNs in response to developmental signals that promote MN formation *in vivo* [6-9]. Recent studies have further shown that MNs can be similarly produced from induced pluripotent stem cells (iPSC) including those derived from ALS and SMA patients [10-12], and through transcription factor-mediated reprogramming of fibroblasts [13]. A remaining challenge, however, is to establish methods to evaluate the function of normal and diseased MNs obtained from these sources in a physiologically relevant setting.

An important step towards this goal is the development of *in vitro* assays to measure the synaptic activity of MNs at neuromuscular junctions, as many studies have pointed to synaptic dysfunction as an early readout and possibly an initiating event in MN disease progression [14, 15]. ESC and iPSC-derived MNs have previously been shown to exhibit many molecular and physiological properties associated with mature MNs [12, 16, 17]. Moreover, when transplanted into the embryonic chick spinal cord [9, 18, 19] or peripheral nerve of mice [20], these neurons appear to be capable of extending axons towards peripheral muscle targets. Despite these successes, relatively little attention has been placed on direct measurements of the communication

between stem cell-derived MNs and muscle cells. In part, this reflects the inherent difficulties in isolating connected pairs of cells in mass culture or transplantation settings.

In this study, we report the development of low-density culture conditions that encourage the formation of neuromuscular junctions between isolated ESC-derived MNs and muscle cells. This system enables the direct measurement of synaptic communication through dual patch clamp recordings. In this setting, MNs form neuromuscular junctions containing functionally important synaptic proteins, and these synapses exhibit both spontaneous and stimulus-evoked transmitter release. Together, these findings constitute an important advance in validating the functional identity of stem cell-derived MNs and providing a platform for defining their synaptic properties under normal and diseased conditions.

MATERIALS AND METHODS

Differentiation of mESCs. *Hb9::EGFP* mESCs [9] were maintained and differentiated into MNs as previously described [9, 21]. Briefly, mESCs were plated on 60 mm bacterial petri dishes in core MN medium to elicit embryoid body (EB) formation. Core MN medium consisted of a 1:1 mixture of Dulbecco's Modified Eagle's Medium/F12 (DMEM/F12) and Neurobasal Medium supplemented with Knockout Serum Replacement, Glutamax, and 2-mercaptoethanol (560 nM), Penicillin/Streptomycin, and Primocin (50 µg/ml; Invivogen). Except as noted, media components were obtained from Invitrogen. After 1 d in culture, EBs were pipetted through a 100 mm strainer to remove large aggregates. The next day, EB culture media was replaced with MN differentiation medium [core MN medium containing N2 supplement (1x), Retinoic Acid (1 mM; Sigma) and Purmorphamine (1.5 mM; EMD Biosciences)]. After 5 d of differentiation, EBs were dissociated using papain (0.5 U/ml; Worthington) in HBSS for 20 min at 37^{o}C with gentle trituration. Cells were collected by centrifugation and washed with MN differentiation medium prior to plating with muscle cells.

Co-culture of MNs and C2C12 muscle cells. C2C12 cells (CRL-1772) were obtained from the American Type Culture Collection and cultured in myoblast growth medium [DMEM supplemented with 15% fetal bovine serum (FBS), L-glutamine (1 mM) and antibiotics as above]. When the cells reached 60-70% confluence, they were washed with PBS and transferred to muscle differentiation medium [DMEM with 0.5% FBS, insulin (10 mg/ml)-transferrin (5.5 mg/ml)-selenium (39 nM), L-glutamine (1 mM) and antibiotics]. After 2 d, the medium was supplemented with cytosine arabinoside (Ara-C; 10 mM), and cells were cultured for another 2 d to eliminate dividing cells. Differentiated myotube cultures were dissociated using trypsin (0.05%) and plated at low density on Matrigel-coated 35 mm culture dishes (1,200 cells/dish) in differentiation medium containing Ara-C. 1-2 d after muscle cells were plated, 1,500 mESC-derived MNs were added to each dish and the medium was changed to core MN medium supplemented with N2 (1x), Brain-Derived Neurotrophic factor (10 ng/ml), Glia-Derived Neurotrophic Factor (10 ng/ml), and Ciliary Neurotrophic Factor (10 ng/ml); neurotrophic factors were obtained from Prospec. Within 1-2 d, motor axons made contact with muscle cells, and functional nerve-muscle contacts were observed for at least 6-7 d.

Fluorescence microscopy and immunostaining. Cultures were fixed in 3% paraformaldehyde in PBS for 15 min, washed twice with PBS, permeabilized with 0.1% Triton X-100 in PBS for 15 min, and blocked in 10% normal goat serum in PBS for 15 min. Primary antibodies (0.5-2 mg/ml) were added and specimens were incubated for 12-16 h at 4°C. After extensive PBS washes specimens were incubated with secondary antibodies (Alexa 594 goat anti-mouse or goat anti-rabbit IgG; Invitrogen) for 1h followed by PBS washes. The following primary antibodies were used: Slc18a3 (VAChT, Millipore; AB1588); Slc5a7 (choline transporter 1 (ChT1), Millipore; AB5966)); Sv2 (Developmental Studies Hybridoma Bank); Snap25 (Stressgen; VAP-SV0002); synaptophysin (Syp, Sigma; S-5768); syntaxin 1a (Stx1a, Stressgen; VAM-SV013). Nicotinic acetylcholine (ACh) receptors were detected through bath application of

Alexa 594-a-bungarotoxin (Invitrogen) to the cultures prior to fixation. Epifluorescence images were obtained using an Olympus IX70 inverted microscope equipped with a Sensicam cooled CCD camera (PCO) and a Lambda 10 shutter (Sutter Instruments) controlled by Axon Instruments Imaging Workbench. Images were processed using Adobe Photoshop and CorelDRAW software.

Electrophysiology. Cultures were screened for isolated MN-muscle cell pairs where the axon branched minimally and the axon terminal formed a visible contact with a muscle cell that was < 0.1 mm from the cell body. Patch pipettes were sealed sequentially onto both cells using methods described in [22]. Pipette solutions were in mM, muscle: K-gluconate (140), Hepes (10), $CaCl_2$ (1), $MgCl_2$ (1), EGTA (11), QX-314 (5); neuron: K-gluconate (140), Hepes (10), EGTA (1), Mg-ATP (4), Na-GTP (0.3). The bath solution for recording was in mM: NaCl (120), KCl (1.9), KH_2PO_4 (1.2), Na-bicarbonate (20), $CaCl_2$ (2.2), $MgCl_2$ (1.4), Hepes (7.5). In all cases, pH was adjusted to 7.2. Cells with resting potentials < -30 mV were discarded. After an initial period to record at least 25 spontaneous miniature excitatory post synaptic currents (mEPCs) in the muscle cell (voltage clamped at -80 mV), MNs (maintained in current clamp mode at approximately -70 mV) were stimulated by 0.5 msec current injections of increasing amplitude from +0.5 to +6 nA. Data were collected using Axopatch 2B patch clamp amplifiers with 4-pole Bessel filtering at 5 kHz. Signals were digitized and stored using pClamp and Axotape software (Axon Instruments) and analyzed using pClamp and miniAnalysis (Synaptosoft).

RESULTS

ESC-derived MNs form cholinergic synapses on muscle cells under low-density co-culture conditions

To evaluate the synaptic activity of ESC-derived MNs, we first developed culture conditions that were amenable to patch clamp analysis of MN-muscle pairs. The initial step was

to test whether cells could form synaptic contacts when plated at low density (1,200 muscle cells and 1,500 *Hb9::EGFP*$^{+}$ MNs per 35 mm dish). We reasoned that such conditions might encourage the preferential growth of motor axons to nearby partners and minimize non-synaptic contacts made when cells are plated at high densities. Under these conditions, each culture dish yielded 1-4 isolated MN-muscle cell pairs with *Hb9::EGFP*$^{+}$ axons projecting towards spindle-shaped muscle cells (**Fig. 4-1 A, B**). At the point of contact between the axons and muscle cells there was a varicose enlargement of the terminal bouton (**Figs. 4-1 and 4-2**). Bouton diameter ranged from 3-11 mm in diameter with a mean diameter of 6.9 ± 2.0 mm (n = 65) and was easily distinguished from motor neuron soma, which were typically > 20 mm in diameter. This geometry of neuron-muscle pairing was sufficiently common that it enabled the reliable identification of nerve and muscle cells that were likely to have made functional synaptic contacts. The presence of a-bungarotoxin (BTX) staining (**Fig. 4-1 C-E**) further indicated that nicotinic ACh receptors preferentially accumulated at these sites.

We next used immunofluorescence microscopy to investigate whether other macromolecules characteristic of cholinergic synapses were present at the nerve-muscle contacts. Proteins associated with ACh metabolism including Slc18a3 (VAChT) and the high affinity choline transporter Slc5a7 were detected at these sites along with the SNARE proteins Snap25 and Syntaxin 1a (**Fig. 4-2 A-L***)*. Concomitantly, synaptic vesicle proteins such as synaptophysin and SV2 were also present (**Fig. 4-2 M-R**). These results were representative of data obtained from at least two separate culture dishes for each antibody. In each dish, at least 4 neuromuscular junctions were imaged and every *Hb9::eGFP*$^{+}$ terminal showed immunoreactivity for these presynaptic proteins. Collectively, these data indicate that sites of contact between ESC-derived MNs and muscle cells contain components of the molecular machinery associated with cholinergic synapses.

Neuromuscular synapses formed *in vitro* are functional and trigger both spontaneous and evoked muscle contractions

To determine whether the nerve-muscle contacts formed in culture exhibit the functional properties of neuromuscular junctions, we sealed patch clamp pipettes onto MN-muscle pairs. Current injection into the ESC-derived MNs initially elicited passive membrane responses in the MNs, but no electrical response in muscle cells beyond the stimulus artifact (**Fig. 4-3 A**). However, once threshold was exceeded, the MNs fired an action potential. With a brief delay (1-3 msec), MN action potentials were followed by an excitatory post-synaptic current (EPC) in the muscle cells (**Fig. 4-3 A**). These EPCs are reminiscent of the classical electrophysiological signature of synaptic communication between MNs and muscle cells observed in en-bloc preparations [23].

From 60 dishes examined, 111 neuron-muscle pairs with geometries similar to that shown in Fig. 4-1 A were identified. Successful patches (where the resting potential in both cells was > -30 mV) were obtained for ~37% of these pairs (41/111), of which ~90% (37/41) showed functional synaptic responses as illustrated in Fig. 4-3 A. Overall, muscle resting membrane potentials averaged -53.6 ± 9.5 mV; S.D., while neuron resting potentials were 40.9 mV ± 9.4 mV; S.D. The records in Fig. 4-3 A also illustrate the variability in the synaptic delay, amplitude and time course of EPCs. Scatter plots summarize the observed range of synaptic delays, EPC amplitudes, EPC rise times, and EPC decays (**Fig. 4-4 A-D**). In particular, EPC amplitude varied from <100 pA at some synapses on day 3 to >1 nA on 4 day (**Fig. 4-4 A**). EPCs were abolished by the addition of the nicotinic ACh receptor antagonist, *d*-tubocurarine (10 mM, n = 3 trials; Fig. 3B), confirming the cholinergic nature of these EPCs. EPCs were similarly eliminated by replacement of extracellular Ca^{2+} with 10 mM Mg^{2+} (n = 3 trials; data not shown). Moreover, in parallel experiments using a patch pipette on the neuron alone, triggering of neuronal action potentials led to visible muscle contractions in ~20% of the trials evaluated (3/15; data not shown). Collectively, these data indicate that the neuromuscular junctions formed in these

cultures exhibit stimulus-evoked and Ca^{2+}-dependent neurotransmitter release capable of triggering muscle contraction.

An important advantage of the dual patch configuration is that it enables one to conduct additional quantitative analyses of both spontaneous and evoked synaptic events at these neuromuscular junctions. We thus evaluated the profile of spontaneous miniature (m) EPCs recorded in muscle cells for which evoked EPCs were also obtained (**Fig. 4-5 A-D**). The mEPC amplitude distribution (**Fig. 4-5 B**) is typical of the skewed Gaussian distribution observed at 70% of the nerve-muscle contacts in these cultures. Cumulatively, mEPC frequencies ranged from 0.04-0.30 Hz, with mEPC frequencies < 0.1 Hz characteristic of 3 d old cultures and > 0.1 Hz after 4 days in culture (**Fig. 4-5 C**). Although we have not yet undertaken a systematic evaluation of the quantal content of the EPCs in this system, it is important to note that EPCs such as that shown in Fig.4-5 A are very likely comprised of multiple quanta. This conclusion derives from the fact that the amplitude of this EPC is at least five times greater than the largest mEPC (**Fig. 4-5 A, B, D**). Based on this criterion, multi-quantal EPCs were observed in ~95% (36/37) of the neuromuscular junctions from which mEPC/EPC recordings were obtained. Taken together, these data indicate that mESC-derived MNs are capable of coupling action potentials to the synchronous release of multiple quanta at these nerve-muscle contacts to elicit muscle contractions.

DISCUSSION

The definitive feature of MNs is their ability to form functional neuromuscular junctions and thereby drive the contraction of skeletal muscle cells. Our study provides critical evidence that ESC-derived MNs can exhibit robust synaptic communication with muscle cells under simplified *in vitro* culture conditions. Empirically, this is a significant observation, as the use of stem cell-derived MNs for regenerative purposes or disease modeling requires that the cells faithfully mimic their natural counterparts in both molecular and functional properties. Our data

show that ESC-derived MNs express several proteins, including nicotinic ACh receptors, Slc18a3 (VAChT), the high affinity choline transporter Slc5a7, and SNARE proteins found at native neuromuscular junctions, and exhibit both spontaneous and action potential-dependent, multi-quantal secretion of ACh to trigger post-synaptic potentials and muscle contraction. These results further provide an important extension to previous studies that have used bath application of glutamate to evoke post-synaptic potentials and muscle contraction in high-density MN-muscle cell cultures [13, 16, 24]. Moreover, the ability to quantify the functional properties of individual nerve-muscle contacts offers the opportunity to rigorously assess the impact of a variety of experimental manipulations on these synaptic events.

To define the synaptic activity of MN-muscle pairs, our investigation was intentionally restricted to the differentiated progeny of mESCs and C2C12 muscle cells. Our data indicate that MN-muscle synapses formed under these simplified conditions recapitulate many features of neuromuscular communication seen *in vivo*. For example, the frequency of spontaneous mEPCs (0.04-0.3 Hz) is within the range reported for muscle fibers of late embryonic and early post-natal rodents [25-28]. Similarly, the rise and decay times of EPCs are within the range observed for developing rat neuromuscular junctions [25]. It is important to note that while functional, MN-muscle synapses formed under these conditions typically survived for a maximum of 8-9 days in culture. This limitation might reflect a lack of support provided *in vivo* by other cells including astrocytes and Schwann cells or presynaptic inputs to the MNs from spinal interneurons. The low-density culture conditions established in this study provide a suitable platform for evaluating the influence of different cell types in future work. Nevertheless, we have found that similar co-culture of human ESC and IPSC-derived motor neurons with muscle cells results in synaptic contacts that persist for several weeks (JAU, KLA, and BGN, unpublished data), suggesting that at least some aspects of synaptic stability are inherent to the MNs themselves and highly variable between species.

During embryonic development, different classes of MNs exhibit a high degree of selectivity in their choice of muscle targets [29, 30]. However, we infer from the present results that the programs that dictate motor innervation patterns are sufficiently malleable such that ESC-derived MNs can form functional synapses on C2C12 cells. Although this observation is not surprising given the promiscuity of mammalian MNs for forming neuromuscular junctions *in vitro* [31], precise matching of MN and muscle subtypes might nevertheless be crucial for ensuring full synaptic activity and stability [32]. Progress has recently been made in understanding the mechanisms underlying MN fate selection [29, 33, 34], and it should be fruitful to determine whether this information can be harnessed to bias the differentiation of mESC-derived MNs to favor the innervation of specific classes of muscle cells both *in vitro* and *in vivo*.

Another important use for this co-culture system will be for modeling neuromuscular disorders. There is abundant evidence for an early and profound impairment of neuromuscular transmission in amyotrophic lateral sclerosis [35], and we showed previously that mutant forms of superoxide dismutase 1 (SOD1) alter the morphology and survival of hESC-derived MNs *in vitro* [36]. Consequently, conditional expression of mutant SOD1 in MN-muscle co-cultures is likely to provide an informative system for clarifying the impact of SOD1 mutant alleles on nerve-muscle communication. Similarly, recent data suggest that proprioceptive circuits may be particularly vulnerable in spinal muscular atrophy [37]. The *in vitro* system developed here might accordingly be expanded to assess the underlying cellular and molecular mechanisms that contribute to this decline in synaptic input to MNs. Thus, in addition to their utility for helping to answer fundamental biological questions, these co-cultures have clear applications in addressing problems of medical significance.

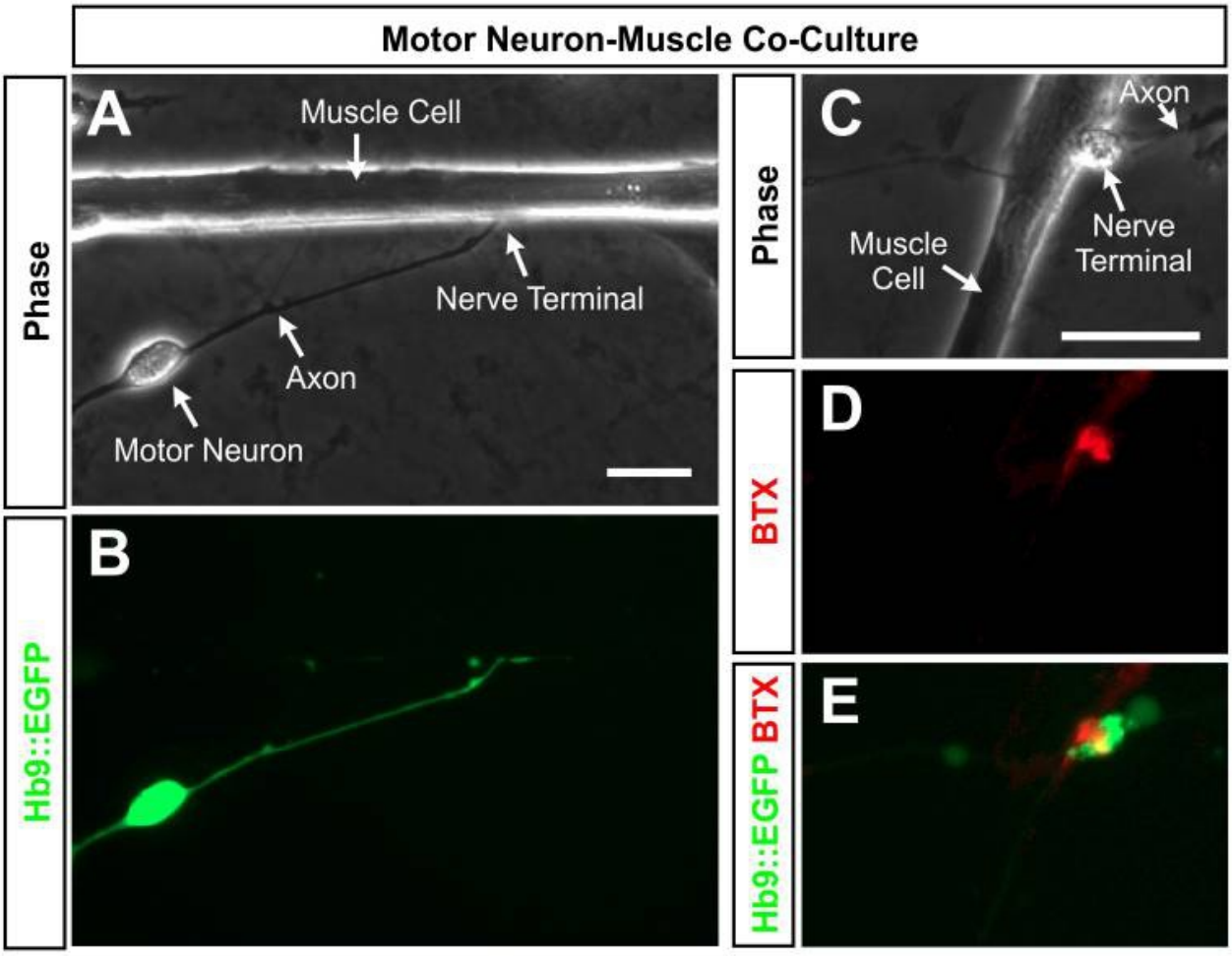

Figure 4-1 Morphology of neuromuscular junctions formed *in vitro* by mESC-derived MNs.

(**A, B**) Brightfield and fluorescence images showing an *Hb9::EGFP*$^{+}$ ESC-derived MN extending an axon to contact a muscle cell under low-density cell culture conditions.

(C-E) The adjacent trio of images shows a representative axonal varicosity contacting a muscle cell stained for nicotinic ACh receptors using fluorescent a-bungarotoxin (BTX) overlaid with *Hb9::EGFP* fluorescence in the MN terminal bouton. Scale bars are 20 μm.

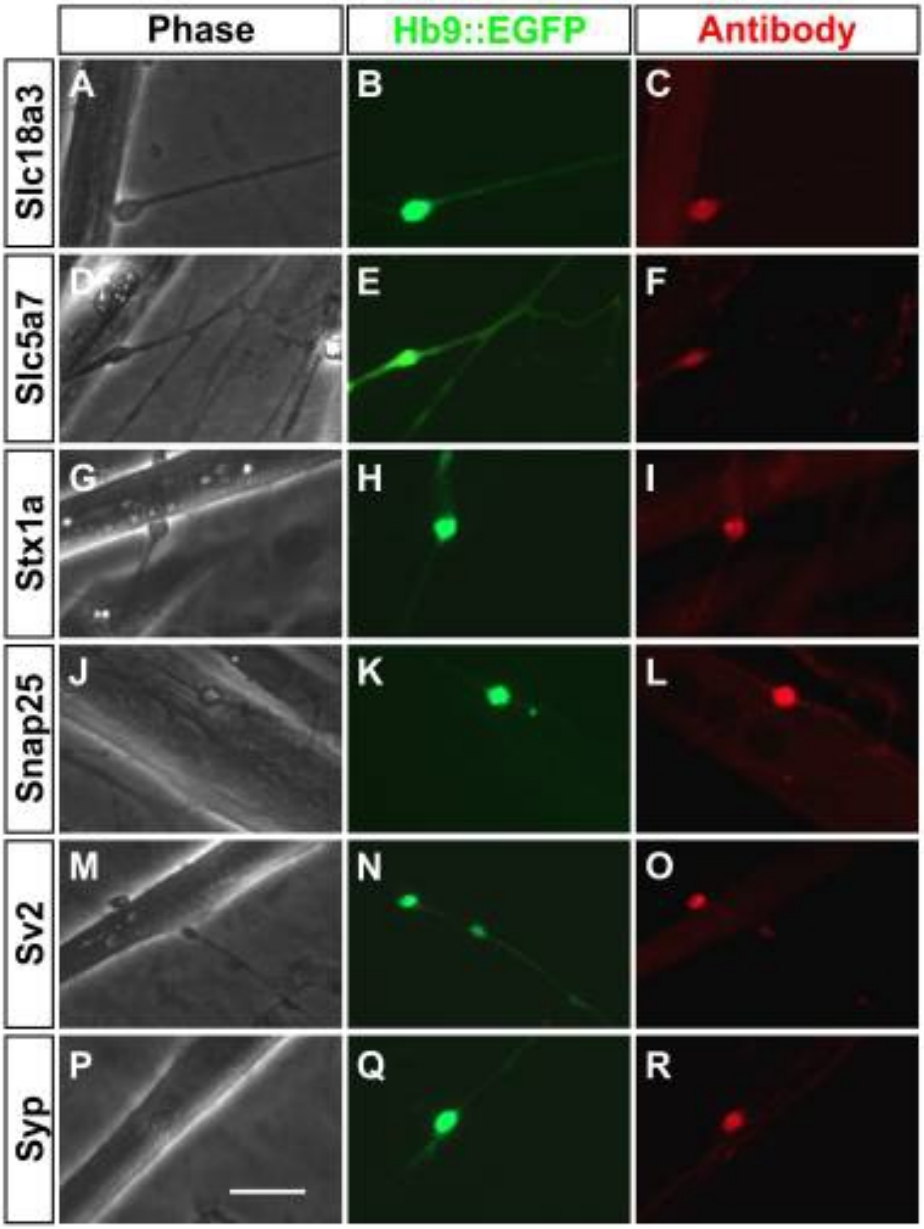

Figure 4-2 mESC-derived MNs form cholinergic synapses with muscle cells *in vitro*. Immunofluorescence analysis of proteins expressed at nerve terminals of mESC-derived Mns.

(**A, D, G, J, M, P**) Brightfield images of axon terminals contacting muscle cells

(**B, E, H, K, N, Q**) Green fluorescence associated with the *Hb9::EGFP* MN reporter

(C, F, I, L, O, R) Red fluorescence corresponding to antibody staining for the indicated presynaptic proteins: Slc18a3 (VAChT), Slc5a7 (ChT1), Syntaxin 1a (Stx1a), Snap25, Sv2, and Synaptophysin (Syp). Scale bar is 20 μm.

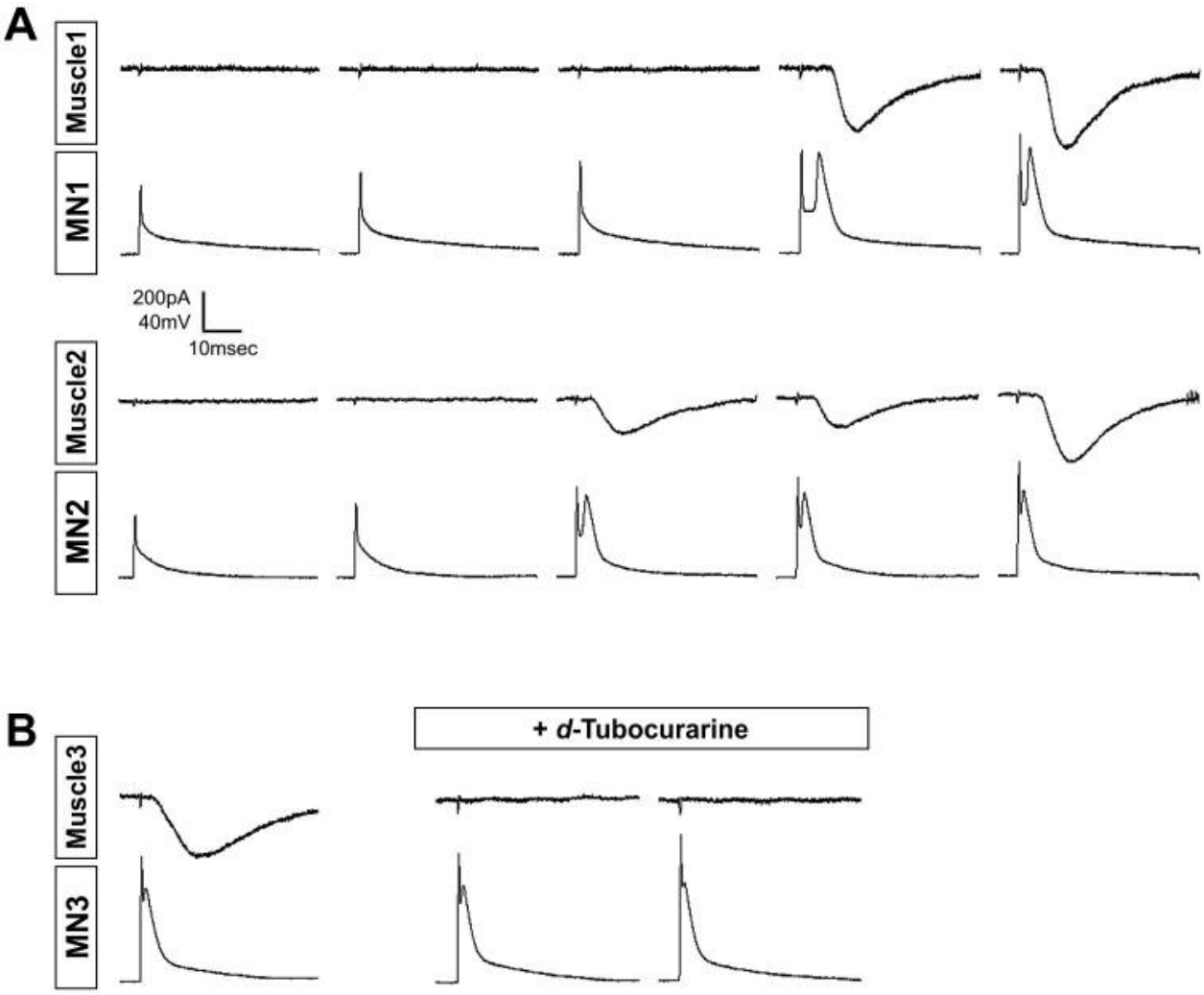

Figure 4-3 mESC-derived MNs trigger a post-synaptic response in muscle cells only when MNs fire action potentials.

(**A**) In each pair of recordings, the lower trace shows the MN response to depolarizing currents of increasing amplitude. For both MN1 and MN2, current was increased in 0.5 nA steps from 2.5 nA on the left to 4.5 nA on the right. Stimuli were delivered at 30 s intervals. MN responses were initially passive, but upon reaching threshold, MNs typically fired a single action potential with this stimulus duration. Each MN action potential elicited an EPC of variable amplitude after a delay of 1-3 msec. (**B**) Addition of d-tubocurarine (10 mM) eliminated the stimulus-evoked EPC, but did not affect the MN action potential.

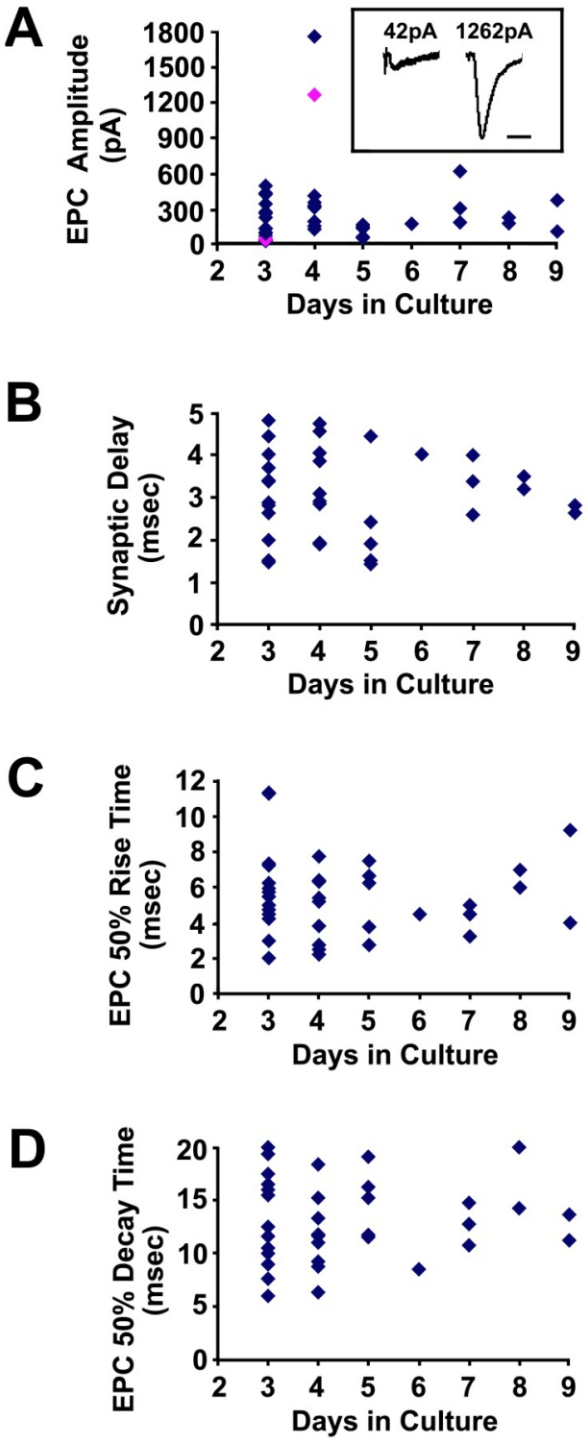

Figure 4-4 Quantification of the properties of mESC-derived MN-muscle synapses.

Scatter plots show the variability of the following parameters as a function of days in co-culture

(**A**) EPC amplitudes, where each point is the largest EPC recorded at each synapse. Inset shows representative EPCs that correspond to the fuchsia diamonds (time scale is 25 msec)

(**B**) Synaptic delay, measured from the peak of the MN action potential to the start of the EPC

(**C**) EPC rise time

(**D**) EPC decay time.

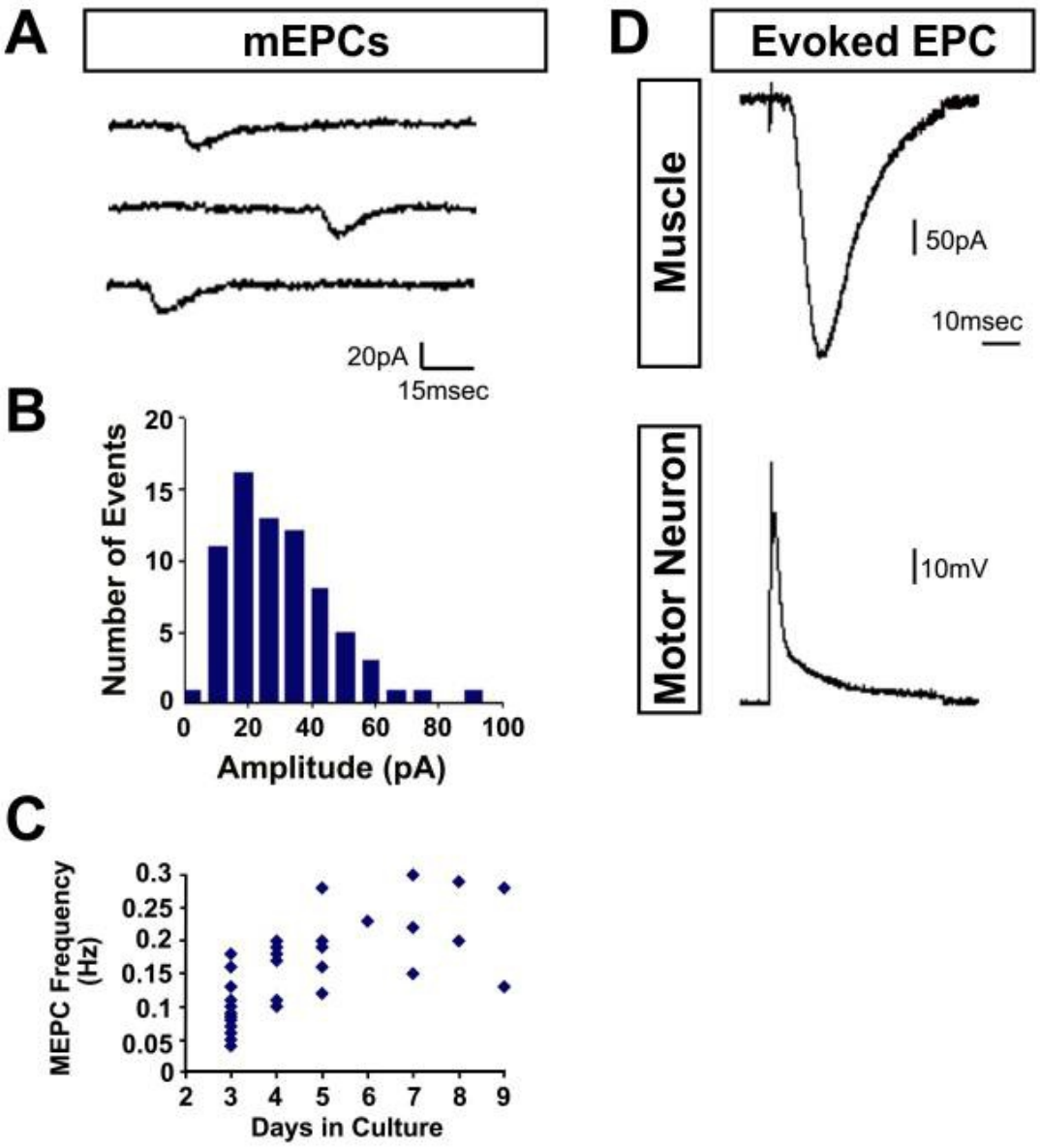

Figure 4-5 mESC-derived MNs exhibit both spontaneous and evoked synaptic currents at neuromuscular junctions formed *in vitro*.

Patch pipettes were sealed onto MNs and muscle cells making contact as shown in Fig. 1.

(**A, B**) Records of spontaneous mEPCs in muscle cells and their amplitude distribution.

(**C**) Scatter plot of mEPC frequency over different times in culture.

(**D**) Current injections into MNs triggers action potentials that elicit multi-quantal EPCs in muscle cells.

BIBIOLOGRAPHY

1. Boillee, S., Vande Velde, C. & Cleveland, D.W. ALS: a disease of motor neurons and their nonneuronal neighbors. *Neuron* **52**, 39-59 (2006).

2. Monani, U.R. Spinal muscular atrophy: a deficiency in a ubiquitous protein; a motor neuron-specific disease. *Neuron* **48**, 885-896 (2005).

3. Pasinelli, P. & Brown, R.H. Molecular biology of amyotrophic lateral sclerosis: insights from genetics. *Nat Rev Neurosci* **7**, 710-723 (2006).

4. Vande Velde, C., Dion, P.A. & Rouleau, G.A. Amyotrophic lateral sclerosis: new genes, new models, and new mechanisms. *F1000 Biol Rep* **3**, 18 (2011).

5. Wee, C.D., Kong, L. & Sumner, C.J. The genetics of spinal muscular atrophies. *Curr Opin Neurol* **23**, 450-458 (2010).

6. Lee, H.*, et al.* Directed differentiation and transplantation of human embryonic stem cell-derived motoneurons. *Stem Cells* **25**, 1931-1939 (2007).

7. Li, X.J.*, et al.* Specification of motoneurons from human embryonic stem cells. *Nat Biotechnol* **23**, 215-221 (2005).

8. Singh Roy, N.*, et al.* Enhancer-specified GFP-based FACS purification of human spinal motor neurons from embryonic stem cells. *Exp Neurol* **196**, 224-234 (2005).

9. Wichterle, H., Lieberam, I., Porter, J.A. & Jessell, T.M. Directed differentiation of embryonic stem cells into motor neurons. *Cell* **110**, 385-397 (2002).

10. Dimos, J.T.*, et al.* Induced pluripotent stem cells generated from patients with ALS can be differentiated into motor neurons. *Science* **321**, 1218-1221 (2008).

11. Ebert, A.D.*, et al.* Induced pluripotent stem cells from a spinal muscular atrophy patient. *Nature* **457**, 277-280 (2009).

12. Karumbayaram, S.*, et al.* Directed Differentiation of Human-Induced Pluripotent Stem Cells Generates Active Motor Neurons. *Stem Cells* **27**, 806-811 (2009).

13. Son, E.Y.*, et al.* Conversion of mouse and human fibroblasts into functional spinal motor neurons. *Cell Stem Cell* **9**, 205-218 (2011).

14. Murray, L.M., Talbot, K. & Gillingwater, T.H. Review: neuromuscular synaptic vulnerability in motor neurone disease: amyotrophic lateral sclerosis and spinal muscular atrophy. *Neuropathol Appl Neurobiol* **36**, 133-156 (2010).

15. Dadon-Nachum, M., Melamed, E. & Offen, D. The "dying-back" phenomenon of motor neurons in ALS. *J Mol Neurosci* **43**, 470-477 (2011).

16. Miles, G.B.*, et al.* Functional properties of motoneurons derived from mouse embryonic stem cells. *J Neurosci* **24**, 7848-7858 (2004).

17. Patani, R.*, et al.* Retinoid-independent motor neurogenesis from human embryonic stem cells reveals a medial columnar ground state. *Nature communications* **2**, 214 (2011).

18. Soundararajan, P., Miles, G.B., Rubin, L.L., Brownstone, R.M. & Rafuse, V.F. Motoneurons derived from embryonic stem cells express transcription factors and develop phenotypes characteristic of medial motor column neurons. *J Neurosci* **26**, 3256-3268 (2006).

19. Peljto, M., Dasen, J.S., Mazzoni, E.O., Jessell, T.M. & Wichterle, H. Functional diversity of ESC-derived motor neuron subtypes revealed through intraspinal transplantation. *Cell Stem Cell* **7**, 355-366 (2010).

20. Yohn, D.C., Miles, G.B., Rafuse, V.F. & Brownstone, R.M. Transplanted mouse embryonic stem-cell-derived motoneurons form functional motor units and reduce muscle atrophy. *J Neurosci* **28**, 12409-12418 (2008).

21. Wichterle, H. & Peljto, M. Differentiation of mouse embryonic stem cells to spinal motor neurons. *Current protocols in stem cell biology* **Chapter 1**, Unit 1H 1 1-1H 1 9 (2008).

22. Poage, R.E., Meriney, S.D., Gundersen, C.B. & Umbach, J.A. Antibodies against cysteine string proteins inhibit evoked neurotransmitter release at Xenopus neuromuscular junctions. *J Neurophysiol* **82**, 50-59 (1999).

23. Fatt, P. & Katz, B. An analysis of the end-plate potential recorded with an intracellular electrode. *J Physiol* **115**, 320-370 (1951).

24. Guo, X.*, et al.* Neuromuscular junction formation between human stem-cell-derived motoneurons and rat skeletal muscle in a defined system. *Tissue engineering. Part C, Methods* **16**, 1347-1355 (2010).

25. Dennis, M.J., Ziskind-Conhaim, L. & Harris, A.J. Development of neuromuscular junctions in rat embryos. *Dev Biol* **81**, 266-279 (1981).

26. Ferguson, S.M.*, et al.* Lethal impairment of cholinergic neurotransmission in hemicholinium-3-sensitive choline transporter knockout mice. *Proc Natl Acad Sci USA* **101**, 8762-8767 (2004).

27. Urbano, F.J.*, et al.* Altered properties of quantal neurotransmitter release at endplates of mice lacking P/Q-type Ca2+ channels. *Proc Natl Acad Sci USA* **100**, 3491-3496 (2003).

28. de Castro, B.M.*, et al.* The vesicular acetylcholine transporter is required for neuromuscular development and function. *Mol Cell Biol* **29**, 5238-5250 (2009).

29. Dalla Torre di Sanguinetto, S.A., Dasen, J.S. & Arber, S. Transcriptional mechanisms controlling motor neuron diversity and connectivity. *Curr Opin Neurobiol* **18**, 36-43 (2008).

30. Landmesser, L.T. The acquisition of motoneuron subtype identity and motor circuit formation. *Int J Dev Neurosci* **19**, 175-182 (2001).

31. Sanes, J.R. & Lichtman, J.W. Development of the vertebrate neuromuscular junction. *Annual review of neuroscience* **22**, 389-442 (1999).

32. O'Brien, M.K., Landmesser, L. & Oppenheim, R.W. Development and survival of thoracic motoneurons and hindlimb musculature following transplantation of the thoracic neural tube to the lumbar region in the chick embryo: functional aspects. *J Neurobiol* **21**, 341-355 (1990).

33. Dasen, J.S., De Camilli, A., Wang, B., Tucker, P.W. & Jessell, T.M. Hox repertoires for motor neuron diversity and connectivity gated by a single accessory factor, FoxP1. *Cell* **134**, 304-316 (2008).

34. Rousso, D.L., Gaber, Z.B., Wellik, D., Morrisey, E.E. & Novitch, B.G. Coordinated actions of the forkhead protein Foxp1 and Hox proteins in the columnar organization of spinal motor neurons. *Neuron* **59**, 226-240 (2008).

35. Wishart, T.M., Parson, S.H. & Gillingwater, T.H. Synaptic vulnerability in neurodegenerative disease. *J Neuropathol Exp Neurol* **65**, 733-739 (2006).

36. Karumbayaram, S.*, et al.* Human embryonic stem cell-derived motor neurons expressing SOD1 mutants exhibit typical signs of motor neuron degeneration linked to ALS. *Dis Model Mech* **2**, 189-195 (2009).

37. Ling, K.K., Lin, M.Y., Zingg, B., Feng, Z. & Ko, C.P. Synaptic defects in the spinal and neuromuscular circuitry in a mouse model of spinal muscular atrophy. *PLoS One* **5**, e15457 (2010).

CHAPTER 5 – Conclusions and Implications for Motor Neuron Disease

One of the main objectives of stem cell biology is to generate faithful representations of endogenous cell populations, with the hope of modeling and treating human disease. This objective requires extensive knowledge of different signaling pathways required for the development of all cell populations in the body. One especially challenging and rewarding area has been the generation of different cell types of the central nervous system from pluripotent stem cells. Spinal motor neurons (MNs) are a diverse population of highly specialized cells, required for all voluntary and involuntary muscle movement. Diseases that directly target MNs are life threatening and often fatal, with very few effective treatments available. Characterization of animal models has resulted in increased understanding of MN biology and disease, but has not successfully translated into new treatments for patients. Because of this, a large amount of effort has been directed towards using human stem cells for alternative methods of modeling MN disease and cellular replacement strategies

In chapter two, I presented a detailed characterization of human spinal cord and MN development during the first trimester. Interestingly, the processes of MN development and organization are largely conserved between humans and mice, validating the use of mouse models for investigating spinal cord development. However, there are several small differences in motor pool size between human and mouse embryonic lateral motor column (LMC) MNs, suggesting some species-specific developmental processes. Interestingly, human embryonic stem cell (hESC)-derived MNs only express markers of cervical MNs, therefore only representing a subset of endogenous populations. In addition, medial motor column (MMC) and LMC MN markers are disproportionately expressed by hESC-derived MNs at different times during the maturation period, with very few $FOXP1^{+}$ LMC-like MNs generated overall. Despite these differences, human embryonic and hESC-derived MNs appear to functionally mature over

the same time period, as determined by their expression of CHAT and electrophysiological properties. Overall, it appears that hESC-derived MNs are functionally equivalent to embryonic populations, but do not represent the full population of MNs found *in vivo*.

In chapter three, I presented an alternative approach for broadening the diversity of stem cell-derived MNs. Foxp1 misexpression during mouse embryonic stem cell (ESC) differentiation is sufficient to push newly born MNs from an MMC fate to an LMC fate. Interestingly, Foxp1 misexpression results in stem cell-derived MNs that express motor pool markers and axon guidance receptors of both dorsal and ventral LMC MN populations. Furthermore, Foxp1-programmed MNs preferentially innervate distal limb muscles *in vivo* after transplantation. This approach can also be applied to hESC-derived MNs, as shown by overexpression of a caudal Hox protein (HOXC10) to increase the diversity of stem cell-derived MNs.

Finally, in chapter four, I demonstrated that stem cell-derived MNs are capable of forming neuromuscular junctions (NMJs) with muscle cells *in vitro*. Presynaptic and postsynaptic proteins co-localize between MN axon terminals and myotubes in a low density co-culture system. Upon stimulation of action potentials (APs) in stem cell-derived MNs, C2C12 myotubes exhibit stereotypical excitatory post-synaptic currents. Therefore, stem cell-derived MNs can be used to successfully model NMJ maturation *in vitro*.

Together, this work demonstrates that standard human and mouse ESC differentiation protocols result in a biased subset of total MN populations, but this subset can be expanded through MN fate determinant overexpression. Furthermore, different ESC-derived MN subtypes display appropriate functional behaviors *in vitro* and *in vivo*. This is very significant for future studies of human MN development, as it signifies that *in vitro* assays can substitute for difficult *in vivo* experiments. This work also proposes several interesting questions. First, how do different MN fate determinants alter cell fate decisions? Although several gene targets of Foxp1 in MNs have been previously hypothesized (Lhx3, Hb9)[1, 2], currently little evidence exists of its

direct and downstream targets. A previous study found that Lhx3 bound a different set of genes when co-expressed with either Isl1 or Phox2a to specify spinal or cranial MN populations, respectively[3]. Therefore, it is likely that MN fate determinants act differently in separate cell populations throughout the spinal cord. Overexpression of different MN fate determinants during stem cell differentiation presents a unique system for answering these questions. Secondly, how are different MN populations affected by MN disease? The majority of studies that model MN diseases with stem cell-derived MNs do not take into account the diversity of spinal MNs *in vivo*. Interestingly, many patients have reported initial muscle weakness in arms and legs[4]; therefore, it is possible that limb-innervating MNs have increased sensitivity to cellular damage. It would be exciting to use Foxp1-programmed MNs to investigate any potential differences. And finally, can early symptoms of MN diseases be accurately recapitulated *in vitro* using MN and muscle co-culture assays? Now that we know NMJ formation and maturation can be modeled *in vitro*, it will be important to examine any possible synaptic defects associated with MN disease. To further discuss these last two questions in the next section, I briefly describe MN disease and how stem cells have contributed to current understanding.

Amyotrophic lateral sclerosis

Amyotrophic lateral sclerosis (ALS), also known as Lou Gehrig's disease, is a fatal neurodegenerative disease that usually presents itself late in adulthood. The disease results in progressive muscle weakness, ultimately resulting in paralysis and death from respiratory failure within 3 to 5 years after diagnosis[5]. Approximately 5,600 people in the United States are diagnosed with ALS each year and there are no current effective treatments or cure for the disease[5]. ALS typically starts with limb weakness in about two-thirds of patients and usually involves both upper and low MN dysfunction[4]. The majority (~90%) of ALS cases are sporadic, meaning that there is no family history of the disease. However, analysis of familial ALS patients (~10% of total cases) has revealed insight into mechanisms of the disease. The first gene

identified to play a role in ALS was superoxide dismutase 1 (SOD1), which accounts for ~20% of familial ALS cases[6-8]. SOD1 is a constitutively expressed protein that catalyzes the dismutation of superoxide radicals and protects the cell against reactive oxygen species[5]. More than 160 mutations in SOD1 have been reported – the most well studied being the G93A mutation that has been used to create an ALS mouse model[9]. The toxic mechanisms of SOD1 mutations remain unclear, but there is growing evidence that they result in misfolded SOD1 protein that gains toxic functions causing ER stress, mitochondrial dysfunction, and disruption of axonal transport. In addition to SOD1, additional mutations in other genes have been identified, including TDP43, FUS, C9ORF72, UBQLN2, and P62[5]. Expanded hexanucleotide repeats in C9ORF72 have recently been found to be the most common cause of ALS and frontal temporal dementia (FTD), found in ~30% of familial and 5% of sporadic cases[10, 11].

Mouse models of ALS have replicated certain aspects of human symptoms. Transgenic mice expressing high levels of the human SOD1 protein containing the G93A mutation display progressive muscle weakness resulting in paralysis and reduced lifespan (~5-6 months)[9]. However, these animals overexpress human SOD1 at very high non-physiological levels. Another mouse model that expresses a common ALS-associated FUS mutation (FUS-R521C) has been found to exhibit evidence of DNA damage, dendritic and synaptic defects, and abnormalities in motor function[12]. However, animal models of other ALS mutations, such as TDP43 and C9ORF72, have not been as widely studied as the G93A mouse.

Scientists have recently turned towards using hESCs and ALS patient-derived induced pluripotent stem cells (iPSCs) to model disease processes *in vitro*. Overexpression of mutant SOD1 in hESC-derived MNs was found to result in decreased MN survival and electrophysiology defects, compared to control MNs.[13] Human iPSC lines have been generated from ALS patients with SOD1, TDP43, and C9ORF72 mutations and display some disease characteristics upon differentiation into MNs, such as decreased MN survival[14-16]. Recently, transcriptional profiling of SOD1 mutant iPSC-derived MNs identified candidate genes that were

significantly affected by the disease mutation[16]. In addition, non-cell autonomous roles for SOD1 have been identified through the culturing of MNs with wild type and mutant glial cells[17]. While these studies have shown that hESC and hiPSC-derived MNs recapitulate some characteristics of ALS, the majority of disease processes have not been observed *in vitro*.

Spinal muscular atrophy

Similar to ALS, spinal muscular atrophy (SMA) is characterized by a loss of spinal MNs, resulting in progressive muscle weakness and atrophy, paralysis, and death. SMA affects 1 in every 6,000 live births and is the primary genetic cause of infant mortality[18]. SMA is caused by homozygous genetic disruption of the Survival Motor Neuron1 (SMN1) gene, which is expressed constitutively and been implicated in pre-mRNA splicing, mRNA transport, and axon growth[18]. The severity (and type) of SMA depends largely upon the expression level of SMN protein. Unlike other animals, humans have a duplicated SMN1 gene (SMN2) that contains a single nucleotide change in exon 7 that disrupts its splicing, resulting in very little functional protein[19]. SMA type I is the most common and severe form of the disease, with symptoms typically appearing around 6 months of age and death occurring before 2 years. There are no effective treatments at present, but current strategies focus on increasing levels of SMN protein, potentially through gene therapy, affecting alternative splicing, or increasing protein stability[18].

Because SMA is a single-gene disease, many different animal models have been created, including *C. elegans*, *Drosophila*, zebrafish, and mouse models[18]. Mice have only the SMN1 gene and knocking out SMN1 results in early embryonic lethality[20]. Therefore, most studies have used mice that lack SMN1 in combination with transgenic SMN2 expression ($SMN1^{-/-}$; $SMN2^{tg/tg}$; $SMN\Delta7^{tg/tg}$), which exhibit symptoms similar to patients with intermediate type II SMA[21]. These mice are born with normal numbers of MNs, but exhibit NMJ defects, muscle weakness, and 50% MN loss by postnatal day 9[21].

Recently, human stem cells have also been used to model SMA *in vitro*. SMA patient fibroblasts have been converted into iPSCs, which display certain disease characteristics upon differentiation into spinal MNs[22]. Although SMA iPSCs initially generated normal numbers of MNs, significant reductions in MN number and cell size were found after an additional two weeks of culture[22]. Interestingly, treatment with valporoic acid or tobramycin resulted in increased SMN protein production[22]. Another group used single-stranded oligonucleotides to convert the SMN2 gene into an SMN1-like gene in SMA patient derived iPSCs[23]. Transplantation of these corrected SMA iPSC-derived MNs into a SMA mouse model of SMA reduced disease symptoms and extended lifespan.[23]

Although these studies represent important advances in understanding SMA disease pathogenesis, relatively little work has been done to examine the earliest events in the course of the disease. This process has been difficult to determine from patients, largely because of the difficulty in obtaining tissue biopsies. From work with SMA mouse models, the earliest structural defects were seen with NMJ postnatal maturation, including a loss of acetylcholine receptor clustering at MN axon terminals[24]. These results suggest a “dying-back” mechanism of axon degeneration, similar to what is seen in other neurodegenerative diseases.

Future directions for modeling and treating MN disease with stem cells

A large amount of work has been done over the past several decades to understand the diverse cellular mechanisms of different MN diseases. While the majority of insight has resulted from animal models, it is important to confirm any findings and potential treatments with human cells before use in patients. In this regard, human stem cell-derived MNs have provided a valuable tool. However, several issues remain that will need to be addressed in the next several years. First of all, many (if not all) studies characterize ALS and SMA hiPSC-derived MNs in isolation without muscle cells, which does not provide insight into the initiation of disease. Now that NMJ formation and maturation can be observed *in vitro*, it will be important to perform these

studies with the addition of muscle cells, astrocytes, and Schwann cells. This will also provide important information on whether ALS and SMA are strictly MN-specific diseases, or whether other cell types are affected. If ALS and SMA hiPSC-derived MNs exhibit defects in NMJ maturation or stability, these co-cultures will then also provide valuable assays for screening drugs and identifying early disease biomarkers.

A second issue is the functional maturation of stem cell-derived MNs. From our work in chapter two, we found that hESC-derived MNs exhibited electrophysiological properties similar to human embryonic MNs. However, MNs and NMJs are known to undergo further maturation and diversification at postnatal ages. Spinal MNs are further organized into slow-twitch fatigue-resistant (S), fast-twitch fatigue-resistant (FR), and fast-twitch fatigable (FF) subclasses, which are responsible for different types of muscle movement[25]. Unfortunately, the molecular characteristics distinguishing these MNs are not clearly defined, thereby making it difficult to assess whether these MNs are generated from stem cells. Interestingly, these subclasses display varying degrees of vulnerability in ALS and SMA, with S MNs being the most resistant and FF the most vulnerable[26]. It is very likely that late-stage disease processes will not occur in stem cell-derived MN cultures, so there is a great need for methods to accelerate maturation of human stem cell-derived neurons. One approach has been overexpression of progerin in iPSC-derived dopaminergic neurons to induce DNA damage and other characteristics of aging[27]. While this method is not ideal, it represents an important step towards solving this problem.

In conclusion, this thesis provides important insights into human development and how well stem cell-derived cell populations mimic endogenous populations. Now that alternative differentiation methods and *in vitro* assays are available, hopefully a new era of understanding for neurodegenerative disease is just around the corner.

BIBLIOGRAPHY

1. Rousso, D.L., Gaber, Z.B., Wellik, D., Morrisey, E.E. & Novitch, B.G. Coordinated actions of the forkhead protein Foxp1 and Hox proteins in the columnar organization of spinal motor neurons. *Neuron* **59**, 226-240 (2008).

2. Dasen, J.S., De Camilli, A., Wang, B., Tucker, P.W. & Jessell, T.M. Hox repertoires for motor neuron diversity and connectivity gated by a single accessory factor, FoxP1. *Cell* **134**, 304-316 (2008).

3. Mazzoni, E.O.*, et al.* Synergistic binding of transcription factors to cell-specific enhancers programs motor neuron identity. *Nat. Neurosci.* **16**, 1219-1227 (2013).

4. Kanning, K.C., Kaplan, A. & Henderson, C.E. Motor neuron diversity in development and disease. *Annu. Rev. Neurosci.* **33**, 409-440 (2010).

5. Ajroud-Driss, S. & Siddique, T. Sporadic and hereditary amyotrophic lateral sclerosis (ALS). *Biochim. Biophys. Acta* (2014).

6. Siddique, T.*, et al.* Linkage analysis in familial amyotrophic lateral sclerosis. *Neurology* **39**, 919-925 (1989).

7. Siddique, T.*, et al.* Linkage of a gene causing familial amyotrophic lateral sclerosis to chromosome 21 and evidence of genetic-locus heterogeneity. *N. Engl. J. Med.* **324**, 1381-1384 (1991).

8. Rosen, D.R.*, et al.* Mutations in Cu/Zn superoxide dismutase gene are associated with familial amyotrophic lateral sclerosis. *Nature* **362**, 59-62 (1993).

9. Gurney, M.E.*, et al.* Motor neuron degeneration in mice that express a human Cu,Zn superoxide dismutase mutation. *Science* **264**, 1772-1775 (1994).

10. Renton, A.E.*, et al.* A hexanucleotide repeat expansion in C9ORF72 is the cause of chromosome 9p21-linked ALS-FTD. *Neuron* **72**, 257-268 (2011).

11. DeJesus-Hernandez, M.*, et al.* Expanded GGGGCC hexanucleotide repeat in noncoding region of C9ORF72 causes chromosome 9p-linked FTD and ALS. *Neuron* **72**, 245-256 (2011).

12. Qiu, H.*, et al.* ALS-associated mutation FUS-R521C causes DNA damage and RNA splicing defects. *J. Clin. Invest.* **124**, 981-999 (2014).

13. Karumbayaram, S.*, et al.* Human embryonic stem cell-derived motor neurons expressing SOD1 mutants exhibit typical signs of motor neuron degeneration linked to ALS. *Disease models & mechanisms* **2**, 189-195 (2009).

14. Chen, H.*, et al.* Modeling ALS with iPSCs reveals that mutant SOD1 misregulates neurofilament balance in motor neurons. *Cell Stem Cell* **14**, 796-809 (2014).

15. Sareen, D.*, et al.* Targeting RNA foci in iPSC-derived motor neurons from ALS patients with a C9ORF72 repeat expansion. *Sci Transl Med* **5**, 208ra149 (2013).

16. Kiskinis, E.*, et al.* Pathways disrupted in human ALS motor neurons identified through genetic correction of mutant SOD1. *Cell Stem Cell* **14**, 781-795 (2014).

17. Di Giorgio, F.P., Carrasco, M.A., Siao, M.C., Maniatis, T. & Eggan, K. Non-cell autonomous effect of glia on motor neurons in an embryonic stem cell-based ALS model. *Nat. Neurosci.* **10**, 608-614 (2007).

18. Edens, B.M., Ajroud-Driss, S., Ma, L. & Ma, Y.C. Molecular mechanisms and animal models of spinal muscular atrophy. *Biochim. Biophys. Acta* (2014).

19. Cartegni, L. & Krainer, A.R. Disruption of an SF2/ASF-dependent exonic splicing enhancer in SMN2 causes spinal muscular atrophy in the absence of SMN1. *Nat. Genet.* **30**, 377-384 (2002).

20. Schrank, B.*, et al.* Inactivation of the survival motor neuron gene, a candidate gene for human spinal muscular atrophy, leads to massive cell death in early mouse embryos. *Proc. Natl. Acad. Sci. U. S. A.* **94**, 9920-9925 (1997).

21. Le, T.T.*, et al.* SMNDelta7, the major product of the centromeric survival motor neuron (SMN2) gene, extends survival in mice with spinal muscular atrophy and associates with full-length SMN. *Hum. Mol. Genet.* **14**, 845-857 (2005).

22. Ebert, A.D.*, et al.* Induced pluripotent stem cells from a spinal muscular atrophy patient. *Nature* **457**, 277-280 (2009).

23. Corti, S.*, et al.* Genetic correction of human induced pluripotent stem cells from patients with spinal muscular atrophy. *Sci Transl Med* **4**, 165ra162 (2012).

24. Kariya, S.*, et al.* Reduced SMN protein impairs maturation of the neuromuscular junctions in mouse models of spinal muscular atrophy. *Hum. Mol. Genet.* **17**, 2552-2569 (2008).

25. Davis-Dusenbery, B.N., Williams, L.A., Klim, J.R. & Eggan, K. How to make spinal motor neurons. *Development* **141**, 491-501 (2014).

26. Arbab, M., Baars, S. & Geijsen, N. Modeling motor neuron disease: the matter of time. *Trends Neurosci.* (2014).

27. Miller, J.D.*, et al.* Human iPSC-based modeling of late-onset disease via progerin-induced aging. *Cell Stem Cell* **13**, 691-705 (2013).